Delay and Queue Length Estimation at Signalized Intersections Using Archived Automatic Vehicle Location and Passenger Count Data from Transit Vehicles

by

Sahar Tolami Hemmati

A thesis
presented to the University of Waterloo
in fulfillment of the
thesis requirement for the degree of
Master of Applied Science
in
Civil Engineering

Waterloo, Ontario, Canada, 2015

AUTHOR'S DECLARATION

I hereby declare that I am the sole author of this thesis. This is a true copy of the thesis, including any required final revisions, as accepted by my examiners.

I understand that my thesis may be made electronically available to the public.

Abstract

Signalized intersections are typically the capacity bottlenecks within urban road networks. The performance of signalized intersections is typically quantified on the basis of average vehicle delay and maximum queue lengths. In practice, these measures of performance are commonly estimated using tools that implement the methods from the Highway Capacity Manual. These methods, which have been derived from deterministic and stochastic queuing theory, estimate delay and queue length on the basis of geometry, signal timings, turning movement counts (TMC), vehicle stream composition, etc. The cost and effort required to acquire these data, and particularly the TMCs, result in TMCs being collected for a single day every several years. Thus, estimates of intersection performance are often several years out of date and do not capture day-to-day and seasonal variations in conditions that occur throughout the year.

Many transit agencies have deployed Automatic Vehicle Location (AVL) and Automatic Passenger Count (APC) systems on their fleet of transit vehicle. This thesis proposes a methodology to estimate the stopped delay and maximum queue length at signalized intersections on the basis of archived AVL/APC data. This provides the advantage of being able to: (1) estimate intersection performance on the basis of field measurements rather than models; (2) no additional cost or effort is required to acquire the data; and (3) performance can be evaluated throughout the year.

Unlike previous methods, the proposed methodology is applicable to intersections with near-side transit stations. The proposed model is evaluated using both simulation and field data and shown to provide satisfactory results.

Acknowledgements

I would like to gratitude to all those who have supported me during my graduate studies.

Firstly, I like to express my deep appreciation and thanks to my supervisor, Professor Bruce Hellinga, for his guidance and help.

I sincerely appreciate all the help and information Reid at Grand River Transit has provided me for this research.

I wish to thank my friends Alina and Camila for all the emotional support, comradery, entertainment, and caring they provided.

I would like to express my gratitude to my family, particularly my parents Nassrin and Mozaffar, for their unconditional love, support, and unwavering belief in me. Without their support, I would not be the person I am today. Thanks to Nasim and Pedram that have always been my role models. Their continuous love, support and encouragement fuel all my endeavours.

Last but not least, I would like to thank Sina whose love, passion and patience cannot go unmentioned. Thanks for being my rock.

Table of Contents

List of Figures

List of Tables

Chapter 1
Introduction

1.1 Background

Intersections are considered the capacity bottlenecks of the arterial road network. Much of the delay experienced within the arterial road network is experienced at the signalized intersections. The performance of signalized intersections is commonly quantified in terms of the average vehicle delay and the maximum queue length where the average delay is typically mapped to a categorical scale called Level of Service (LOS) for which A is best and F is worst. Unsatisfactory levels of service typically lead to the implementation of measures to improve the LOS, such as retiming of the traffic signals, changes to geometry, or other measures. Queue length estimates are typically used to determine the required length of turning lanes, planning suitable locations and expected operations of upstream driveways or intersections, or identifying opportunities for implementing transit priority measures such as queue jump lanes. For these reasons it is important for transportation authorities to have a system with which they can evaluate the performance of the intersections within their network and on the basis of these data prioritize the allocation of resources for intersection improvements.

All agencies share two common challenges:

1. Identifying the problematic/inefficient intersections within the arterial road network.
2. Obtaining reliable signal delay data under existing conditions in a timely and cost effective manner.

Conventionally, delay and queue length measures are estimated using software tools that implement the Highway Capacity Manual methodology (HCM, 2010). Regardless of which tool is used, the analysis requires input data such as traffic counts, signal timings, pedestrian volumes, traffic stream composition, and saturation flow rates. The accuracy of the measures of performance provided by the software tools depends on the accuracy of the input data.

In recent years, many transit agencies have deployed Automatic Vehicle Location (AVL) and Automatic Passenger Counting (APC) systems on their fleet of public transit vehicles. AVL systems utilize GPS and wireless communication systems to track the position of the transit vehicle in real time. APC systems utilize sensors on the transit vehicle to count the number of passengers boarding and alighting the transit vehicle at each transit station. Typically the data from the AVL and APC systems are combined with schedule data and archived into a unified historical database. The availability of this database provides bus location and passenger activity data (i.e. number passengers boarding and alighting) for large portions of the arterial network by time of day, day of week, etc. Being able to use the archived AVL/APC data to quantify the performance of signalized intersections provides the obvious cost savings of not having to conduct dedicated field data collection surveys, and also provides the benefit that performance can be evaluated over the entire year, rather than the current norm in which data (e.g. turning movement counts) are collected for a single day (or at best a small number of days).

AVL/APC systems are deployed by public transportation agencies to ensure safety, efficiency and quality of service for transit users. The main applications of AVL/APC data are in real-time transit operations monitoring and control (Furth et al., 2006). However, AVL/APC data have been used by researchers for other applications as well. Yang and Hellinga (2012) proposed a method for estimating the delay and queue length at signalized intersections from archived AVL/APC data, but their method was not applicable for intersection approaches with a near-sided transit station[1] (i.e. stations located just upstream of the intersection stop line).

1.2 Motivation

There is no systematic cost effective tool available to evaluate and rank the performance of the signalized intersections within an arterial network. AVL/APC data are available for every

[1] The term *transit station* is used to refer to any location designated for passenger boarding and alighting. The term *stop* is used to refer to an event in which the transit vehicle becomes stationary.

signalized intersection approach traversed by a transit route and therefore provide an opportunity to evaluate the performance of signalized intersections without the need for additional instrumentation and at no additional cost for data acquisition.

The study by Yang and Hellinga (2012) illustrated the potential of using archived AVL/APC data for estimating delay and maximum queue length at signalized intersections. However, their method is not applicable to approaches containing a near-sided transit station. This restriction imposes a significant limitation for the application of the model because near-sided transit stations are very common.

Given the cost associated with estimating signal delay by conventional methods and the fact that near-sided transit stations are common in transit networks, there is substantial benefit to developing a method to estimate the delay and queue length at signalized intersections containing a near-sided transit station. In this research a methodology is proposed to use archived AVL/APC data for estimating the delay and queue length at signalized intersection approaches containing a near-sided transit station.

1.3 Problem Definition

Typically, the AVL/APC data are stored in two sets of records, (1) trip-level records and (2) stop-level records. The information pertaining to individual transit trips such as the trip's date and time, route and direction are stored in trip-level records. The information regarding individual stops are archived in stop-level records. AVL/APC systems can be configured to provide stop data in three ways:

1. *Fixed Frequency* – The position of the transit vehicle is recorded at a fixed time frequency.
2. *Event Based* – Data are recorded when a predefined event occurs.
3. *Combined Fixed Frequency and Event Based* – Data are recorded at a fixed time interval and when a predefined event occurs.

The AVL/APC systems are usually event based and therefore are the focus of this thesis. Events of interest typically include: *Planned Stops* (transit vehicle makes a scheduled stop at a transit station regardless of passenger demand); *On Call Stops* (transit vehicle stops at a transit station to board or discharge passengers); *Unscheduled Stops* (transit vehicle stops at a location that is not a transit station); *Drive Through* (transit vehicle passes by a planned or on call stop without stopping). For the purposes of this thesis *scheduled stops* will refer to both *planned* and *on call stops.*

For intersections with near-sided transit stations, stops occurring within the service zone of the transit stations are deemed as *scheduled stops* and stop events outside of the service zones are defined as *unscheduled stops*. Service zone is the distance from the transit station that the transit vehicle is allowed to stop to let passengers board and alight the vehicle.

The events are triggered either by the location of the transit vehicle relative to the known transit stations or the speed of the transit vehicle. For each recorded event, the following information is provided:

- Type of event (i.e. *scheduled stop*)
- Date and time
- Route and direction that transit vehicle is serving
- GPS coordinates
- Passenger activity (number of passengers boarding or alighting)
- Scheduled and actual times of arrival and departure of the transit vehicle
- Total length of time that the transit vehicle is stopped

When an intersection approach does not contain a transit station, then it is likely that the majority of recorded bus stop events upstream of the stop-line, defined as *unscheduled stops*, are caused by the traffic signal. However, for intersections with a near-sided transit station, the bus stop events on the approach can be caused by either the traffic signal or the bus stopping to serve passengers at the transit station, or a combination of both.

At an intersection without any transit stations, vehicles approaching the intersection during the red interval must stop and wait for the green interval. This will create a backward moving formation shockwave. At the onset of the green interval, the queued vehicles will discharge from the intersection at the saturation flow rate, causing a backward moving dissipation shockwave. The location at which the formation and dissipation shockwave meet represents the tail of the queue. The maximum stopped delay is experienced by the vehicle arriving at the stop-line at the onset of red interval and experiences a delay equal to the red interval. The minimum delay is experienced by the vehicle that arrives at the tail of the queue when the queue has nearly dissipated. Therefore, the emerging pattern of delay at the signalized intersection is that which is presented in Figure 1-1(a); where the maximum stop delay equal to red interval occurs at the stop-line and delay decreases linearly to zero at the tail of the queue upstream of the intersection. In an ideal world without sources of variability (i.e. variability of traffic, incidents, parking maneuvers, etc.) the unscheduled stop records of transit vehicles' that occur within the vicinity and upstream of the intersection are expected to follow the described pattern by shockwave theory. These observations can be used to estimate the delay and queue length at signalized intersections.

However, at an intersection with near-sided transit station, the emerging pattern of transit vehicles' stop observations won't be consistent with the pattern describe by shockwave theory, as illustrated in Figure 1-1(c). A transit vehicle approaching such intersections during the green interval may stop to allow passengers to board and alight the transit vehicle. Depending on when the transit vehicle arrives at the station relative to the green interval and the duration of its dwell time, the bus may either leave the intersection during the green interval (depicted by the green line in Figure 1-1(b)) or face the red interval and must wait for the unset of the green interval (depicted by the black line in Figure 1-1(b)). At any rate, these stop observations are not a reflection of signal operation and should not be considered for stopped delay calculations. On the other hand the stop observations that occur when the transit vehicles arrives at the transit station

during the red interval must be considered for the stopped delay calculations. Therefore, the primary challenge is to setup a method to deduce which *scheduled stop* observations are due to the signal operation and which are the result of transit operation (i.e. serving passengers at the transit station).

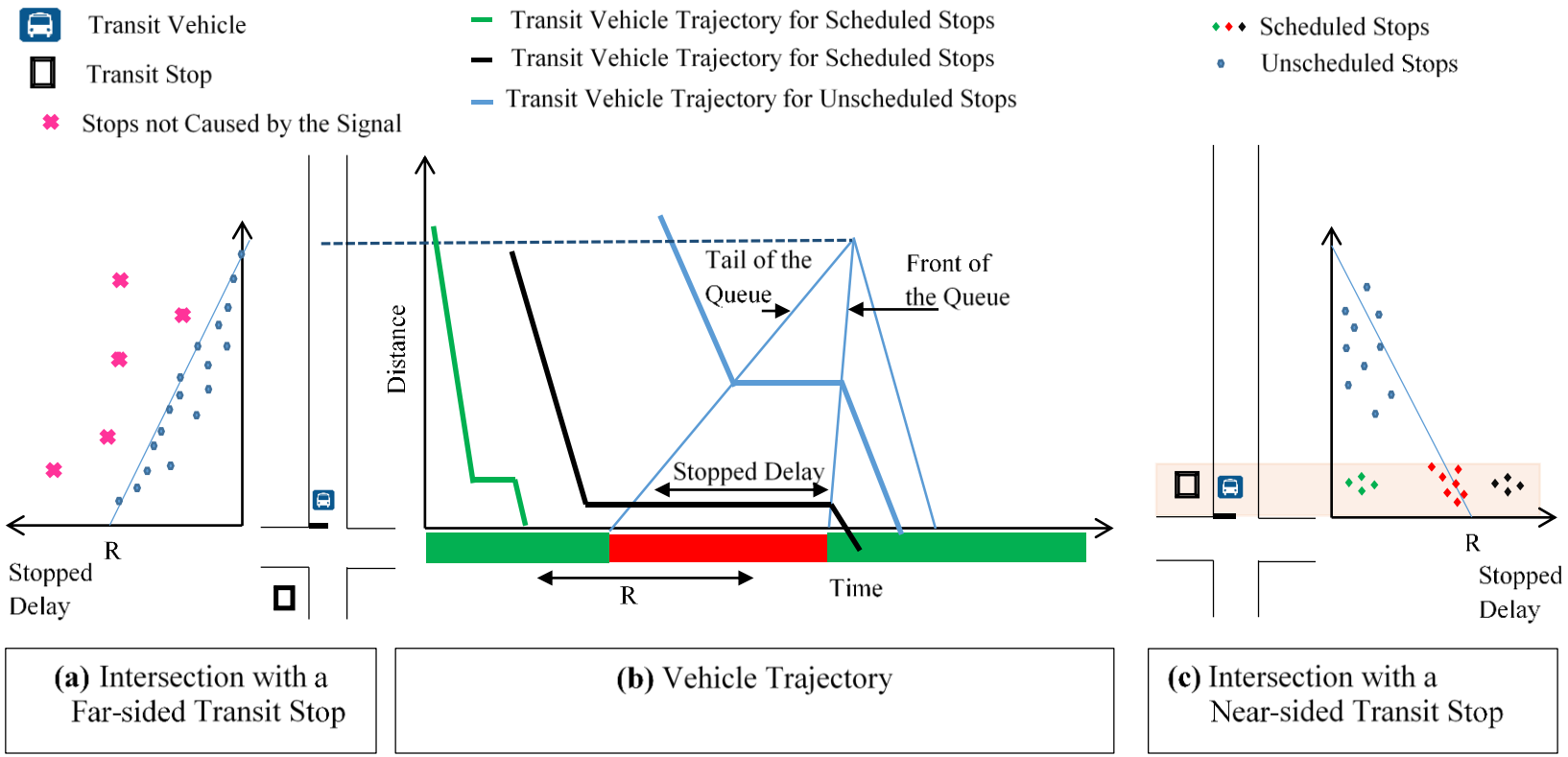

Figure 1-1: Comparison of the Interaction between the Transit Vehicles at Intersection with & without Near–sided Transit Station.

Furthermore, not all *unscheduled* stops observed upstream of the intersection are caused by the traffic signal operation. Transit vehicles may incur stop delay as a result of parking maneuvers, incidents, service vehicles blocking the lane, construction activities, detours, emergency vehicle activity, or other geometric or traffic control devices (e.g. at grade rail-road crossings).

For example, Figure 1-2 depicts a roadway segment between an upstream and a downstream signalized intersection and an at-grade railway crossing in between the intersections. The stopped delay observations depicted are associated with vehicles travelling from right to left (i.e. in the direction of the arrow). The stopped delay observations that are not caused by the traffic signal operation and are the result of the buses stopping at the rail crossing need to be excluded from the delay estimation.

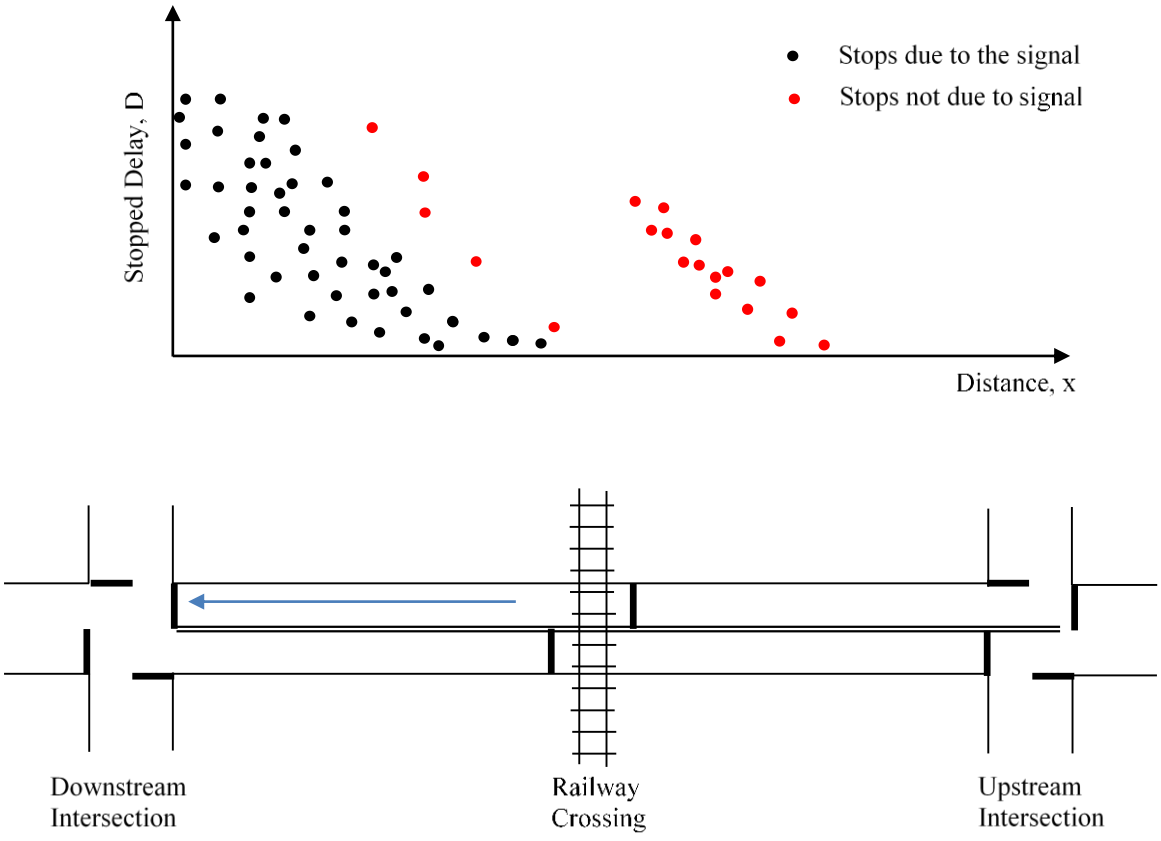

Figure 1-2: Stopped Delay Caused by Multiple Sources.

In order to properly estimate transit vehicle delays for intersections with near-sided transit stop, the methodology must be able to automatically differentiate between the stop observations caused by the traffic signal operations from those caused by transit operations. The methodology must determine which stop observations occur because the signal was red and which stops are merely associated with the transit vehicle's necessity to serve passengers. Furthermore, the methodology must distinguish which *unscheduled* stops are due to signal and other causes.

1.4 Scope and Objectives

The objective of this thesis is to develop a model to evaluate performance and prioritize signalized intersections within the road network using AVL/APC data. This thesis endeavours to answer the following questions:

1. How can archived AVL/APC data be used to automatically quantify the performance of signalized intersection approaches (in terms of average vehicle stopped delay and maximum queue length), including those approaches that contain a near-sided transit station?
2. How accurate are these estimates?
3. How can these estimates be used to prioritize intersections for improvement countermeasures?

1.5 Thesis Organization

The organization of this thesis is as follows: Chapter 2 describes relevant previous studies. Chapter 3 describes the proposed methodology. The evaluation of the proposed methodology is described in Chapter 4. An application of the proposed methodology to the field data is presented in chapter 5. Chapter 6 contains conclusions and recommendations.

Chapter 2
Literature Review

Delay estimation and queue length estimation at signalized intersections has been extensively studied in literature. This chapter provides a brief description of the Highway Capacity Manual procedure for evaluating the performance of signalized intersections. Furthermore, this chapter presents previous research on measuring signalized delay and queue length using microscopic simulation software and direct field measurements.

2.1 Delay at Signalized Intersections

Figure 2-1 depicts a space-time diagram for a section of roadway controlled by a signalized intersection. Two vehicle trajectories are depicted. Trajectory A represents a hypothetical vehicle traversing the roadway and having to decelerate and stop for the traffic signal. Trajectory B represents the same hypothetical vehicle but in this case, the signal is green and the vehicle does not need to adjust its speed. On the basis of these trajectories we can define several different delays.

Deceleration delay is the time required for a vehicle to reduce speed from the approach speed to come to a stop. Stopped delay is the time the vehicle is stationary. Acceleration delay is the time required for the vehicle to increase speed from stopped to cruise speed. The sum of deceleration, stopped, and acceleration delay is called control delay (or total delay) and is the difference between the times when Trajectory B and Trajectory A reach location P2 downstream of the signalized intersection.

The Highway Capacity Manual (HCM) quantifies the level of service (LOS) of an intersection on the basis of control delay.

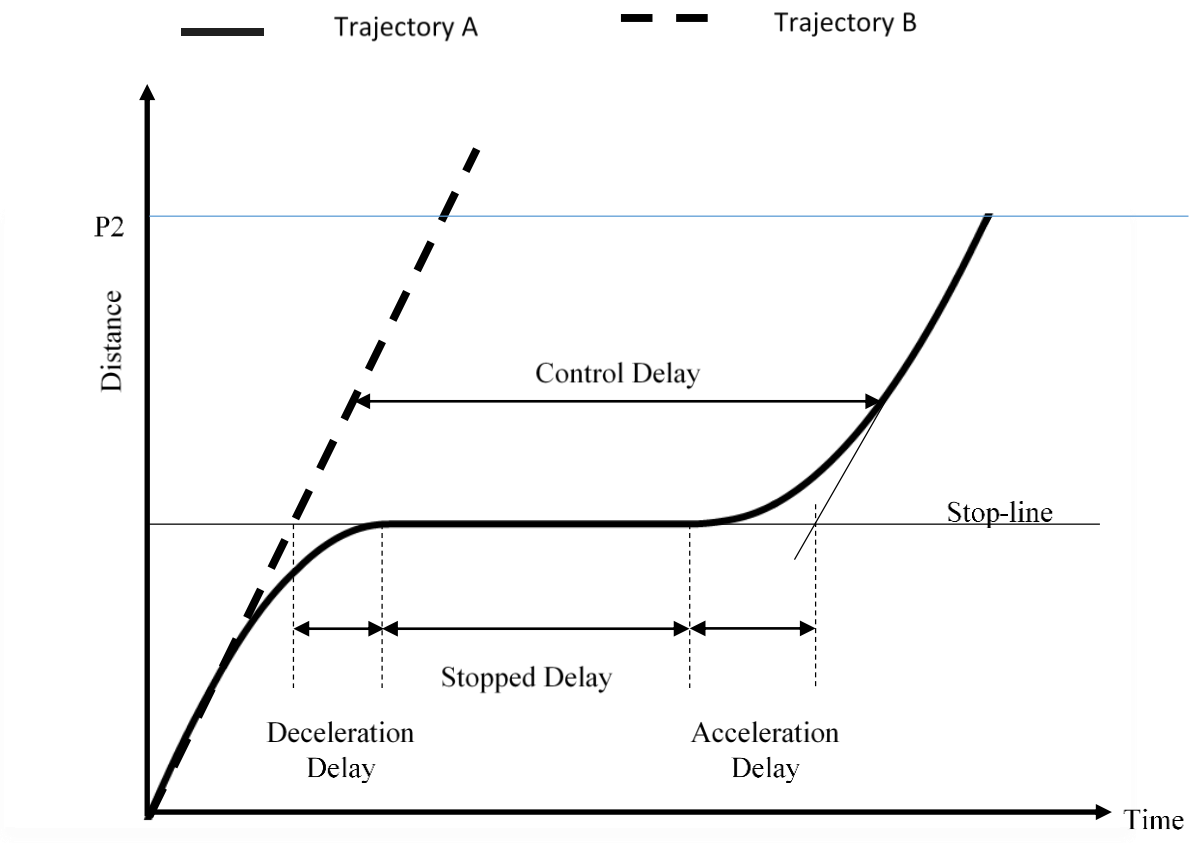

Figure 2-1: Definition of Signal Control Delay Components [Source: Click, 2003]

The HCM provides an analytical model, based on Webster's delay formula, to estimate average control delay for a given lane group, presented in Equation (1) (HCM, 2010). HCM defines lane group as one or more lanes that either (1) exclusively serve one movement, (2) exclusively serve turning movements or (3) each lane share by more than 1 movement (HCM, 2010).

$$d = d_1(PF) + d_2 + d_3 \quad \textbf{(1)}$$

Where, d_1 is uniform delay and represents the delay that is expected to occur when arrivals have uniform time headways; Incremental delay, d_2, accounts for both random fluctuations in arrivals demand and also the predominant over-saturation condition over the analysis period. The initial

queue delay, d_3, estimates the delay incurred due to an initial queue not served during the previous cycle. PF is a progression factor and accounts for the quality of signal coordination. When signals are well coordinated, then vehicles from the upstream intersection arrive at the downstream intersection when the downstream signal is green and therefore PF is close to zero. However, if coordination is very poor, then vehicles from the upstream intersection arrive at the downstream intersection when the downstream signal just turns red and therefore PF is greater than 1. The equations for d_1, d_2, and d_3, as defined by the HCM are provided below:

$$d_1 = \frac{0.5C\left[1-\left(\frac{g}{C}\right)\right]^2}{1-\left[\min(X,1)\left(\frac{g}{C}\right)\right]} \quad \textbf{(2)}$$

$$d_2 = 900T\left[(X-1)+\sqrt{(X-1)^2+\frac{8kIX}{cT}}\right] \quad \textbf{(3)}$$

$$d_3 = \frac{1800Q_b(1+u)T_t}{(cT)} \quad \textbf{(4)}$$

where

C = cycle length, seconds
T = duration of analysis, hours
g = effective green time, seconds
X = Degree of saturation (X = v/c)
c = capacity, vehicle/hour
k = incremental delay factor, unitless
I = upstream filtering factor, unitless
Q_b = Initial queue at the start of period T, vehicles
T_t = duration of unmet demand in period T, hours
u = delay parameter.
v = Volume, veh/hr

The HCM model requires many inputs such as traffic volume, initial queue, signal timings and so on. Obtaining this information is costly and the values change frequently (i.e. for actuated signals the timings change on the basis of traffic conditions; traffic demand changes by time of day, day of week, month of year, etc.) Consequently, at best the HCM method provides an approximate estimate of intersection performance.

In practice, software tools are used to estimate average delay and maximum queue length. Studies such as, Benekohal et al, (2002) and Washburn and Larson (2002), compare the ability of traffic simulation models to estimate the performance measures at the signalized intersections. Mulandi et al (2010) evaluated the performance of signal timing optimizations calculated by Synchro, TRANSYT-7F, CORSIM and VISSIM and found obvious differences in the performance of these simulation and optimization tools. The conclusion of these studies is that different software models may provide very different estimates of the measures of performance of interest for the same set of input conditions. Furthermore, there does not appear to be unanimous agreement among researchers on which model(s) most accurately reflect real-world conditions (Almohanna, 2014). These findings also suggest that direct field observations rather than models may provide the most accurate estimates of the performance measures of interest.

Extensive studies have used direct measurements of delay and queue length from an intersection for performance evaluation instead of HCM procedures. Olszewski (1993), Mousa (2002), Mazloumi et al (2010) traced the trajectories of vehicles between a predefined entrance and exit point to measure average delay. Olszewski used two screen lines and estimated control delay by subtracting the free flow travel time from the observed travel time. Olszewski (1993) noted that stopped delay is easier to measure, however control delay is a better measure for evaluating the signal operation.

Mousa (2002) set up 12 lines at an intersection to measure the average deceleration, acceleration, and stopped delay of the intersection approach. Each line was assigned to one observer, to denote

the time the randomly selected vehicle passed their assigned line. The recorded data was used to trace the trajectory of 182 vehicles.

Mazloumi et al. (2010) deployed two surveyors to each intersections to records the plate number and passing time of the vehicles passing predefined locations. Due to the sheer volume of vehicles traversing the intersections, only vehicles with a specific colour were recorded. The control delay of the vehicles was calculated as the differences between the observed and the free flow travel times. The average delay for the intersection approach was computed as the weighted average of the lane groups based on their traffic volume at 5 minute intervals.

Even though high level of detailed information about different components of delay can be acquired by manual screening of traffic flow, these methods suffer from being labour intensive and time consuming. Furthermore, the measurement errors inherent in these methods are hard to control as they are dependent on the skills and attentiveness of the observers.

Skabardonis and Geroliminis (2005) calculated signal delay by using second by second traffic signal events and vehicle actuation data. This technique requires high resolution traffic volume data and precise signal timings which are not typically available.

Sharma et al. (2007) proposed input-output and hybrid techniques in which the queueing theory is used to estimate the delay and maximum queue length. The method requires loop detectors at both the upstream of the intersection approach and at the stop-line. The upstream detectors are used to track the arrivals at the intersection over time. The stop-line detectors are used to measure the number of departures. These two flow profiles are used to estimate the queue and the delay. These methods have the ability to estimate delay and maximum queue length for each cycle. However, they require upstream and stop line detectors on each approach; infrastructure that is not available in many jurisdictions. Moreover, the phase change information for the traffic signal needs to be readily available. Collecting these data for a wide-area arterial system is often complicated because traffic signals within a network are often operated and maintained by multiple agencies.

Benekohal et al (1992) measured approach delay by using video image processing system. However, this approach relies on the camera's ability to cover the area within which deceleration and acceleration of vehicles occur. In general, video processing technologies such as automated number (license) plate recognition (ANPR) systems are not ideal for network analysis due to the expensive cost of instrumentation. Furthermore, they may be less well suited to areas experiencing adverse environmental conditions such as snow, ice, etc.

Quiroga and Bullock (1999) measured control delay by finding critical points (i.e. when vehicles stopped and started deceleration and acceleration) in GPS data. Similarly, Ko et al. (2008) used GPS data to estimate components of control delay. The speed profile was used to estimate stopped delay and the acceleration profile was utilized to estimate deceleration and acceleration delay. Ko et al. method determines the starting critical points for stopped time interval (t_2 and t_3 in Figure 2-2(a)) and searches backward for a critical point when acceleration is non-negative and searches forward when the acceleration is non-positive. For cases with no stopped time the start of the search is set to the point at which the sign of acceleration changes (t_2 in Figure 2-2(b)). For cases where multiple stops are identified, the stop closer to the downstream intersection is used as the starting point for the search of critical points and the other stops are assumed not to be associated with the signal. However, this assumption results in underestimation of delay during congestion periods.

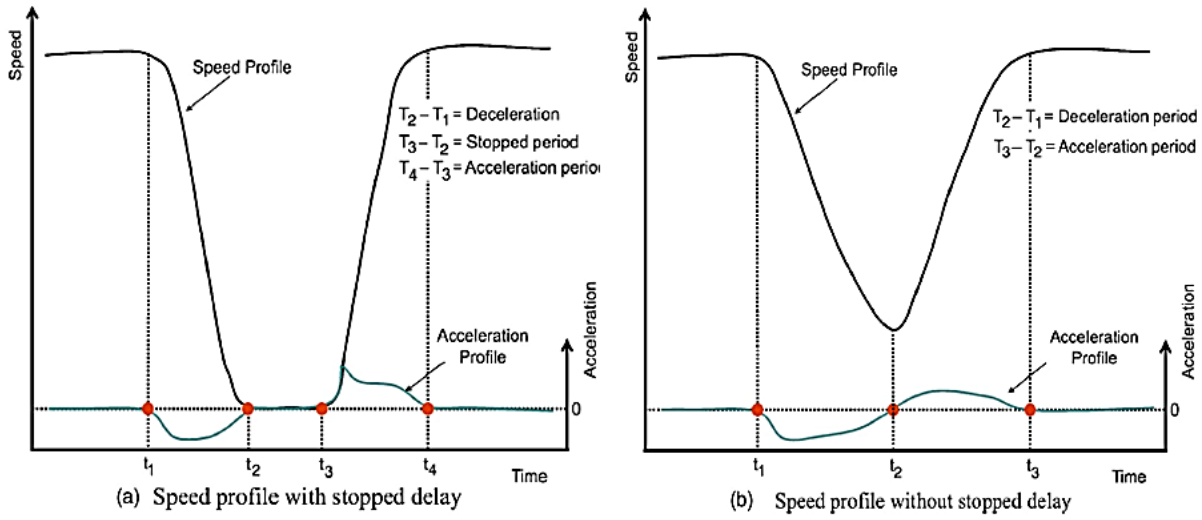

Figure 2-2: Speed and Acceleration Profile Obtained From GPS Data [Source: Ko et al. with Permission from ASCE]

Vehicle re-identification techniques have also been used to obtain intersection delays. Kwong et al. (2008) proposed a scheme in which the individual vehicle signatures are obtained from wireless magnetic sensors placed at the two ends of the segment. The travel time of a vehicle can be obtained by matching the vehicle's signature at two consecutive sensors. The signal phases can be deduced by looking at the start and end of the first vehicle in the queue. Although, this procedure does not require measurements of signal settings, it does require both ends of the intersection to be equipped with magnetic sensors. Although the proposed methodologies provide accurate delay measurements, they tend to be expensive in terms of time and resources. Alternatively, AVL/APC data can be used to evaluate the performance of signalized intersections within a wide-area arterial network in a timely and cost effective manner.

2.2 Applications of AVL/APC Data

In recent years, the deployment of AVL/APC systems on public transit vehicles has provided agencies with a new source of data. AVL/APC systems use GPS sensors (for position, speed, and

heading) and passenger counting sensors, along with transit route and schedule information to (a) track the position of the transit vehicle relative to the scheduled location for real-time command and control at a temporal resolution on the order of every second; and (b) to create an archived database containing records associated with events of interest rather than all of the GPS data.

AVL/APC data provide valuable information to transit agencies and enable them to monitor the quality of service and assist service planning. Furth et al. (2006) outlined the application of AVL/APC data in monitoring schedule adherence using time-point records, passenger crowding analysis and route mapping with stop events. Mandelzys (2010) proposed a method to evaluate transit schedule adherence and identifying causes of poor performance using time-point records.

AVL/APC data have been used by researchers for other applications such as real-time traveler information (Farhan et al., 2002), transit signal priority (Lin, 2002; Liu et at., 2007), transit route performance measurement (Liao and Liu, 2010), and ridership and operational performance analysis (Golani, 2007).

The AVL/APC data can also be used to estimate the performance of signalized intersections. Yang and Hellinga (2012) proposed a method to estimate the stopped delay and maximum queue length at signalized intersections on the basis of archived AVL/APC data. A summary of their methodology is provided in the following section.

2.2.1 Intersection performance evaluation using AVL/APC data in the absence of near-sided Transit Stations

Yang and Hellinga (2012) modelled the formation and dissipation of traffic queues on an approach to a signalized intersection using shockwave theory under the assumption of uniform arrivals and a fixed time signal timing plan. As illustrated in Figure 2-3, consider an intersection operating in an under-saturated condition (i.e. the arrival demand is less than the capacity). During the red interval (r) vehicles arriving at the intersection cannot proceed and must queue

until the signal turns to green. This results in a backward moving formation shockwave which represents the movement of the tail of the queue upstream of the intersection.

During the green interval the vehicles discharge from the queue at the saturation flow rate, resulting in a backward moving recovery shockwave. The location at which the recovery shockwave meets the formation shockwave represents the maximum extent of the queue.

The stopped delay experienced by a vehicle is a function of the time the vehicle arrived at the tail of the queue. The maximum stopped delay, which is experienced by the vehicle that arrives at the stop-line just at the start of the red interval, is equal to the duration of the effective red interval. A vehicle that arrives at the tail of the queue when the queue is almost entirely dissipated experiences minimum stopped delay. Vehicles arriving after this time and before the start of the next red interval will not incur any stopped delay. Therefore, the largest delay is expected to occur for vehicles that stop close to the stop-line and the magnitude of stopped delay decreases linearly as the stop location moves further upstream, until the tail of the queue is reached.

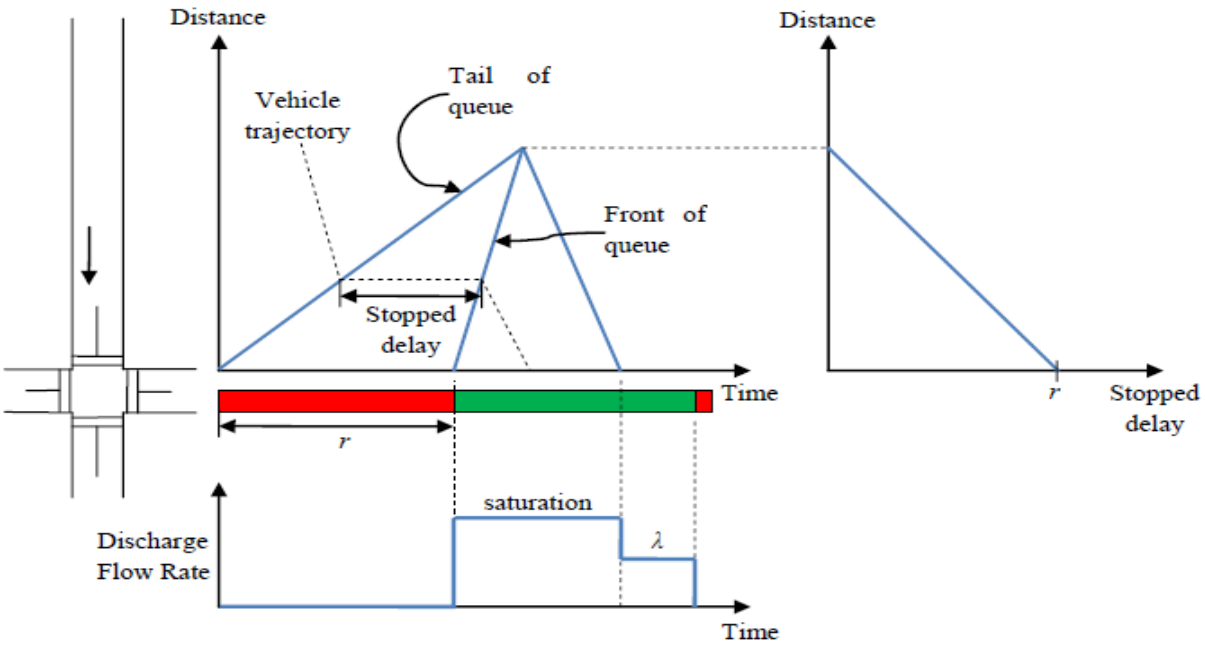

Figure 2-3: Queue Pattern Analysis Using Shockwave Theory for Under-saturated Conditions [Source: Yang, 2012]. Where r Represents Red interval and λ is the Vehicle Arrival Rate.

The magnitude of average stopped delay and maximum queue length experienced at a signalized intersection is a function of both the red interval duration and the volume to capacity ratio (v/c). If the red interval increases, vehicles will incur longer stopped delay and the maximum queue will reach further upstream. Similarly, if the v/c ratio increases the maximum queue length moves upstream and hence more vehicles are queued at the intersection waiting for the green interval.

When the approach is oversaturated, demand exceeds capacity, and the queue that forms during the red interval cannot be completely discharged during the same cycle. These vehicles remain un-served and form an initial queue at the start of the red interval of the next cycle. This results in the formation of a fourth shockwave with the same slope as the former recovery shockwave,

as illustrated in Figure 2-4. The stopped delay experienced by the vehicles within the queue is close to the red interval. The maximum queue length of the second cycle will be longer then the first cycle. The queue would theoretically grow to infinity until the demand subsides or supply increases. One can see that when the approach is over-saturated the queue patterns change from cycle to cycle.

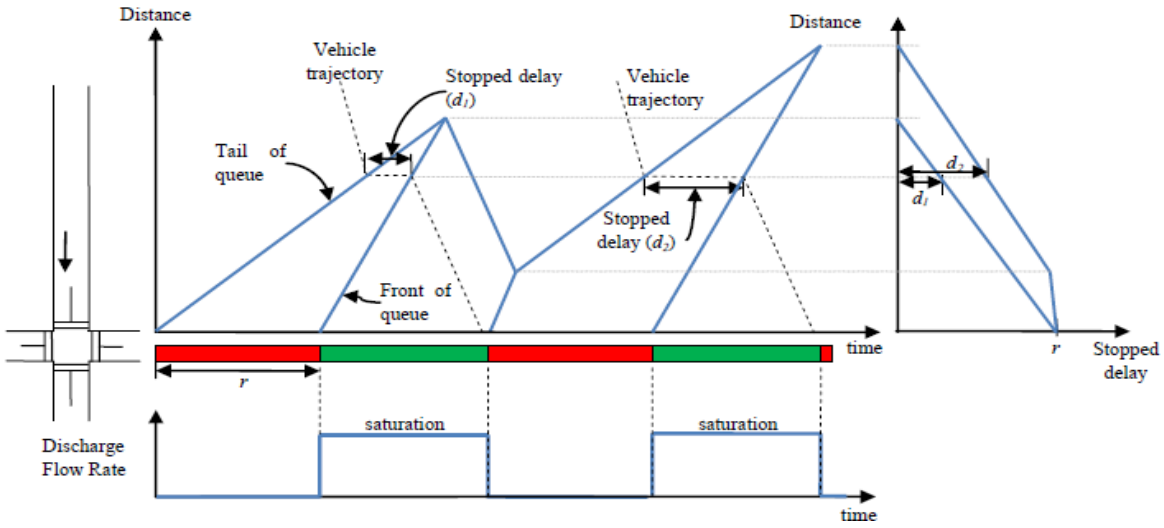

Figure 2-4: Queue Pattern Analysis using Shockwave Theory for Over-saturated Conditions [Source: Yang, 2012]

If the study period is selected such that the traffic demand and signal timings remain relatively constant during the analysis, then the queue formation and dissipation over the different cycles should maintain a relatively constant pattern.

Furthermore, if no transit station exists on the approach, then a transit vehicle can be expected to be impacted by the queue formation and dissipation in almost the same way as other motorized vehicles on the approach. Thus, the stopped delays experienced by transit vehicles and captured within the AVL/APC data, can be considered to be an unbiased sample of the stopped delays experienced by the population of vehicles traversing the approach.

On the basis of this assumption, Yang and Hellinga (2012) proposed a method in which the AVL/APC *unscheduled stops* are used to determine the delay and queue length. The method consists of the following four steps which are applied to each direction of each bus route:

1. Define route segments within GIS software. A segment is defined as the link between two consecutive signalized intersections.
2. Using GIS software, identify all of the *unscheduled* stop observations associated with each route segment, and compute the distance from the location of the stopped delay observation to the downstream signalized intersection.
3. Plot stopped delay versus distance for each route segment and fit a boundary line (BL) to the *unscheduled* stop observations. The BL separates the stop events associated with the signalized intersection from other causes of unscheduled stops such as parking maneuvers or other geometric characteristics.
4. The observations under the BL are deemed as stops caused by the traffic signal operation and are used to estimate the performance measures such as average stopped delay and maximum queue length for a particular intersection approach.

The selection of the optimal BL from a set of candidate BLs is based on the expectation that the cumulative number of observations due to the signalized intersection will increase relatively quickly as a function of distance from the stop-line until the maximum queue is reached (Figure 2-5A). The transit vehicles are expected to stop less frequently beyond the tail of the queue. If the segment contains other geometric or traffic control features upstream of the stop-line, the cumulative number of observations is expected to increase quickly as a function of distance from such features as depicted in Figure 2-5B.

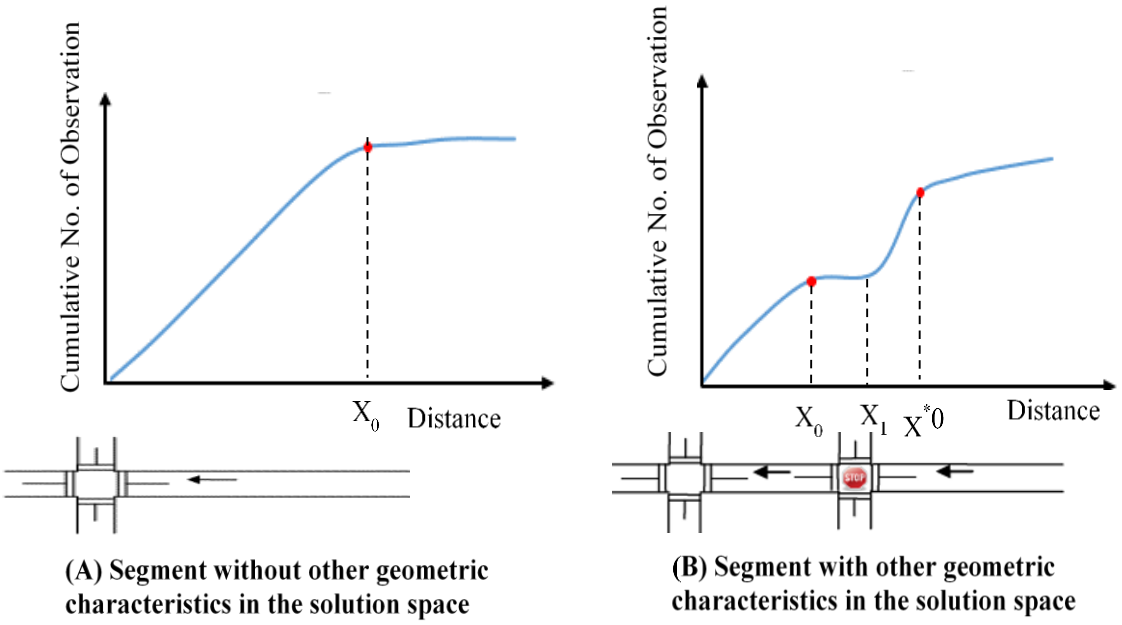

Figure 2-5: Distribution of Cumulative Number of Stopped Delay Observations as a Function of Intermediate Traffic Control Devices

The process to determine the optimal BL is described below and illustrated in Figure 2-6. First, a solution space is defined within which the delay envelope resides. The solution space is defined by setting upper bound limits for the X and Y-axis. The upper bound limit on the X-axis is defined by the farthest upstream observations within the segment, $\boldsymbol{X_{p2}}$. The upper bound limit for the Y-axis is defined by maximum delay, $\boldsymbol{d_{max}}$, which is calculated as the 99th percentile of the stopped delay observations located within 50 meters of the stop-line. The delay defined by the boundary line follows a piece-wise linear function:

$$d = \begin{cases} d_{\max} & 0 \le x \le X_{p1} \\ d_{\max} + bx & X_{p1} < x < X_{p2} \end{cases} \quad (b < 0) \qquad \textbf{(5)}$$

Where, *d* and *x* are delay and distance to the stop line, respectively. The variable X_{P1} defines whether the intersection operates at under-saturated or over-saturated conditions. If X_{P1} is zero the intersection is under-saturated and if X_{P1} is greater than zero then the intersection is oversaturated.

A series of candidate boundary lines are defined and evaluated with each line connecting a feasible pair of X_{p1} and X_{p2} within the solution space. For each candidate boundary line, the density of stopped delay event (*DS*) is defined as the cumulative number of stopped delay observations (*Ns*) divided by the area (A) defined by the delay envelope boundary line (i.e. DS = N_s/A). The candidate boundary line with the smallest change in density with respect to the other candidate boundary lines, is selected as the optimal BL and the value of $\boldsymbol{X_o}$ represents the estimate of the maximum extent of the queue.

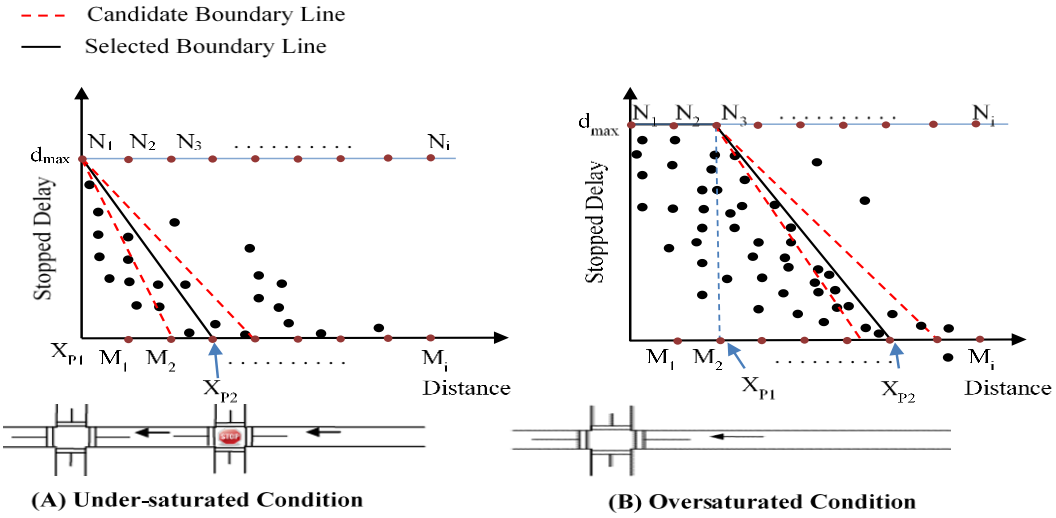

Figure 2-6: Candidate Boundary Line Selection

This methodology assumes that the relationship between stopped delay and location is linear. However, in reality variations in traffic composition, driving behaviour, arrival rate, signal timing and discrepancies in AVL/APC system's determination of stop events influence the

linearity of this relationship. These variations challenge the accuracy of the boundary line algorithm proposed by Yang and Hellinga (2012). The selection of the BL needs to be robust to capture the variability in traffic. There are 3 main issues associated with the boundary line selection process proposed by Yang and Hellinga (2012). In the following sections we illustrate these issues using AVL/APC data from the bus routes in the Region of Waterloo under operation of Grand River Transit (GRT). Data from the months of September to November, 2013 are used. The data include only the PM peak (4:30 PM – 6:00 PM) weekday non-holiday days.

1. The first issue lies with the setup of the problem within ArcGIS and is illustrated in Figure 2-7. As mentioned previously the road network is divided into route segments bounded by an upstream (indicated by point A in the figure) and a dowsntream (point B) signalized intersection. These segments are represented as a polyline within the ArcGIS framework. Yang (2012) created a spatial buffer zone around the polyline route segment to identify the stopped delay observations associated with the route segment and to measure the distance of the observation within the buffer zone to the downstream intersection. However, for some segments, the unscheduled stop observations from the adjacent road segments are captured by the buffer zone (i.e. the points shown within the red circle in Figure 2-7 are captured as stop observations on Ottawa street, where infact they are vehicles stopping on Alpins road because of the signal control at Ottawa and Alpine intersection). These observations should not be associated with the segment of interest.

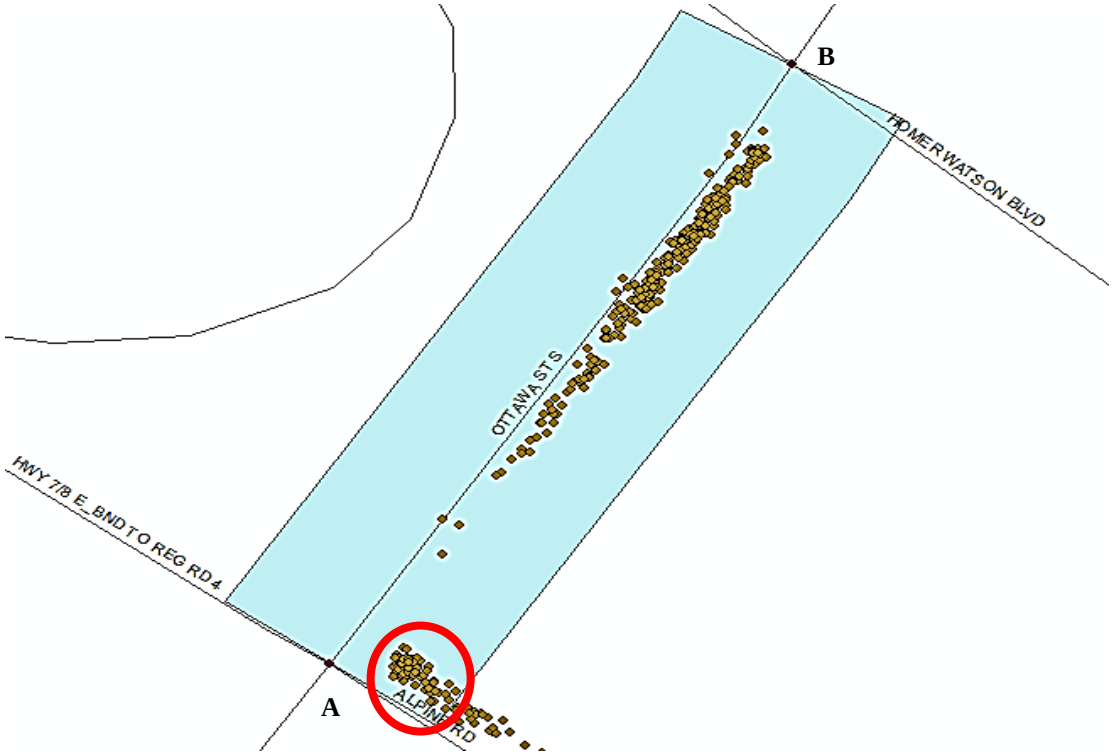

Figure 2-7: Invalid Stopped Delay Observations Captured by the Buffer Zone in the ArcGIS

2. The second issue is regarding the data points captured by the boundary line that are caused by other geometric characteristics or traffic controls. Figure 2-8 is an example of such a case. The downstream intersection is University Avenue at Hazel, represented by point A, and the upstream intersection, point B, is at the Wilfrid Laurier University pedestrian crossing signal. There is a parking lot entrance 75 meters from the stop line. It is suspected that the stopped delay observations in the oval (in Figure 2-8B) are not caused by the traffic signal due to the lack of observations between 35 and 80 meters from the stop line. It would be reasonable to speculate that the buses may be stopping in response to vehicles entering or existing the parking lot. However, there may be other explanations but no other influencing causes were observed from the data and the geometry of the segment. If these observations are not due to the signal operation they must be removed from the analysis.

3. Lastly, the distance of the observations are measured from the center of the intersections and not the stop line associated with an approach. This caused the overestimation of the maximum queue length estimation.

The method proposed by Yang and Hellinga (2012) is restricted to signalized intersection approaches which do not contain a near-sided transit station. To this end, this study seeks to build upon the previous work and proposes a method which can be applied to signalized intersection approaches that contain a near-sided transit station. The efforts will also endeavour to improve the method used to select the boundary line to field data in order to address the aforementioned deficiencies.

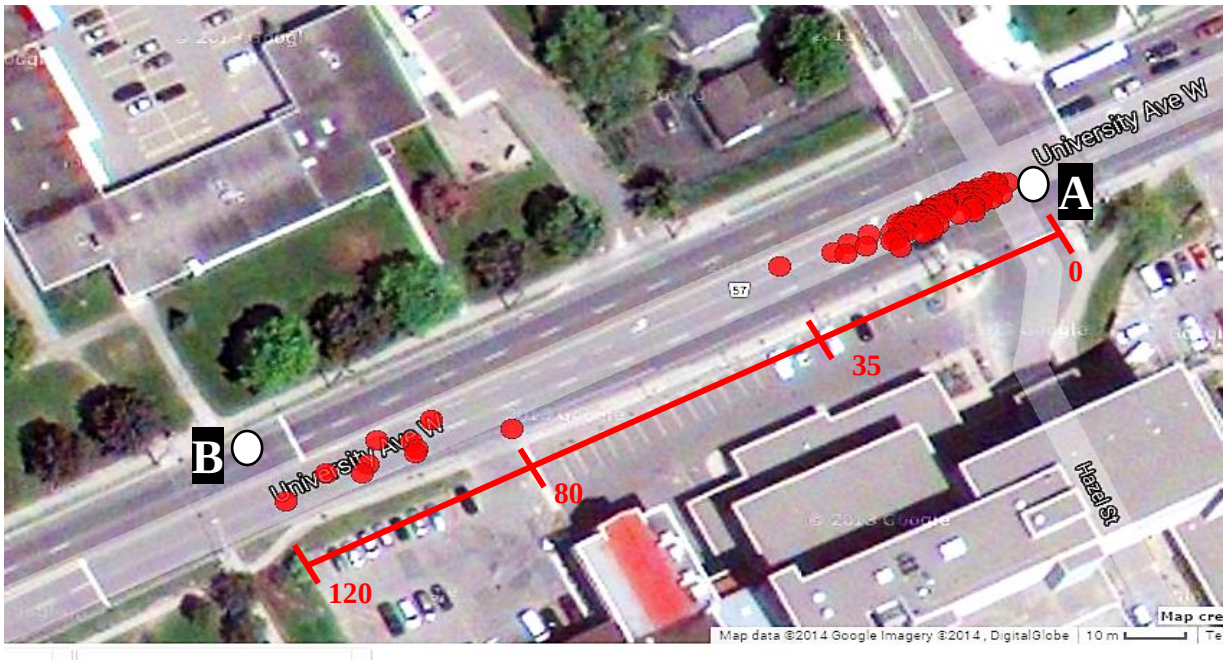

(A) The Unscheduled Stop Observations Superimposed on Google Maps

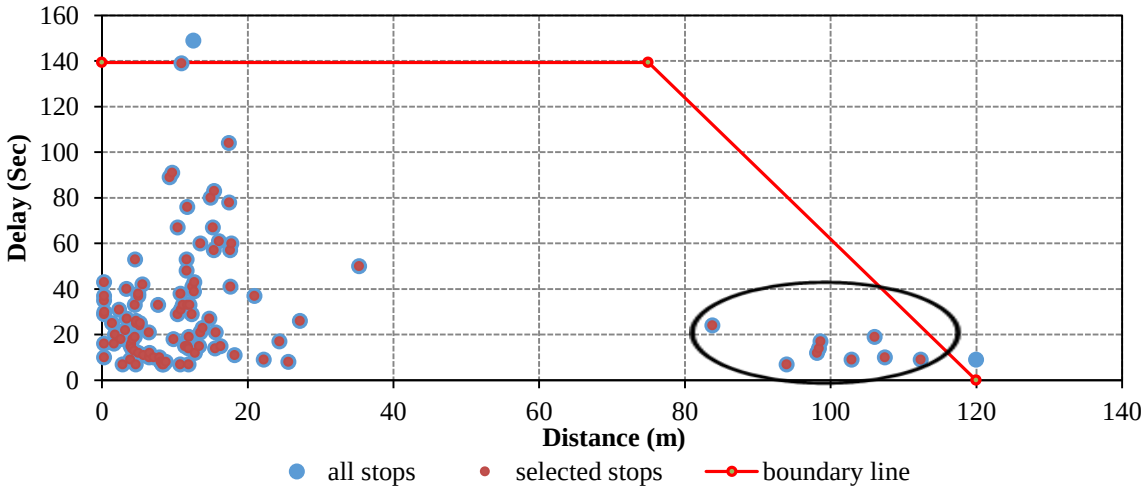

(B) Delay vs. Distance Plot Showing the Error in BL Calibration

Figure 2-8: Boundary Line Calibrated to Stop Observations of University at Hazel Intersection

Chapter 3
Field Data

The models described and calibrated in the next chapter make use of field data collected from Grand River Transit (GRT), the public agency providing public transit within the Region of Waterloo located in southwestern Ontario, Canada. At the time of this study, GRT operated 66 bus routes within the region and serviced approximately 21 million trips annually. GRT has 2724 transit stations, 1328 of which are considered to be near-sided stops (i.e. located just upstream of a signalized intersection). The agency has a fleet of 240 buses all of which are equipped with AVL systems and APC data is collected by 90% of the fleet (GRT, 2011).

The GRT bus routes traverse 435 signalized intersections. Only 44 signalized intersections within the Region's road network are not traversed by at least one bus route and therefore no data are available in the AVL/APC database for these intersections. The majority of these 44 signalized intersections are located in the outskirts of the Region of Waterloo, as shown in Figure 3-1.

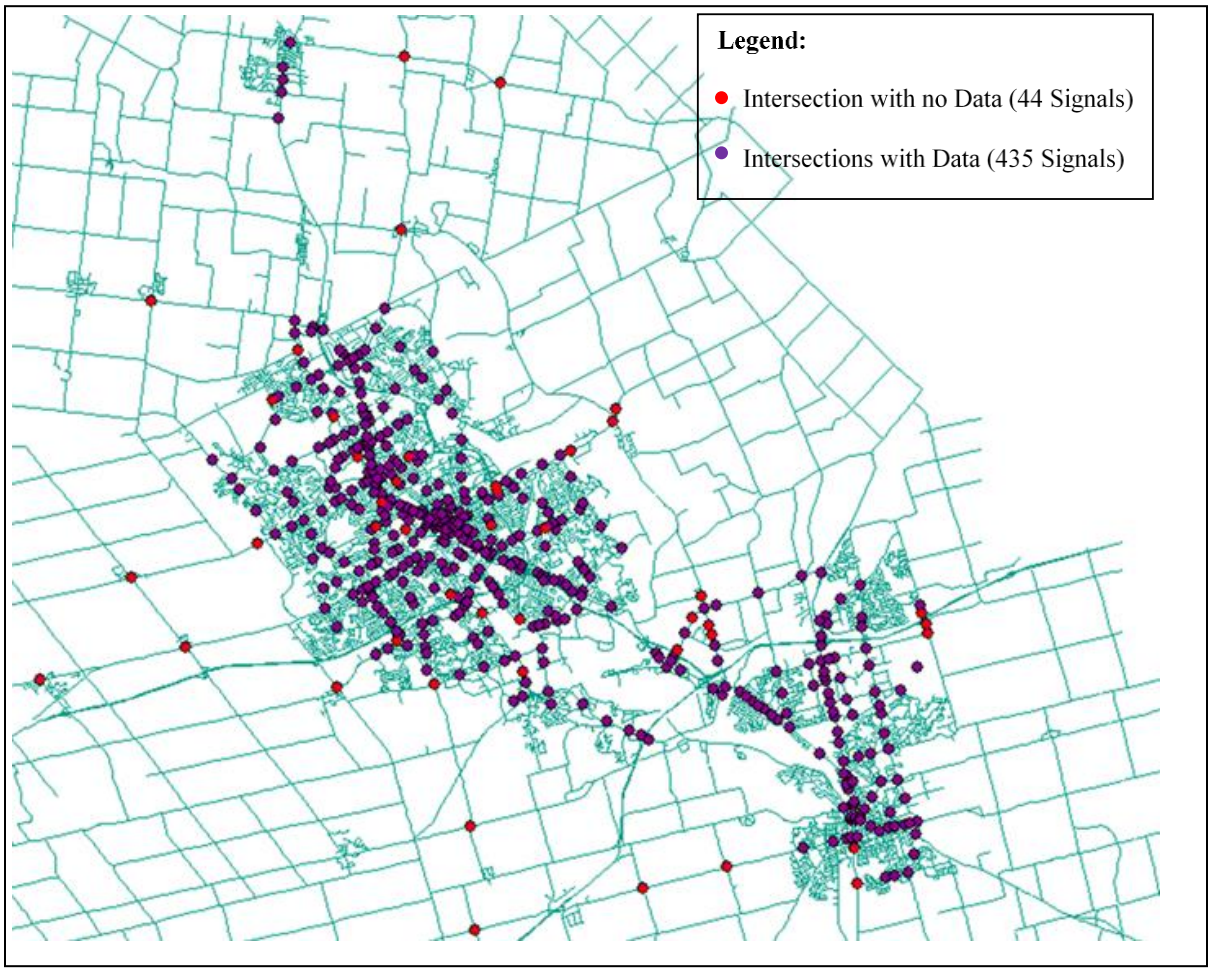

Figure 3-1: The Intersections with Automatic Vehicle Location /Automatic Passenger Count Data Available

The AVL/APC database contains event-based records meaning that records are generated and recorded in the database for a specified set of events rather than at a constant time interval (e.g. every 5 seconds). The database contains both trip-level and stop-level records. The structure and field description of trip-level records and stop-level records are presented in Figure 3-2 and Figure 3-3, respectively.

Fields	Type	Description
id	Number	Index (Primary Key)
course_id	Number	Reference to the course (Foreign Key for report_course_start.id)
op_day	Date	Operation date
line_no	Number	Line number (transit route number)
route_no	Number	Route number
course_no	Number	Course number
run_no	Number	Block index
vehicle_no	Number	Vehicle number
act_start_time	Number	Actual start time
act_start_time_hhmmss	String	Actual start time (as string)
actual_end_time	Number	Actual start time at the final recorded stop of trip (seconds past midnight)
actual_end_time_hhmmss	String	Actual start time at the final recorded stop of trip (as string)
sched_start_time	Number	Scheduled start time (seconds past midnight)
sched_start_time_hhmmss	String	Scheduled start time (as string)
sched_end_time	Number	Scheduled start time at the final recorded stop of trip (seconds past midnight)
sched_end_time_hhmmss	String	Scheduled start time at the final recorded stop of trip (as string)
route_direction	String	Route direction – no validation check
trip_no	Number	Trip number – no validation check
trip_id	Number	Reference to the ID in report_definition_trip
trip_type	Number	Trip type – no validation check 0 = Service Journey 1 = Unspecified Dead Run 2 = Outgoing Dead Run 3 = Interlink (Dead Run) 4 = Incoming Dead Run
destination_no	Number	Destination number – not utilized
destination_name	String	Destination name – not utilized
stopsequence	String	Stop sequence (lists the stop numbers on the trip)
odometer	Number	Odometer (m)
passenger_data	Number	Status of passenger counters 1 = At least one observation recorded
quality	Number	Percentage of scheduled stops versus actual stops recorded
pattern_completeness	Number	Same as quality field
data_source	Number	Code indicating data source

Figure 3-2: Description of Fields Within Trip-level Records [Source: Mandelzys, 2011]

Fields	Type	Description
id	Number	Index (Primary Key)
trip_id	Number	Reference to the trip (Foreign Key for report_trip_start.id)
op_day	Date	Operation day
vehicle_no	Number	Vehicle number
stop_no	Number	Stop number
stop_lname	String	Stop long name
stop_sname	String	Stop short name
stop_pos	Number	Stop position (i.e. nearside, farside, etc.) – not utilized
stop_type	Number	Stop type 0 = Stop with schedule time 2 = Stop with doors 3 = Stop without doors 4 = Drive through with schedule time 5 = Stop without schedule time 6 = Drive through without schedule time
prev_sched_stop_id	Number	Reference to the id of the previous record
stop_idx	Number	Index of stop on the pattern (report_definition_route)
sched_arr_time	Number	Scheduled arrival time (seconds past midnight)
sched_arr_time_hhmmss	String	Scheduled arrival time (as string)
sched_dep_time	Number	Scheduled departure time (seconds past midnight)
sched_dep_time_hhmmss	String	Scheduled departure time (as string)
act_arr_time	Number	Actual arrival time (seconds past midnight)
act_arr_time_hhmmss	String	Actual arrival time (as string)
act_dep_time	Number	Actual departure time (seconds past midnight)
act_dep_time_hhmmss	String	Actual departure time (as string)
odometer	Number	Odometer (m)
boarding	Number	Number of passengers boarding
alighting	Number	Number of passengers alighting
load	Number	Load (number of passengers)
e_boarding	Number	Boardings from extra stops
e_alighting	Number	Alightings from extra stops
e_load	Number	Load from extra stops
longitude	Number	Longitude GPS (WGS 84)
latitude	Number	Latitude GPS (WGS 84)
positioning_method	Number	Positioning method of the vehicle 0 = Real position 1 = Plan position

Figure 3-3: Description of Fields Within Stop-level Records [Source: Mandelzys, 2011]

The required data for the proposed analysis is queried from these trip and stop level records. The AVL/APC data for the PM peak (4:30 PM to 6 PM) non-holiday weekdays from September to November 2013 were extracted from the GRT database. For each in-service route and direction the following information is obtained from stop-level records:

- Stop_type
- Act_arr_time
- Act_dep_time
- Boarding
- Alighting
- Longitude
- Latitude

The queried AVL/APC data is exported into geographic information system (GIS) software as a point layer. The stop location of each observation is determined by its longitude and latitude coordinates. The geographic data of transit routes and signalized intersections are also exported into GIS in the form of layers. For each route and direction, the transit route layers are segments such that each segment is enclosed by two signalized intersections. A polygon buffer zone is created around the segment. The stop observations that fall within the buffer zone are selected. In order to prevent stop observations from adjacent road segments being captured by the polygon buffer zone, a circular buffer of 30m radius is created at the upstream intersection. In this methodology the stop observations contained within the overlapping area of the two buffer zones are excluded from the analysis, as illustrated in Figure 3-4.

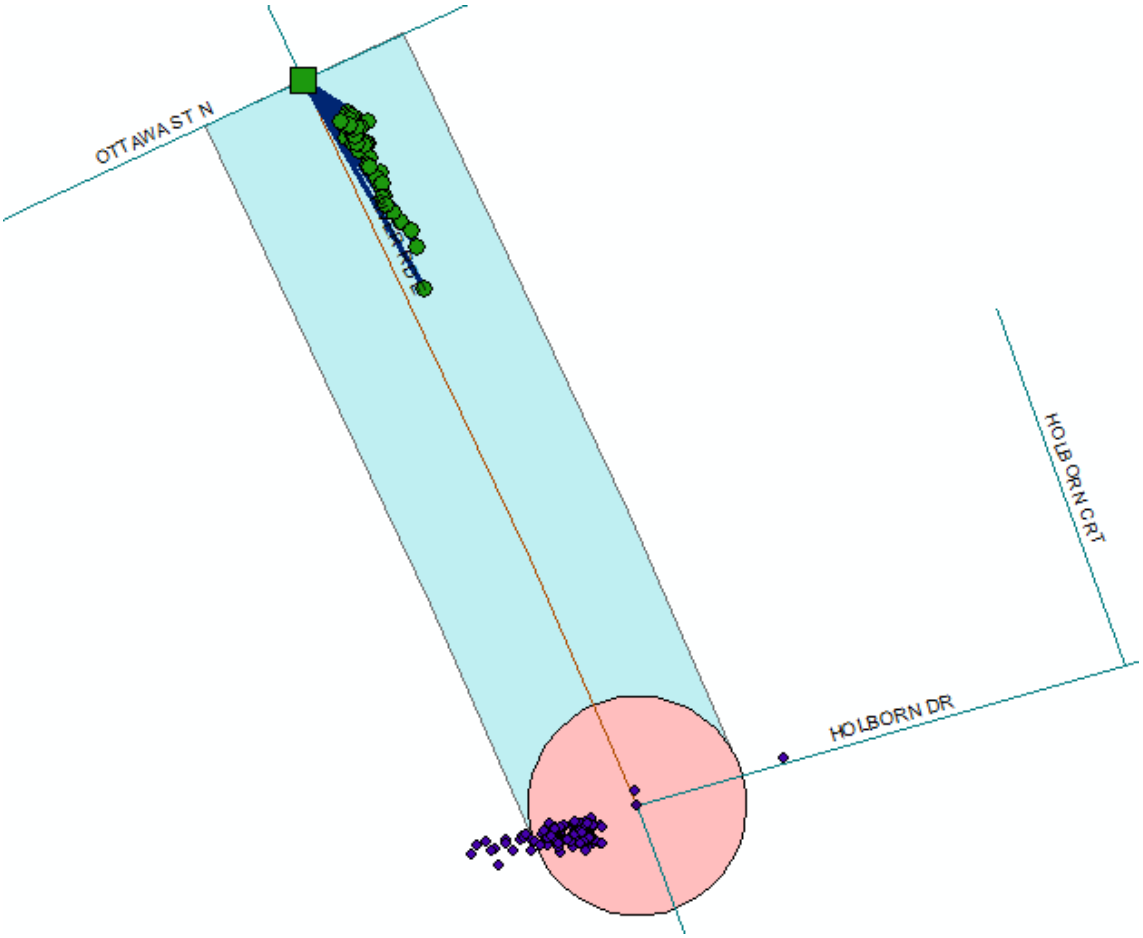

Figure 3-4: Example of a Segment Processed in GIS

The distance between the downstream intersection and the selected stop observations is measured using the network analyst tool in ArcGIS. The magnitude of stop delay (*D*) for *unscheduled stop* observations, defined as the *stop_type 3*, is calculated as the difference between *Act_dep_time* and *Act_arr_time*. For *scheduled stop* observations, defined by *stop_type 0* or *5*, the difference between *Act_dep_time* and *Act_arr_time* represents the total stop time (*TS*) of the bus.

In Figure 3-4, the green circles represent the stop observations selected for analysis, for this given segment. The blue lines represent the distance between the downstream stop line and the stop observation.

This process is carried out for all segments on all routes and directions and the resulting set of data was used throughout the remainder of this thesis.

Within the study period approximately 14,227 trips have taken place from which there are approximately 141,600 unscheduled and 44,400 scheduled stop observations available. The frequency distribution of the total stop time for all unscheduled stops and all scheduled stops is provided in Figure 3-5 and Figure 3-6, respectively. The frequency distribution of the boarding and alighting passengers for all the scheduled stop observations is provided in Figure 3-7 and Figure 3-8, respectively.

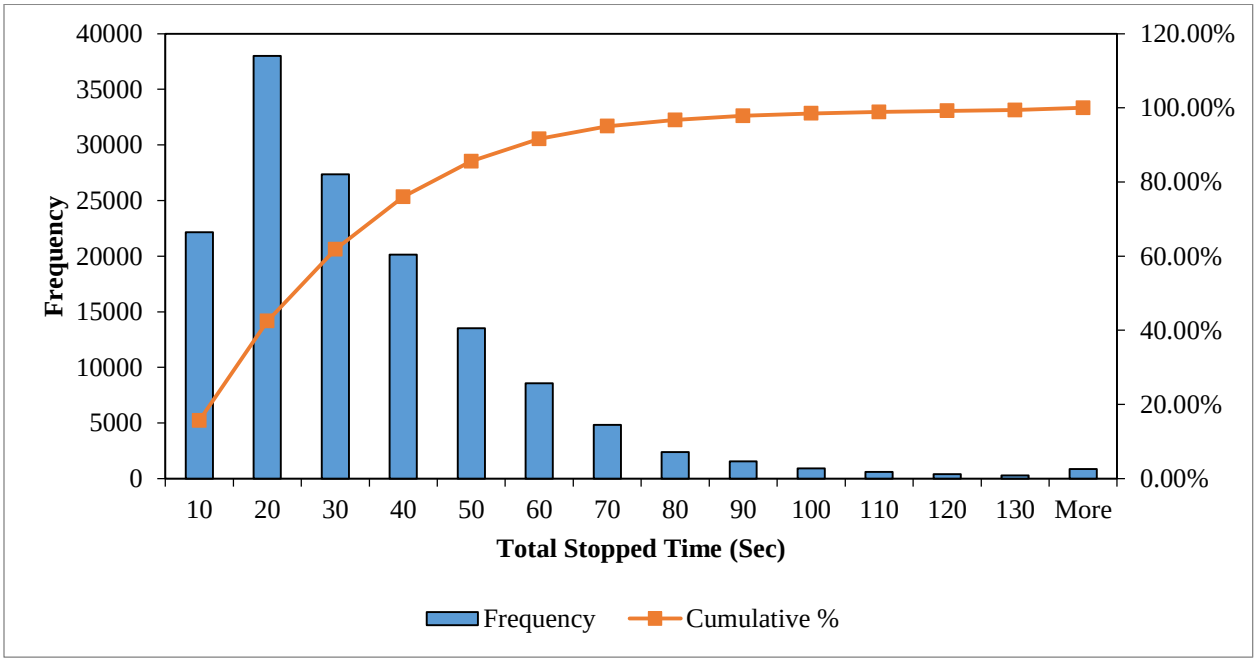

Figure 3-5: Frequency Distribution of Total Stop Time of Unscheduled Stop Observations

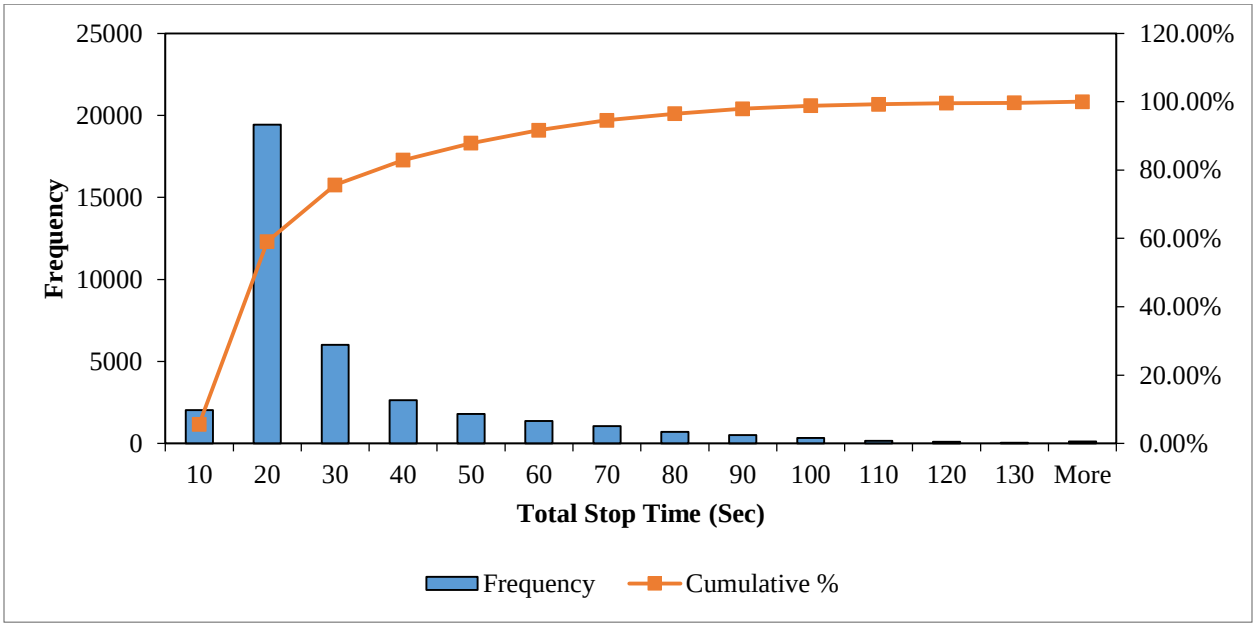

Figure 3-6: Frequency Distribution of Total Stop Time of Scheduled Stop Observations

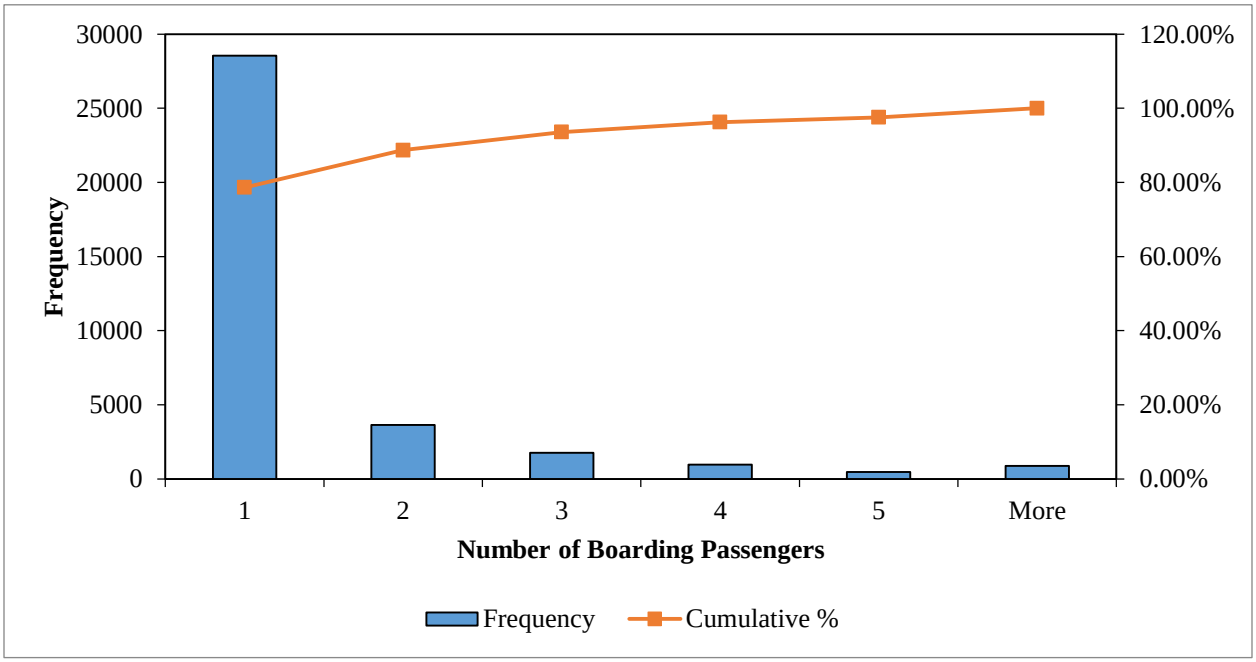

Figure 3-7: Frequency Distribution of the Number of Boarding Passengers

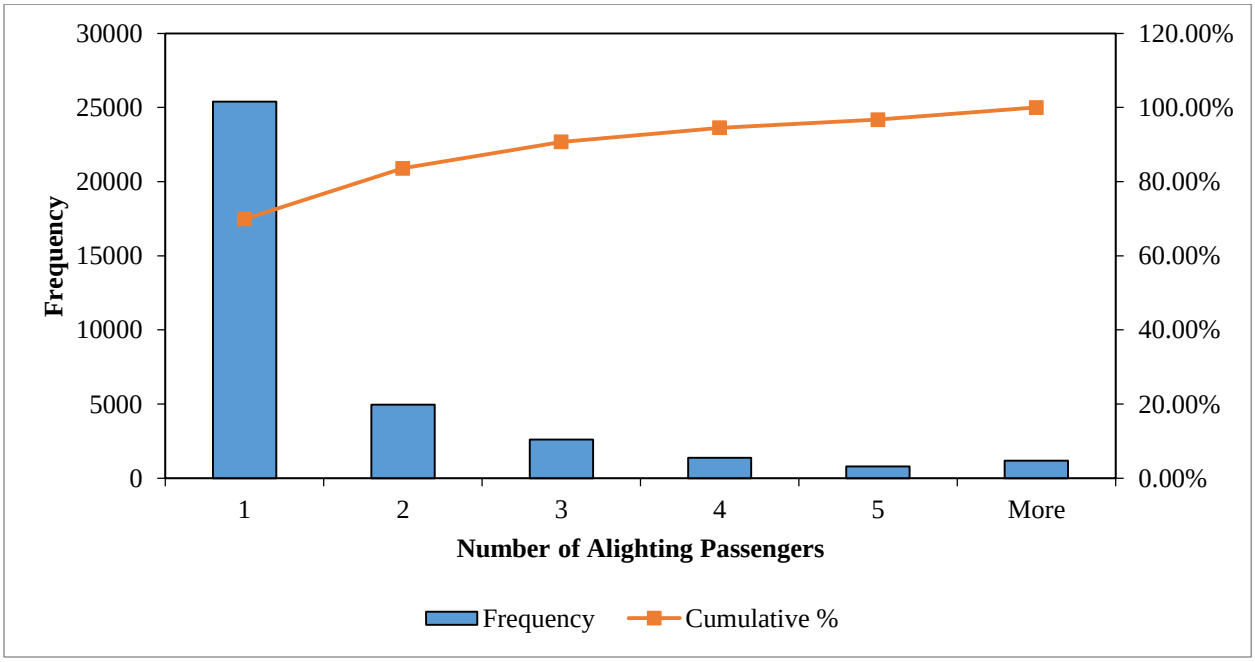

Figure 3-8: Frequency Distribution of the Number of Alighting Passengers

GRT defines a near-sided transit station as the station which is located immediately before the intersection's stop line. Similarly, a far-sided transit station is located immediately after the signalized intersection. Here, near-sided stations are assumed to be located within 40 meters of the downstream stop-line.

The area within which the bus is allowed to stop and permit passenger activity is named the service zone of the transit station. GRT defines the service zone as 10 meters before and 5 meters after the assumed location of the transit station, plus a 6% buffer that is proportional to the difference in distance between the two consecutive transit stations. For example, if the distance between the current and previous stop is 100 meters, then the distance before the stop would be increased by 6 to 16 meters, and the distance after the stop would be increased by 6 to 11 meters. Therefore, anytime the doors open in this 27 meters window the system would recognize that the bus has stopped at the transit station. All the stops that occur within the service zone are deemed as *scheduled stops* (i.e. stop-type 0 and 5). The next chapter describes the proposed method.

Chapter 4
Methodology

The proposed methodology utilizes archived AVL/APC data to evaluate the performance of signalized intersections with near-sided transit stations. For intersections with near-sided transit stations, the interaction between the transit vehicle and the station must be distinguished from the transit vehicle's interaction with the traffic signal. The general framework of the methodology is presented in Figure 4-1.

As described in the previous chapter, the AVL/APC data consists of scheduled stop observations and unscheduled stop observations. No special treatment is required for the unscheduled stop observations because the recorded total stop time (*TS*) is all stopped delay. However, for scheduled stop observations a portion of the total stop time may be attributed to time required for the transit vehicle to board and discharge passengers. Thus, there is a need to treat these observations in order to estimate the stopped delay attributable to the traffic signal. The remainder of this chapter describes the methods for doing this treatment.

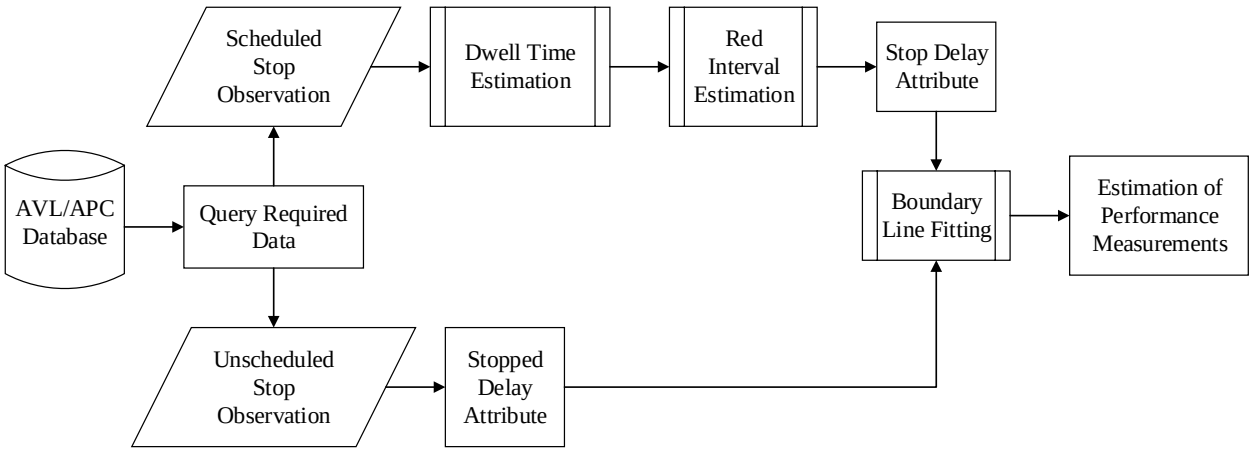

Figure 4-1: Flowchart of Proposed Methodology

4.1 Defining Scenarios

A transit vehicle stopping at a transit station to board and/or discharge passengers generates a *Scheduled Stop* record in the archived AVL/APC data. The length of time for which the transit vehicle is stationary is recorded and is designated as *TS*. The time required to board and discharge passengers is designated as the dwell time (*DW*). Dwell time (*DW*) may comprise all or just a portion of the total stopped time (i.e. $TS \geq DW$). Our objective is to utilize transit vehicles as probe vehicles in order to estimate the stopped delay (*D)* experienced by general purpose vehicles at the intersection.

The transit vehicle's interactions with the transit station and the signal can be categorised into three scenarios as illustrated in Figure 4-2**.**

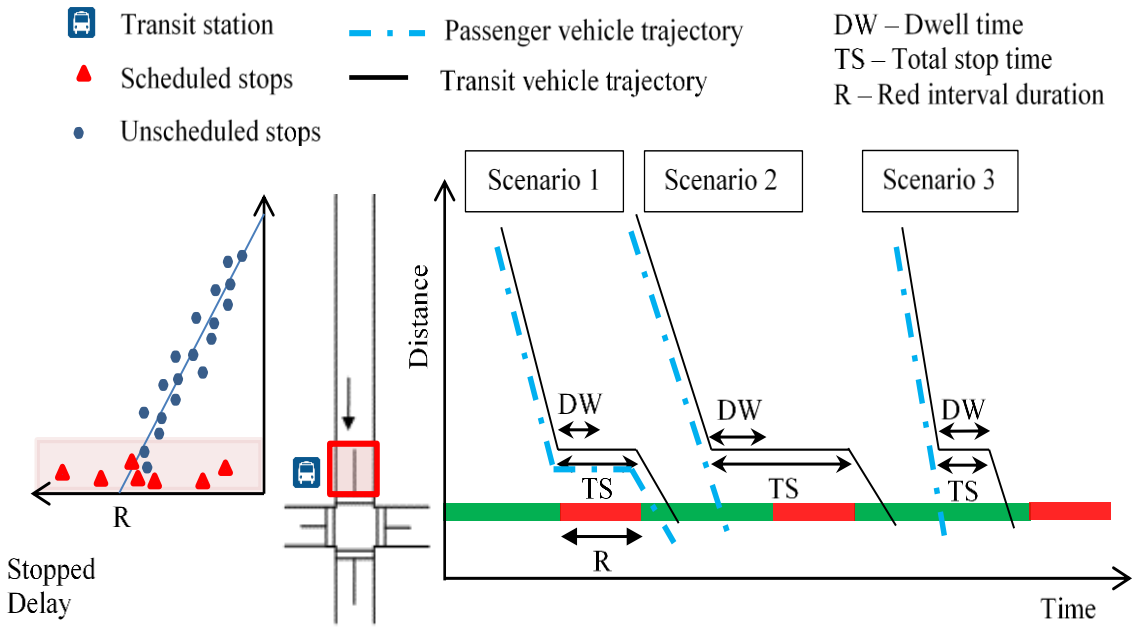

Figure 4-2: Presentation of Delay Estimation Scenarios Using Space Time Diagram

1. In the first scenario, the bus arrives at the transit station during the red interval. The bus serves passengers at the transit station and then waits until the red interval ends before

proceeding. In this case, the delay that would have been experienced by a general purpose vehicle arriving at the intersection at the same time as the transit vehicle is approximately[2] equal to the transit vehicle's total stopped time ($D = TS$), which is less than or equal to the red interval, R ($DW < TS \leq R$).

2. In the second scenario, the traffic signal is green when the bus approaches the transit station. While the passengers are boarding and alighting, the traffic signal turns red and the bus must wait until the signal turns green to clear the intersection. It is noted that in order for the transit vehicle to arrive at the transit station, any unserved queue on the approach must not extend upstream of the transit station and because the transit station is located close to the stop line, any such queue would be small. Therefore, we expect that a general purpose vehicle arriving at the transit station at the same time as the transit vehicle would have been able to travel through the intersection during the green interval and would not have experienced any stop delay ($D = 0$). In this scenario the stop time of the bus is greater than the dwell time and greater than the red interval ($TS > R$ and $TS > DW$).
3. In the third scenario, the bus arrives at the intersection during the green interval, serves passengers at the transit station, and passes through the intersection before the end of the green interval. In this scenario a general purpose vehicle arriving at the same time as the bus would have been able to travel through the intersection during the green interval and would not have experienced any stopped delay ($D = 0$). The duration for which the bus is stationary is equal to the dwell time ($TS = DW$).

Given the total stop time (TS), dwell time (DW), and the red interval (R), each stopped delay observation can be classified as one of the above scenarios and its corresponding delay can be estimated as:

$$D = \begin{Bmatrix} TS & DW < TS \leq R \\ 0 & TS > R \\ 0 & TS = DW \end{Bmatrix} \quad \textbf{(6)}$$

[2] We state approximately because it is possible that a general purpose vehicle may have been able to stop slightly closer to the stop line than the transit vehicle and therefore depart slightly earlier; however, because the transit station is located near to the stop line we assume this error in delay is small compared to TS.

However, from AVL/APC data only the total stop time (*TS*) of the bus is explicitly known. In the following sections, models are presented to estimate the dwell time (*DW*) and the red interval (*R*) using AVL/APC data.

4.2 Dwell Time

The Highway Capacity Manual (2010) defines dwell time as the amount of time the transit vehicle is stationary at the station to serve passengers. It is the summation of time required to open and close the doors plus the time needed to serve passengers at the busiest door (TCQSM, 2013). The factors that affect dwell times are:

1. Passenger demand
2. Transit stations spacing
3. Method of payment
4. Vehicle type (i.e. low floor bus)
5. Distribution of passengers on transit vehicle
6. Wheelchair and bicycle boarding

Section 4.2.1 presents a short summary of previous work on transit dwell time followed by the description of the proposed dwell time estimation model in Section 4.2.2.

4.2.1 Existing Dwell Time estimations Models

The Transit Capacity and Quality of Service Manual (TCQSM) estimates average dwell time based on a linear relationship between passenger activity and their corresponding service time, the lost time due to opening/closing doors and any boarding lost time as shown in equation (7), when hourly passenger boarding and alighting counts are available for a given stop (TCQSM, 2013). The passenger flow time (the time required for all passengers to board and alight the door of their choice) for each bus door is calculated using Equation (8). In absence of local data, the average passenger serving times specified in Table 4-1 can be used.

$$t_d = t_{pf,\max} + t_{oc} + t_{bl} \quad \textbf{(7)}$$

$$t_{pf,i} = P_{a,i} t_{a,i} + P_{b,i} t_{b,i} \quad \textbf{(8)}$$

where

t_d = Average dwell time, seconds
$t_{pf,max}$ = Maximum passenger flow time of all door channels, seconds
t_{oc} = Door opening and closing time, seconds (typically 2-5 seconds)
t_{bl} = Boarding lost time, seconds (time spent waiting for passengers to walk to bus doors from their waiting position at the stop. For stops with 1 loading area[3] t_{bl} is 0, for stops with 3 loading areas t_{bl} is 2.5-9 seconds)
$t_{pf,i}$ = Passenger flow time for door channel *i*, seconds
$P_{a,i}$ = Number of alighting passengers through door channel *i*, persons
$P_{b,i}$ = Number of boarding passengers through door channel *i*, persons
$t_{a,i}$ = Average alighting passenger service time for door channel *i*, second/person
$t_{b,i}$ = Average boarding passenger service time for door channel *i*, second/person

[3] Loading area is defined as curbside space where a single bus can stop and allow passengers to board and alight the vehicle. Bus stops may have one or more loading areas.

Table 4-1: Service Times for Individual Passenger (Source: TCQSM, 2013)

Situation	Average Passenger Service Time (Seconds/Person)	
	Observed Range	Suggested Default
Boarding		
No fare payment	1.75-2.5	1.75
Visual inspection (paper transfer/flash pass/mobile phone)	1.6-2.6	2.0
Single ticket or token into farebox	2.9-5.1	3.0
Exact change into farebox	3.1-8.4	4.5
Mechanical ticket validator	3.5-4.0	4.0
Magnetic strip card	3.7-6.5	5.0
Smart card	2.5-3.2	2.75
Alighting		
Front door	1.4-3.6	2.5
Rear door	1.2-2.2	1.75
Rear door with smart card check-out	3.4-4.0	3.5
NOTE: add 0.5 second/person to boarding times when standees are present. Add 0.5 second/person for non-level boarding (1.0 second/person for motor coaches)		

Studies have analyzed the determinants of dwell time. The majority of studies on dwell time have used regression models to relate transit vehicle dwell time to the passenger activities with varying level of attention to bus types, door use and payment methods.

Dwell time can be expressed as either a sequential or a simultaneous process. In a sequential process passengers would alight first then board Equation (9), as opposed to a simultaneous process where passengers would board and alight at the same time at different doors, Equation (10). However, in reality a little of both processes takes place. In majority of bus services where payment to the driver is required, all passengers board at the front door (closest to the driver), while the majority of alighting passengers step out from the back door and a few may alight at the front door.

$$DW = c + t_a N_a + t_b N_b \quad \textbf{(9)}$$

$$DW = c + \max(t_a N_a, t_b N_{b)} \quad \textbf{(10)}$$

where

DW = Dwell time , seconds

c = Dead time (time to open and close the door plus the lost time due to nature of the process, such as passengers walking up to the door or drivers making sure everything is safe before closing the doors.)

N_b = Number of Boarding Passengers

N_a = Number of Alighting Passengers

t_a = Average alighting passenger service time

t_b = Average boarding passenger service time

York (1993) modified Equations (9) and (10) to account for differences in boarding and alighting due to demographics and payment methods in the form of:

$$DW = c + \sum_{k=1}^{m} t_a N_a + \sum_{l=1}^{n} t_b N_b \quad \textbf{(11)}$$

$$DW = c + \max\left\{\sum_{k=1}^{m} t_a N_a + \sum_{l=1}^{n} t_b N_b\right\} \quad \textbf{(12)}$$

Where, *m* and *n* are the number of categories for boarding and alighting passengers, respectively.

The review of the literature reveals some trends in dwell time duration. Studies (presented in Table 4-2) have observed that alighting service times are shorter than boarding service times. This is because boarding passengers have to pay upon their arrival which increases their service time.

Table 4-2: Summary of Selected Studies on Dwell Time (Source: Tirachini, 2010)

Article	Location	Types of vehicles	Fare collection	Feature	Dead time, *c* (s)	Alighting, *a* (s / pas)	Boarding, *b* (s / pas)
Aashtiani and Iravani (2002)	Tehran, Iran	Two- and three-door buses	–	Dwell time function as input for transit assignment model	12.0	0.99–1.04	1.64–2.00 (from the best model)
Dueker *et al.* (2004)	Portland, USA	Buses	–	Use of archived AVL and APC data, account of lift operations	5.14	1.70 (only linear term)	3.48 (only linear term)
Fernández*et a l.* (2009)	Santiago, Chile	Two-, three- and four-door buses, Metro trains	Contactless card (buses), payment in station (metro)	Marginal boarding and alighting times depending on number of boarders and alighters	Metro: 3.24 Buses: 8.04–9.32	Metro: 0.70 Buses: 1.39–3.32	Metro: 1.13 Buses: 2.05–6.04
Guenthner and Hamat (1988)	Michigan, USA	One-door buses	Cash, tickets and passes	Different fare types found not to affect dwell time significantly	2.25 (plus opening/closing door time)	1.81	5.66 (for all fare payment methods)
TRB (2000)	USA	One- to six-door buses	Prepaid card and cash	Different boarding and alighting times depending on number of doors (rigid and articulated buses)	–	0.4–2.0	0.5–3.0

Table 4-2 (continued): Summary of Selected Studies on Dwell Time (Source: Tirachini, 2010)

Article	Location	Types of vehicles	Fare collection	Feature	Dead time, *c* (s)	Alighting, *a* (s / pas)	Boarding, *b* (s / pas)
Li *et al.*(2006)	Broward, FL, USA	Two-door buses	Prepaid card and cash	Choice model to predict alightings on front and rear doors	–	4.47–4.90	4.59
Lin and Wilson (1992)	MA, USA	One- and two-car trains (light rail)	Outside trains	Differences between model for one- and two-car trains	One car: 8.10–12.50. Two cars: 9.69–15.69	One car: 0.23–1.41. Two cars: 0.36–0.66	One car: 0.55–1.15. Two cars: 0.27–0.42
Rajbhandari*et al.* (2003)	NJ, USA	Buses	No info (data from APC devices)	Nonlinear model is better than linear one	1.32–5.99	1.93–4.63	4.65–6.91
York (1993)	London and Exeter, UK	One- and two-door buses (low floor, steps at entrance)	Prepaid card and cash	Peak/off-peak variation on boarding and alighting times	2.38–8.26	0.99–2.94	1.84–5.49 (passes) 2.74–8.87 (cash) 0.88–4.70 (change giving time)

Kraft and Bergen (1974), York (1993) and Dueker et al. (2004) showed that boarding and alighting service times are shorter during the peak hours in comparison to off peak. The reason is that during the peak hours, passengers are frequent commuters that are familiar with the service and generally in a rush to arrive at their destinations, whereas in the off-peak hours there are more occasional transit users and senior passengers. Their studies also illustrated that the number of steps on the bus impacts the boarding and alighting times where low floor buses have the fastest passenger service times.

Studies have expanded upon Equations (9) and (10) in order to take into account the effect of congestion (crowding) inside the bus as well as at the bus stop. For example, Fernandez et al. (2009) calibrated a piece-wise linear model using data from Santiago which estimates that when there are more than 40 passengers boarding and less than 15 passengers alighting, boarding and alighting service times are slower for bus services. Dueker et al. (2004) used squared terms of passenger activities to account for the diminishing marginal effects of additional boarding and alighting passengers on dwell time. Rajbhandari et al. (2003) proposed linear and non-linear regression models using passenger activity (sum of boardings and alightings) and number of standees (number of passengers in the transit vehicle who are standing rather than seated) as independent variables to estimate dwell time. Rajbhandari et al. (2003) found that the non-linear model (Equation (13)) better explains the variability of dwell time than the linear model (Equation (9)).

$$DW = \alpha(N_b + N_a)^{\beta} \quad \textbf{(13)}$$

Triachini (2010) conducted an extensive study on the determinants of dwell time. He proposed 6 models which evaluates the impacts of passengers' age, crowding, bus configuration (number of steps), fare payment methods and service types (local transit routes vs. intercity transit routes) on dwell time. The result shows that payment methods have a significant impact on dwell time. Slow payment methods such as cash transactions within the bus increase the dwell times, while services with fares paid before boarding the bus have lower dwell times. Triachini also

concluded that demographic distribution of the passengers has an impact on the boarding and alighting service times.

Most studies have used ordinary least square regression to estimate dwell times. The models developed by various authors have shown that passenger activity is the most effective determinant of dwell time. Although the inclusion of other explanatory variables such as payment method, demographic, familiarity with the service, lift activity and so on would increase the accuracy of dwell time estimation, such information is not available with all AVL/APC data.

Furthermore, dwell time models are not readily transferable from one region to the next as the effects on land use, demographics and passenger behaviour inherent in the models may not be representative of other regions. For these reasons a dwell time estimation model is proposed for the AVL/APC data from the Region of Waterloo.

4.2.2 Proposed Dwell Time Estimation Model

A dwell time estimation model was calibrated using Grand River Transit's archived AVL/APC data from 14 far-sided transit stations located in the Region of Waterloo (Figure 4-3). The summary of passenger activity for each of the selected transit stations is provided in Table 4-3. On average there are 2 passengers boarding and 2 passengers alighting, although the maximum passenger activity can reach up to 16 passengers boarding and 15 passengers alighting.

The selected transit stations did not have bus bays or layover times scheduled, and were not influenced by any traffic control features or other geometric characteristics. Therefore, we make the reasonable assumption that the total stopped time recorded in the AVL/APC database is a result of dwell time (i.e. time required to open the doors and to board and discharge passengers).

Figure 4-3: The Location of the Transit Stations Used to Calibrate the Dwell Time Model [Source: Google Map].

Table 4-3: Statistical Summary of Passenger Activity for the 14 Chosen Stations.

	Number of observations	Passenger Activity	Average	Standard Deviation	Minimum	Maximum
Dundas / Cambridge	**50**	**Boarding**	0	0.68	0	2
		Alighting	1	0.73	0	3
King / Blue Springs	**96**	**Boarding**	1	0.87	0	4
		Alighting	1	1.19	0	5
King / Dolph	**123**	**Boarding**	1	1.54	0	10
		Alighting	1	1.09	0	5
Ira needles / Erb	**68**	**Boarding**	1	0.83	0	4
		Alighting	2	2.24	0	13
Bishop /Duke	**52**	**Boarding**	1	0.67	0	3
		Alighting	2	1.50	0	8
University / Phillip	**905**	**Boarding**	2	2.32	0	16
		Alighting	2	2.24	0	15
Victoria / Patricia	**27**	**Boarding**	2	1.25	0	5
		Alighting	0	0.70	0	2
Wellington / Main	**57**	**Boarding**	2	1.33	0	6
		Alighting	0	0.40	0	2
Albert / Long Wood	**118**	**Boarding**	1	1.04	0	5
		Alighting	2	1.45	0	7
King / Sydney	**67**	**Boarding**	2	1.14	0	8
		Alighting	1	0.89	0	5
King / Montrose	**33**	**Boarding**	1	2.00	0	4
		Alighting	1	1.96	0	2
Krug / Lydia	**22**	**Boarding**	0	0.53	0	2
		Alighting	1	0.84	0	3
Queen / Winston	**28**	**Boarding**	1	1.34	0	4
		Alighting	1	0.75	0	3
King / Erb	**245**	**Boarding**	1	1.65	0	4
		Alighting	2	8.52	0	10

Many factors are deemed to be determinants of dwell time in literature such as bus load, number of passengers boarding, number of passengers alighting, fare payment method, use of bike rack or ramp, demographic, etc. However, the GRT's AVL/APC database does not contain a record of all these factors (i.e. fare payment method or ramp usage are unknown). Consequently, a linear regression model was estimated on the basis of the available explanatory variables such as boardings, alightings, load and schedule adherence. Passenger activity was found to be the only statistically significant explanatory variable (Equation (14)). This is reasonable as the literature has found passenger activity as the best determinant of dwell time.

$$\hat{DW}_{OLS} = 16.72 + 1.82N_b + 0.54N_a \quad \textbf{(14)}$$

where,

$\hat{DW}_{OLS}$ = Estimated dwell time based on ordinary least square regression, seconds
N_b = Number of Boarding Passengers
N_a = Number of Alighting Passengers

However, the model is a very poor fit to the data with R^2 = 0.2, as shown in Table 4-4. The model fails to explain the variability in the dwell time. This is due to the fact that there is significant variability in the dwell time as a function of passenger activity, as shown in Figure 4-4. Therefore, a simple regression model based solely on the number of boarding and/or alighting passengers cannot explain a large portion of the variability in the observed dwell times.

Table 4-4: Dwell Time Estimation Regression Results

Regression Statistics					
Multiple R	0.45				
R Square	0.2o				
Adjusted R Square	0.20				
Standard Error	7.33				
Observations	1890				
Analysis of Variance (ANOVA)					
Source of Variability	**Degree of Freedom (df)**	**Sum of Squares (SS)**	**Mean Square (MS)**	**F-test**	**Significance F**
Regression	2.00	26097.95	13048.97	242.80	0.00
Residual	1887.00	101414.20	53.74		
Total	1889.00	127512.14			
	Coefficients	**Standard Error**	**t-test**	**P-value**	
Intercept	16.72	0.26	63.21	0.00	
BOARDING	1.82	0.09	21.04	0.00	
ALIGHTING	0.54	0.09	6.11	0.00	

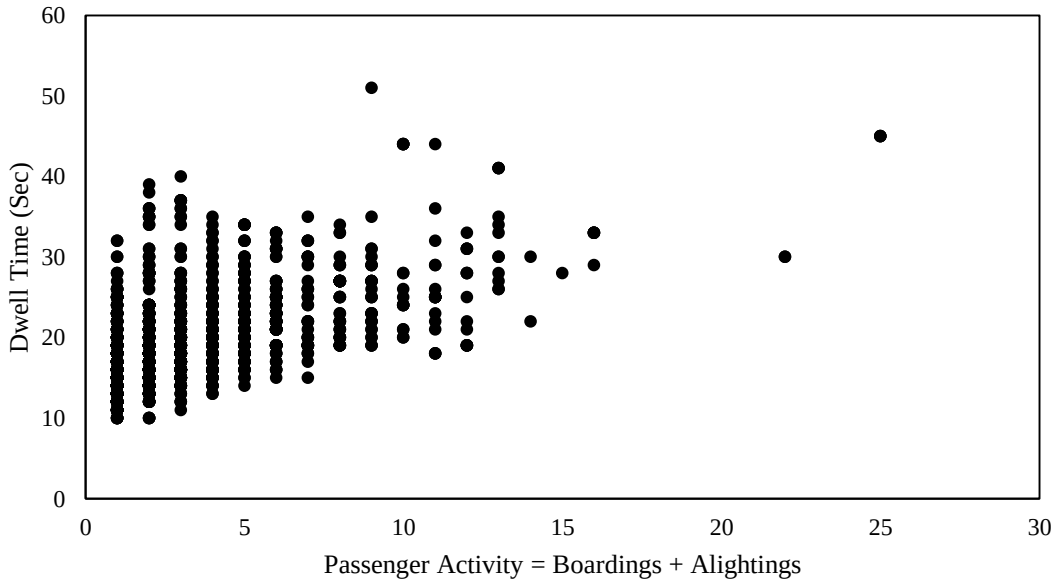

Figure 4-4: Variability of Dwell time Unexplained by Passenger Activity

To improve the dwell time estimation model, a two-stage approach has been adopted. In the first stage, a weighted regression model is calibrated to estimate the average dwell time $\overline{DW}$ as a function of passenger boarding and alighting activity. Then, in the second stage it is shown that dwell time follows the Poisson distribution. A stochastic model is setup in which the average dwell time, $\overline{DW}$, estimated in the first stage is used as the explanatory parameter to create the Poisson distribution. Each of these two stages is described in the following sections.

4.2.2.1 Estimating Mean Dwell Time

The passenger activities were grouped based on the number of passengers boarding (N_b) and alighting (N_a) (i.e. a group is constructed from all observations with one boarding passenger and zero alighting passengers; the next group consists of one boarding and one alighting passenger and so on). The summary of dwell times associated with each passenger activity group is presented in Figure 4-5. The trend of the average dwell time shows that as the number boarding and alighting increases the associated dwell time also increases. It is important to note that for some passenger activity groups only one observation was available, especially those passenger activity groups with large number of boardings and alightings.

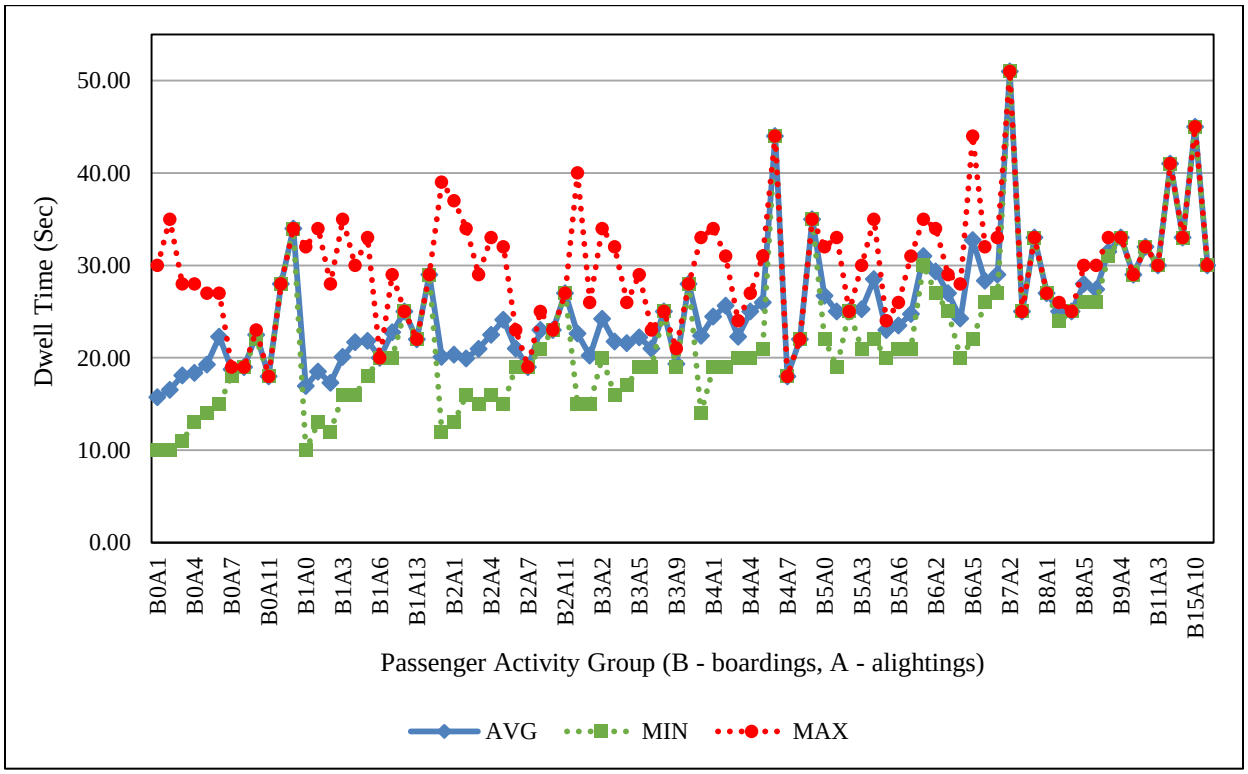

Figure 4-5: Average, Minimum and Maximum Dwell Time for Each Passenger Activity Group

The analysis of the residual plot of the OLS regression, presented in Figure 4-6, revealed that the data may suffer from a heteroskedasticity problem. For OLS the variance of residuals should be constant; meaning the variance of residuals does not vary with the value of the explanatory variables. However, heteroskedasticity in the data violates the assumption that errors are uncorrelated and their variances are constant (i.e. homoscedasticity). For a simple model, the variance may be linearly related to independent variables. The Breusch-Pegan test can be used to ascertain whether the residuals have non-constant variance (Hunter et al, 2005). In the Breusch-Pegan test an auxiliary regression is carried out where a regression model is fitted to the squared residual values with respect to the independent variables, in the following form:

$$\hat{e}^2 = \underline{\beta}\,\underline{X} \quad \textbf{(15)}$$

where

$\hat{e}^2$ = Squared residuals

$\underline{\beta}$ = Coefficients of parameters (P by 1 matrix)

$\underline{X}$ = Explanatory variables (n by P matrix)

Under homoscedasticity conditions the values of β will be zero. The Breusch-Pegan test for heteroskedasticity is a Chi-squared test with p-1 degree of freedoms (where p is the number of independent variables). If the value of observed Chi-squared is greater than the critical Chi-squared then the null hypothesis is rejected and heteroskedasticity is present in the data with respect to at least one of the independent variables.

$$\chi^2_{Observed} = \frac{SSE}{p} \quad \textbf{(16)}$$

$$\chi^2_{Critical} = \chi^2_{(p-1)} \quad \textbf{(17)}$$

where

SSE = Sum of squared of errors

p = Number of independent variables

n = Number of observations

$\chi^2_{critical}$ = Obtained from a Chi-square distribution table

Stata Statistical Software was used to carry out the Breusch-Pegan test. The $\chi^2_{observed}$ value was much larger than $\chi^2_{critical}$ ($\chi^2_{observed}$ = 30.7, $\chi^2_{critical}$ = 0.0), revealing that there is heteroskedasticity present in the data with respect to at least one of the independent variables.

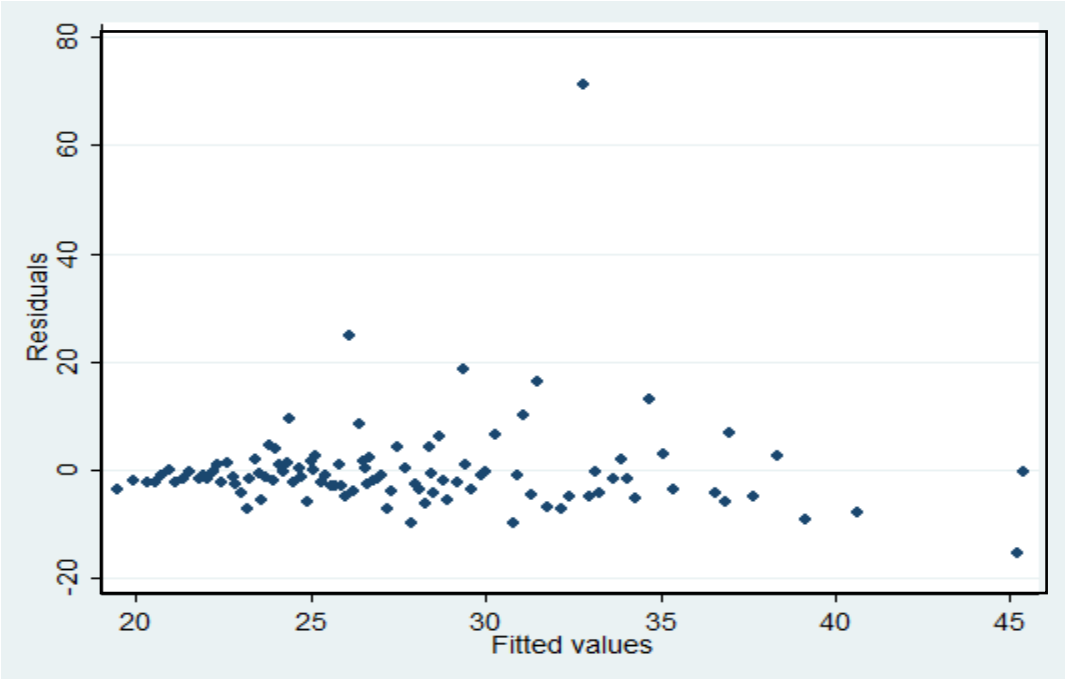

Figure 4-6: Residual Plot of OLS Regression Model for Average Dwell Time

Weighted Least Square (WLS) regression is the method used to account for the heteroskedasticity in the data. Unlike OLS, WLS can account for the inconsistency in the variance across the explanatory variables by applying weights that are inversely proportional to the variance at each level of explanatory variables. The general process for WLS is as follow:

1. Fit Ordinary Least Square (OLS) regression model to the data and obtain the residuals.
2. Estimate the variance function by regressing the squared residuals on the appropriate predictor.
3. Obtain the weights by using the fitted values from the estimated variance function.
4. Use the obtained weights to estimate the regression coefficients.

Stata Statistical Software was used to carry out the WLS regression using passenger activities as predictors. Equation (18) is used to estimate the average dwell time of the bus in the proposed methodology. The analysis of variance for the WLS regression is presented in Table 4-5. The regression constant and parameter coefficients are statistically significant (the Student t-value

and associated P-value for the parameters are: constant: t = 47.54, P-value = 0.00; *Nb:* t = 11.56, P-value = 0.00; *Na*: t = 6.69; P-value = 0.00) and the regression explains 66% of the variation in the observed mean dwell times. Figure 4-7 plots the average dwell time estimated from Equation (18) versus the observed average dwell time.

$$\overline{DW} = 15.47 + 1.99Nb + 0.77Na \quad \textbf{(18)}$$

where

$\overline{DW}$ = Average Dwell time , seconds
Nb = Number of Boarding Passengers
Na = Number of Alighting Passengers

Table 4-5: Weighted Least Squared Regression of the Average Dwell Time with Respect to Passenger Activity

Source of variability	Sums of Square (SS)	Degree of Freedom (df)	Mean Square (MS)			
Model	1327.75	2	663.87	No. of Observations	=	105
Residual	662.01	102	6.49	F(2,102)	=	102.29
Total	1989.77	104	19.13	Probability > F	=	0.000
				R-Squared	=	0.667
				Adjusted R-Squared	=	0.661
				Root Mean Square Error (MSE)	=	2.547

Variables	Coefficients	St. Error	t-test	P>|t|	90% Confidence Level	
Boarding	1.99	0.17	11.56	0.000	1.65	2.33
Alighting	0.77	0.12	6.69	0.000	0.54	1.00
Intercept	15.47	0.32	47.54	0.000	14.82	16.11

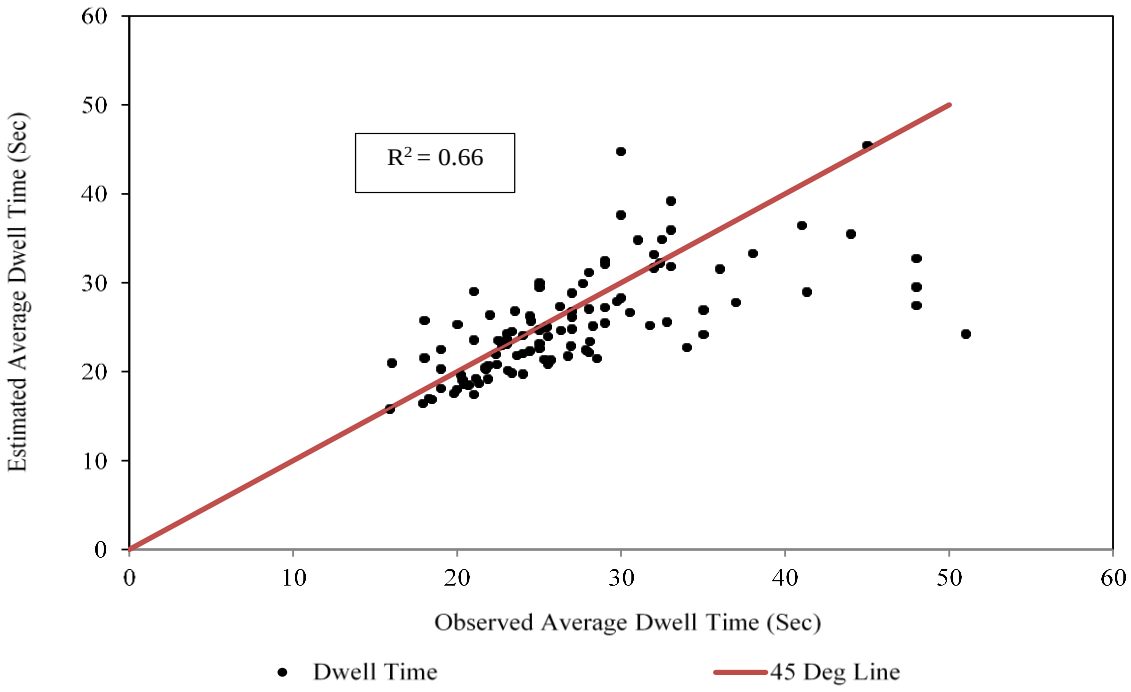

Figure 4-7: Estimated vs. Observed Average Dwell Time

4.2.2.2 Modelling the individual dwell times around the mean

In the second stage, we model the variation in the individual dwell time observations about the mean. An examination of the data revealed that this variation can be described by the Poisson distribution.

As mentioned previously the AVL/APC data have been organized into groups based on passenger activities. The frequency distribution of dwell time for each passenger activity group was constructed. Figure 4-8 is an example of the frequency distribution using the dataset consisting of observations with 1 passenger boarding and zero passengers alighting. Using Easy Fit software it was determined that dwell time follows Poisson distribution, when data is grouped based on passenger activities. The output results from East Fit software are presented in Appendix A.

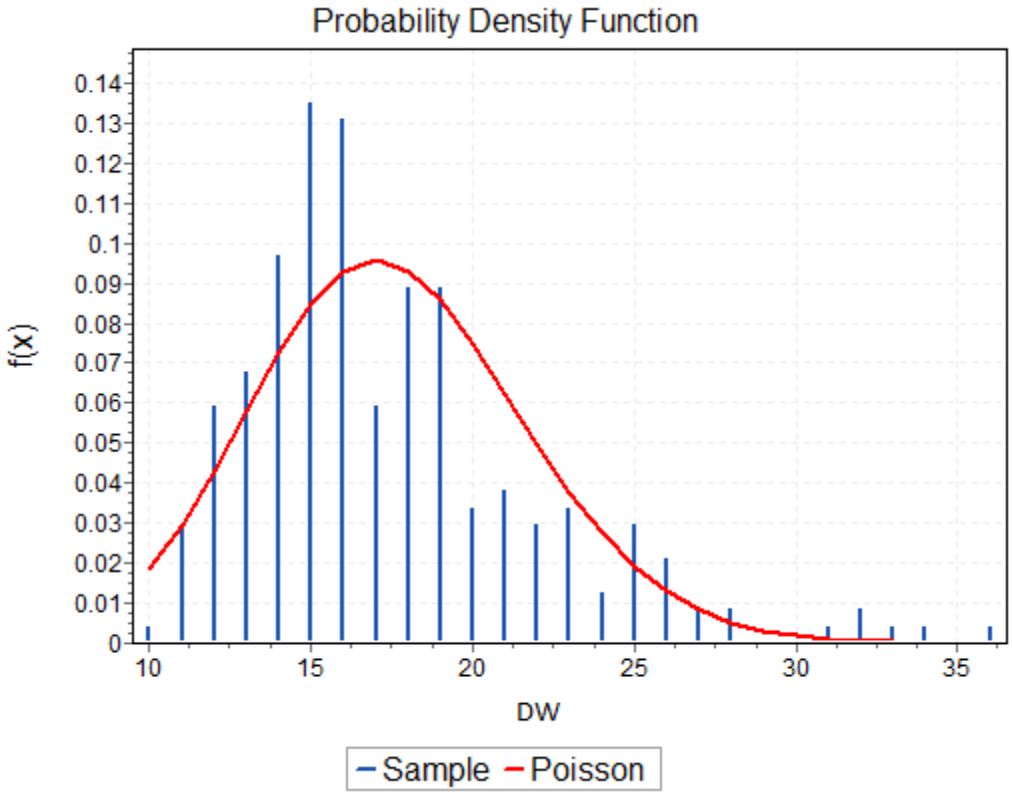

Figure 4-8: The Dwell Time of Sample Passenger Activity Group of 1 Passenger Boarding Following Poisson Distribution

The Poisson distribution is discrete and therefore, dwell time can only be represented as integer values. However, dwell time is measured in seconds, and consequently, this level of precision is adequate. The probability mass function of the Poisson distribution is given in Equation (19).

$$f(Y) = P(Y = DW) = \frac{\overline{DW}^{DW} e^{-\overline{DW}}}{DW!} \quad \textbf{(19)}$$

where

$f(Y)$ = probability that the dwell time for a specific scheduled stop event = Y seconds.
$\overline{DW}$ = average dwell time (seconds) – estimated from Equation (18)
DW = dwell time (seconds) associated with a specific scheduled stop event

Given that a stochastic model is used, the dwell time estimated from Equation (19) can take a wide range of values as illustrated by *f*(*DW*) in Figure 4-9. However, the dwell time cannot be longer than the observed total stop time (*TS*). Therefore, Equation (20) is adjusted to ensure the probability that dwell time exceeds the total stop time is zero. The probability that dwell time (*Y*) will be in the range of *DW* and *DW* + δ given that the total stop time is *TS* is expressed as:

$$f'(DW) = P(Y = DW) \quad = P(DW < Y \le DW + \delta \mid Y \le TS) = \frac{P(DW < Y \le DW + \delta)}{P(Y \le TS)} \tag{20}$$

where

f'(DW) = probability that the dwell time = *Y* seconds given that $Y \le$ TS
δ = a small value of dwell time
TS = total stopped time of the transit vehicle (seconds)

Equation (20) can be expressed in terms of the cumulative distribution function (designated by F) as follows:

$$f'(DW) = P(Y = DW) = \frac{F(DW + \delta) - F(DW)}{F(TS)} \tag{21}$$

The truncated dwell time function is obtained by taking the limit of $\delta \to 0$ which results in:

$$f'(DW) = \lim_{\delta \to 0} \frac{F(DW + \delta)}{F(TS)} = \frac{f(DW)}{F(TS)} \tag{22}$$

The contrast between Equation (19) and Equation (22) is illustrated in Figure 4-9 in which *TS* = 19 seconds.

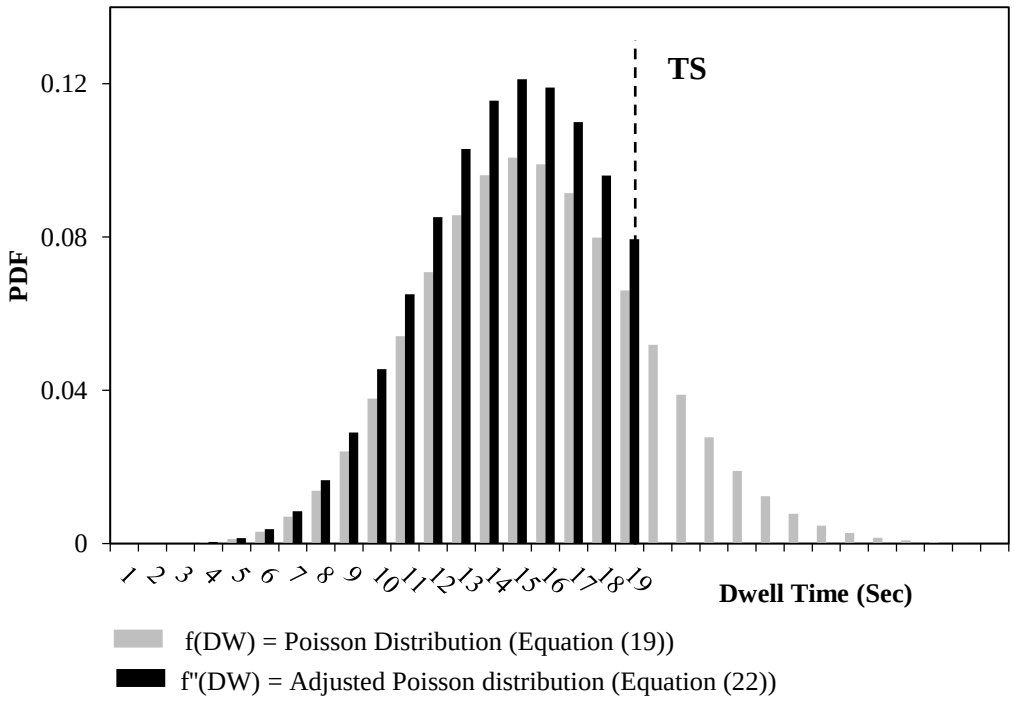

Figure 4-9: Probability Density Function of Dwell Time

This dwell time estimation model is used in the estimation of the red interval of a given intersection, as well as to distinguish between the three different delay scenarios. The performance of the dwell time estimation model is evaluated in Chapter 5.

4.3 Red Interval Estimation Model

Consider a situation in which the bus arrives at the intersection during the green phase, serves passengers at the transit station, and then the signal turns red just as the bus finishes serving passengers at the station. In this scenario the total stop time consists of the dwell time of the bus plus the red interval duration. Assuming that (a) a large database of observations is available; and (b) the red interval is constant within each signal cycle during the analysis period, then the red interval can be estimated as the maximum difference between the total stop time (*TS*) and the dwell time (*DW*). However, the dwell time model developed in the previous section (Equation

(22)) is stochastic, meaning that for each observation a range of valid dwell times can be estimated as a function of the number of passengers boarding and alighting.

Figure 4-10 depicts the elements of the proposed model for estimating the duration of the red interval.

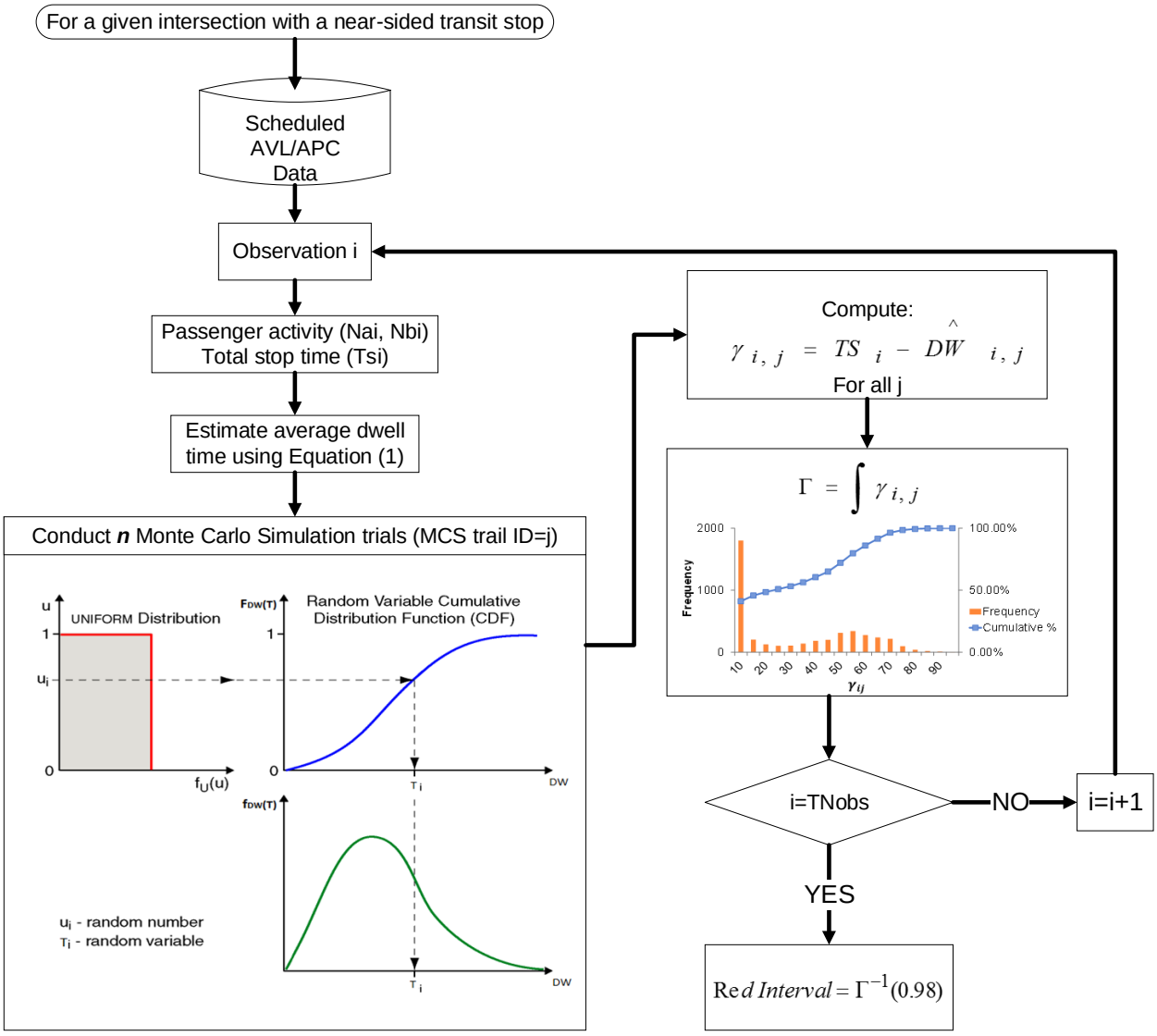

Figure 4-10: Schematics of Red Interval Estimation

As indicated in Figure 4-10, given a database containing AVL/APC data for an intersection approach with a near-side transit station, the following steps are carried out in order to estimate the duration of the red interval.

1. Define i to represent a scheduled stop observation in the AVL/APC database. For observation i, we know the total stop duration (TS_i), the number of passengers boarding (Nb_i), and the number of passengers alighting (Na_i).
2. Use Equation (18) to estimate the mean dwell time ($\overline{DW_i}$).
3. Conduct n Monte Carlo Simulation (MCS) trials (MCS trial ID = j) using Equation (22) ($DW_{i,j}; j = 1, n$)
4. Compute $\gamma_{i,j} = TS_i - DW_{i,j}$ for all j.
5. This process was repeated for all i near-sided scheduled stop observations.
6. The distribution of γ_{ij} is compiled considering all MSC trials for all near-sided observations.
7. Suppose Γ represents the cumulative density function (CDF) of γ_{ij} .The duration of the red interval (R) can be estimated as a specified percentile of Γ. Through the use of simulation, we calibrated this value to be equal to the 95th percentile instead of the largest γ_{ij}, to mitigate the influence of outliers and extreme values.

Once the red interval is estimated, all near-sided *scheduled* observations can be classified into one of the three scenarios identified in Section 4.1 and their corresponding stopped delay (caused only by the traffic signal) can be estimated. Note that for each observation the average dwell time of the n MCS trials is used to distinguish between Scenarios 1 and 3. Next, the stopped delay associated with each *scheduled* observation can be determined. It should be noted that for *unscheduled* stop events, the total stop time is considered as the stopped delay. Finally, the boundary line is fit to the data to distinguish between stop observations due to the signal operation and other causes.

4.4 Boundary Line Algorithm

The boundary line (BL) fitting algorithm needs to be robust to manage the variability in traffic conditions and to distinguish the stopped delay observations caused by the traffic signal operation from the stopped delay observations caused by other factors.

Here a set of modifications are proposed to Yang and Hellinga's (2012) boundary line selection algorithm. These modifications address the following four issues:

1. The data captured from the adjacent road segments, by the GIS buffer, must be excluded from the analysis.
2. The extent of the queue must be measured from the stop line and not the center of the intersection.
3. The BL should exclude stopped observations due to other geometric characteristics or traffic controls.
4. The BL should be improved to account for the variability in traffic. If intersections are incorrectly identified as under-saturated, their stopped delay and maximum queue length will be under-estimated.

To address the first issue, the setup of the problem within the ArcGIS is altered. As illustrated in Figure 4-11, the polyline buffer zone is complemented with a 30 meters circular buffer zone that is centred at the centroid of the upstream intersection (point layer). Stopped delay observations that fall within both of these buffer zones are excluded from the analysis. The 30 meters radius is selected to match the width of the polyline buffer zone.

Furthermore, for each observation the distance is measured from the stop-line and not the center of the intersection as is the case in Yang's work (Yang, 2012).

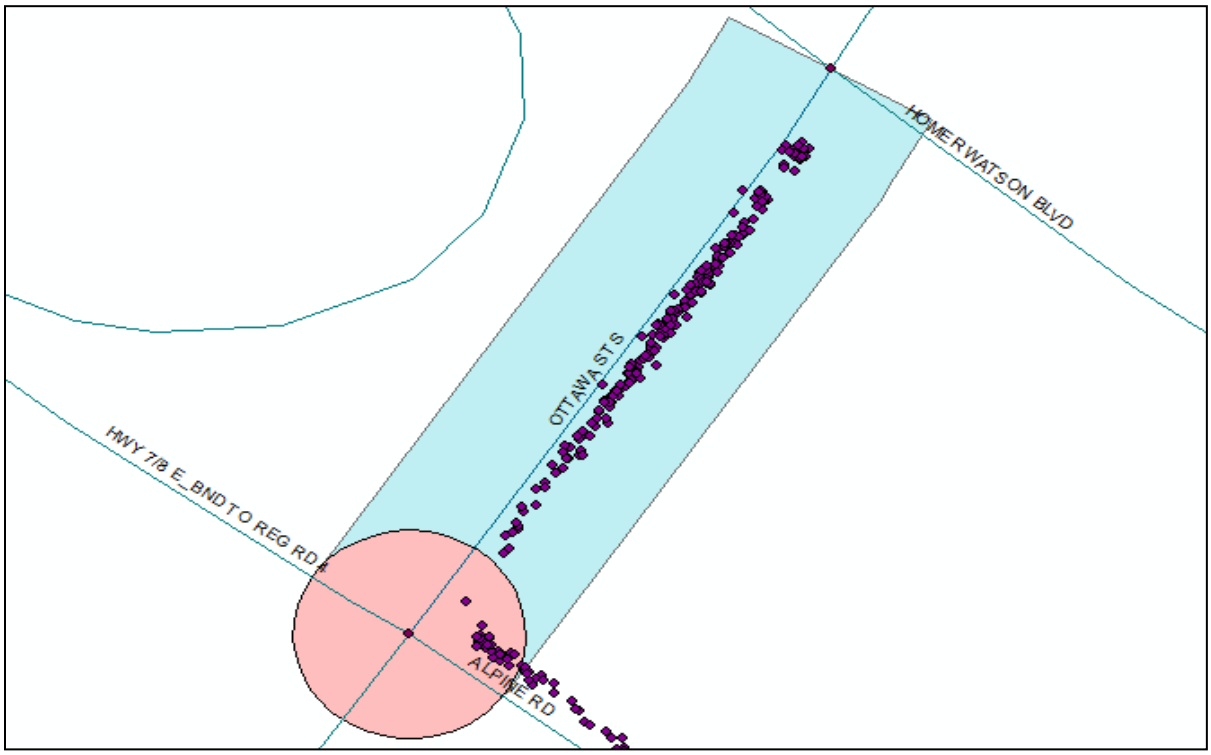

Figure 4-11: Buffer Zone Excluding the Stop Observations Associated With the Adjacent Road

The 3rd and 4th issues are addressed by redefining the solution space and the candidate boundary lines. The determination of the boundary line's X-intercept is redefined as illustrated in Figure 4-12. The boundary line algorithm first determines if there is a significant gap between the distances of stop observations.

If buses are random samples of traffic stream, then the location of transit vehicle's stops are randomly distributed from the stop-line to the tail of the queue. A significant gap between the clusters of stop data may be the result of:

1. Bias in sampling
2. Small sample size

3. Stops caused by other factors than the signal operation (e.g., vehicles queuing to enter a parking lot)

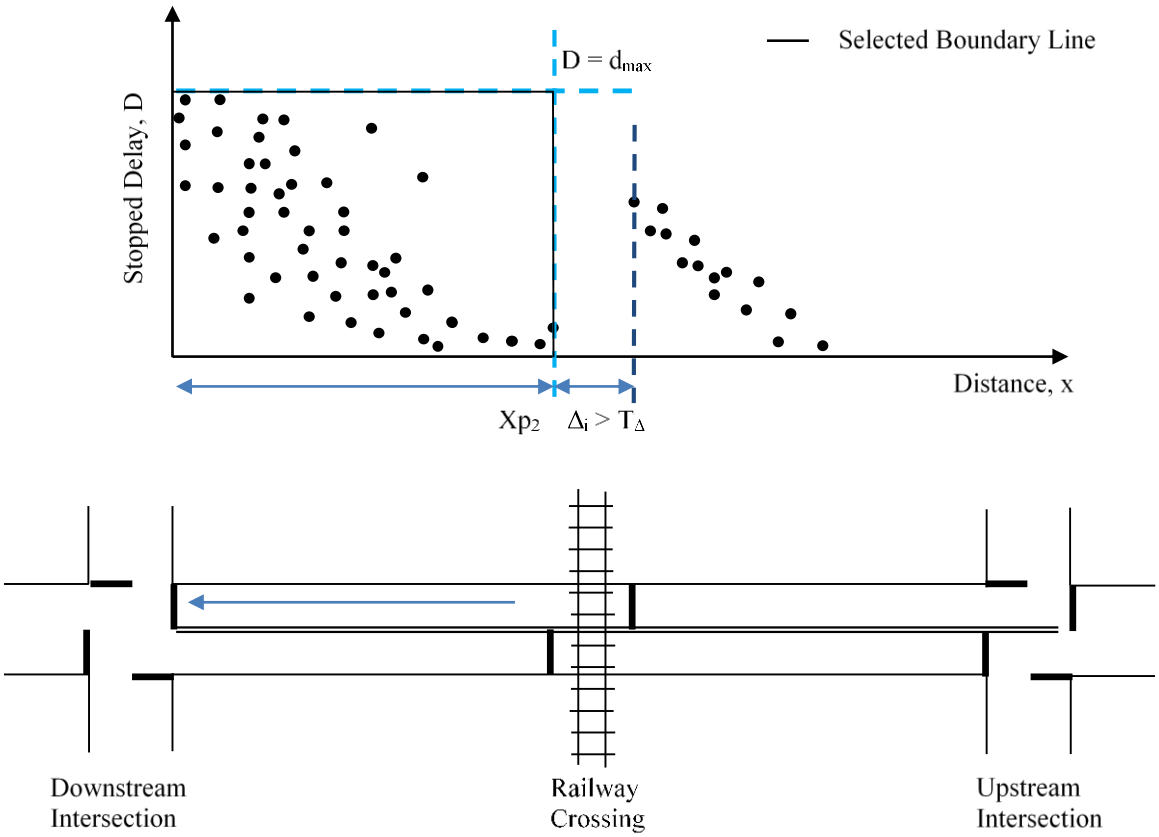

Figure 4-12: Boundary Line Solution Space

Here it is assumed that no bias exists in the sample data. In this study, transit vehicles are used as probe vehicles to evaluate the performance of intersection approach. The major differences between transit vehicles and other vehicles, especially passenger vehicles, are that transit vehicles predominantly travel on the right lane (when multiple lanes are available).

However, the inherent difference in the right lane characteristics is not the source of the gaps within the data. Therefore, no bias is being introduced in maximum queue length calculations as the result of sampling transit vehicle's stop locations at the signalized intersection.

A significant gap in the data may be observed as a result of small sample size. An insufficient sample size provides an incomplete picture of the operational status for a given segment. Gaps within the stop locations of transit vehicles may disappear with a larger dataset. On the other hand, gaps in the data may be observed due to other features such as railway crossing, stop traffic control, parking manoeuvers, etc; such a gap in the data marks the distinction between observations due to signal and other causes.

In this section, we determine the size of gap which distinguishes between the signal operation and other causes. Shockwave theory can be used to determine the threshold length (Δ) of gaps that one would expect to see in data as the result of signal operation for a given number of available observations. The cluster of observations which are located upstream of a spatial gap larger than the threshold are considered to be caused by factors other than the downstream traffic signal.

As an initial research effort, we start with the assumption that the relationship between flow rate (q) and density (k) is triangular, as shown in Figure 4-13. With this assumption, the rate at which queues form and dissipate at the intersection can be calculated. During the red interval the backward moving formation shockwave that travels upstream from the stop line can be represented by Equation (23), while Equation (24), represents the recovery shockwave during the green interval.

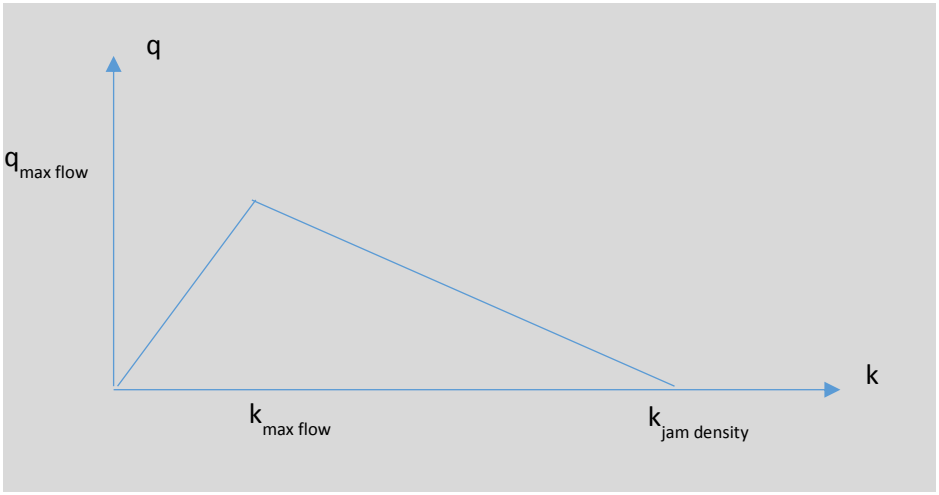

Figure 4-13: Idealized Flow – Density Relationship

$$W_{12} = \frac{q_{arrival\ flow} - q_{stationary}}{k_{arrival\ flow} - k_{jam\ density}} \quad \textbf{(23)}$$

$$W_{23} = \frac{q_{stationary} - q_{\max\ flow}}{k_{jam\ density} - k_{\max\ flow}} \quad \textbf{(24)}$$

The transit vehicles approaching a given intersection and encountering a queue will join the tail of the queue. The location of their stop is a function of when the transit vehicle arrived at the tail of the queue. The time the transit vehicle discharges from the intersection is a function of its location in the queue and the signal timing.

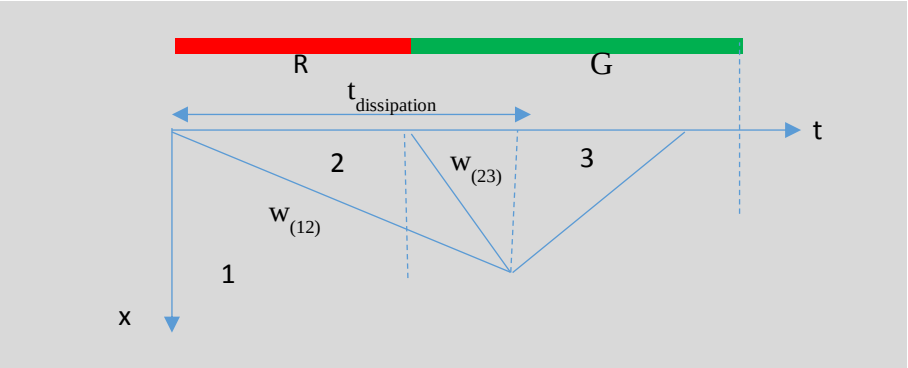

Figure 4-14: Shockwave diagram

A simulation model is used to determine the value of gap threshold (T_Δ) in transit stop observations that distinguishes between signal operation and other causes. Signal timing, arrival flow and the time the transit vehicles arrives at the signalized intersection are used as inputs into the model. The simulation is setup based on the following signal control and road traffic conditions:

- The approach has a constant saturation flow rate
- The average vehicle arrival rate at the approach follows a Normal distribution
- No initial queue is present at the beginning of the evaluation time
- The cycle length is set to be 60 seconds
- The length of the red interval follows the Normal distribution

The simulation process is summarized below:

1. For each trial, the average arrival flow rate ($q_{arrival\ flow}$) in vph is generated based on a Normally distributed[4] random number [N(950,190)].
2. The red interval, R, is randomly chosen based on the Normal distribution[4] [N(30,25)]
3. The green interval, G, is calculated as $G = c - R$

[4] The notation $N(\mu,\sigma^2)$ represent the normal distribution with mean of μ and variance of σ^2.

4. The backward moving formation shockwave, w_{12}, is calculated based on Equation (23);where $q_{stationary} = 0(veh/hr), k_{Jam\ Density} = 125(Veh/km)$ and

   $k_{Arrival\ Flow} = (q_{Arrival\ Flow})(k_{Max\ Flow}) / q_{Max\ Flow}$

5. The backward moving recovery shockwave, W_{23}, is calculated based on Equation (24); Where $q_{Max\ Flow} = 1900(veh/hr), k_{Max\ Flow} = 50(Veh/km)$
6. The time at which the queue dissipates is calculated by Equation (25).
7. The most upstream position of the tail of the queue is determined by Equation (26).
8. The time at which the transit vehicle arrives at the intersection, $t_{transit\_arrival}$, is randomly selected based on the uniform distribution[5], [U(0,60)].
9. The location of the transit vehicle in the queue is determined by Equation (27).
10. For transit vehicles that do join the queue, the time at which they are discharged from the intersection is calculated by Equation (28).
11. The stopped delay of transit vehicle is calculated by Equation (29).

$$t_{Dissipation} = \frac{|W_{12}|(R_i)}{|W_{23}| - |W_{12}|} \quad \textbf{(25)}$$

$$Q_{Max} = |W_{12}|(t_{dissipation})(1000/3600) \quad \textbf{(26)}$$

$$X_{Transit} = \begin{cases} t_{transitarrival}|W_{12}|(1000/3600) & t_{transitarrival} \le t_{Dissipation} \\ The\ transit\ vehicle\ doesn't\ join\ the\ queue. & t_{transitarrival} > t_{Dissipation} \end{cases} \quad \textbf{(27)}$$

$$t_{transitdischarge} = R + \frac{X_{Transit}(1000)}{|W_{23}|(3600)} \quad \textbf{(28)}$$

$$StoppedDelay = t_{transitdischarge} - t_{transitarrival} \quad \textbf{(29)}$$

The analysis of spatial gap between consecutive stop locations is carried out for different datasets, each consisting of a different number of stop delay observations (*n*). Datasets consisting

[5] The notation U(a,b) represent the uniform distribution with defining parameters a and b.

of n=10, 20, 30, …, 200 observations were considered. The procedure above provides the distance from the stop line where the transit vehicle joins the queue and stops for each of the *n* observations. The *n* stop locations are sorted into ascending order. The gap threshold (T_Δ) is determined as the largest distance between consecutive stop observations.

The results, shown in Figure 4-15, indicate that as expected, the maximum gap size decreases as the number of observations increases. A linear regression model was calibrated to the results as shown in Figure 4-15. Both the intercept and slope are statistically significant and the model has a relatively high goodness of fit (R^2 = 0.76). Since the model has a declining linear form a minimum threshold must be set to prevent the value of gap threshold from becoming too small. 7 meters has been chosen as the minimum gap size which corresponds to the width 2 lane of a driveway in order to capture the gap due to other geometric feature which may be present.

Consequently, Equation (30) can be used to determine the value of gap threshold as a function of the number of available stop delay observations.

$$T_\Delta = \max(7, 45.28 - 0.126(N_{observation})) \quad \textbf{(30)}$$

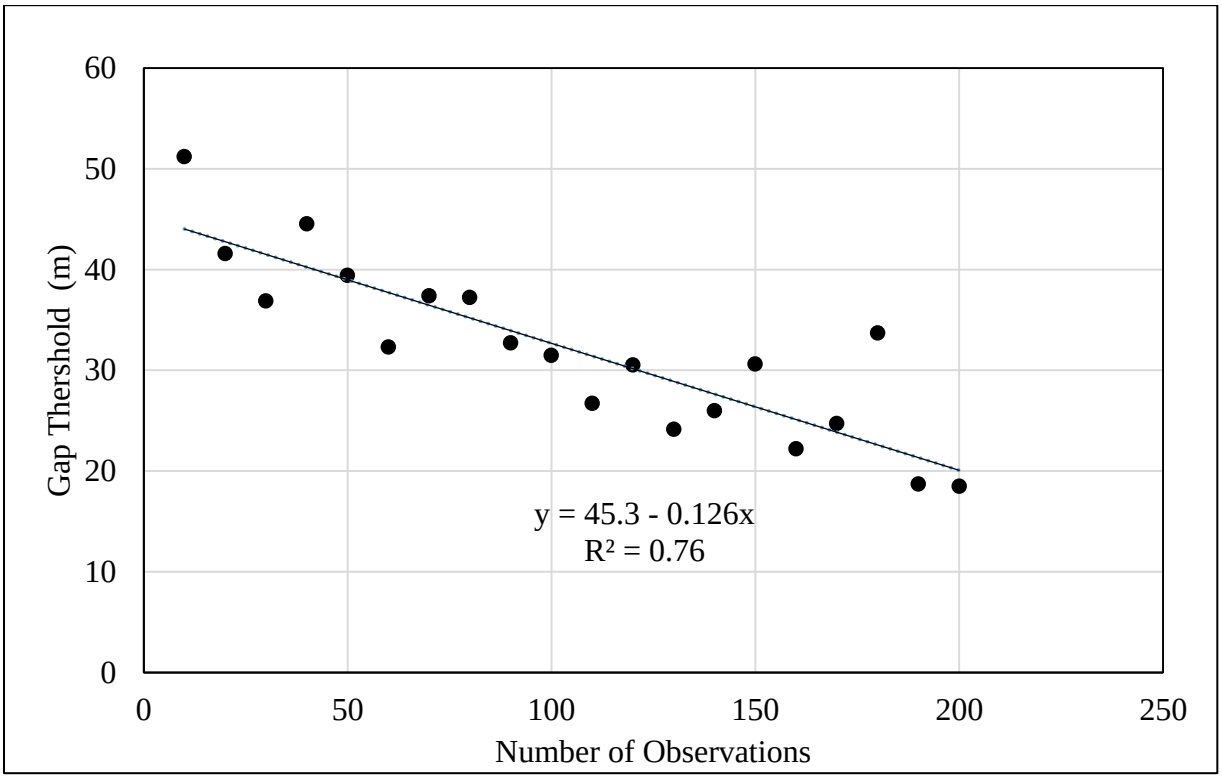

Figure 4-15: Maximum Gap Size vs. Number of Observations Available

For each intersection approach the extent of the queue, X_{p2}, can be computed by undertaking the following steps:

1. The stopped delay observations (i = 1, N) are sorted in ascending order in terms of their distance from the stop-line (x_i).
2. The difference between consecutive x values is calculated for each pair of stopped delay observations ($\Delta_i = x_{i+1} - x_i$, i = 1, N-1).
3. The treshold value is determined by using Equation (30)
4. If the computed difference is greater or equal to a threshold value (T_Δ), then X_{p2} is set equal to the distance corresponding to the previous stopped delay observation .(i.e. if ($\Delta_i \geq T_\Delta$) then $X_{p2} = x_i$ else next i)

Once the extent of the queue is found, the optimal delay envelope within this feasible region can be determined. The shape of the delay envelope is defined as a rectangle enclosed by the line D = d_{max}, and $X_{p2} = x_i$, as shown in Figure 4-16.

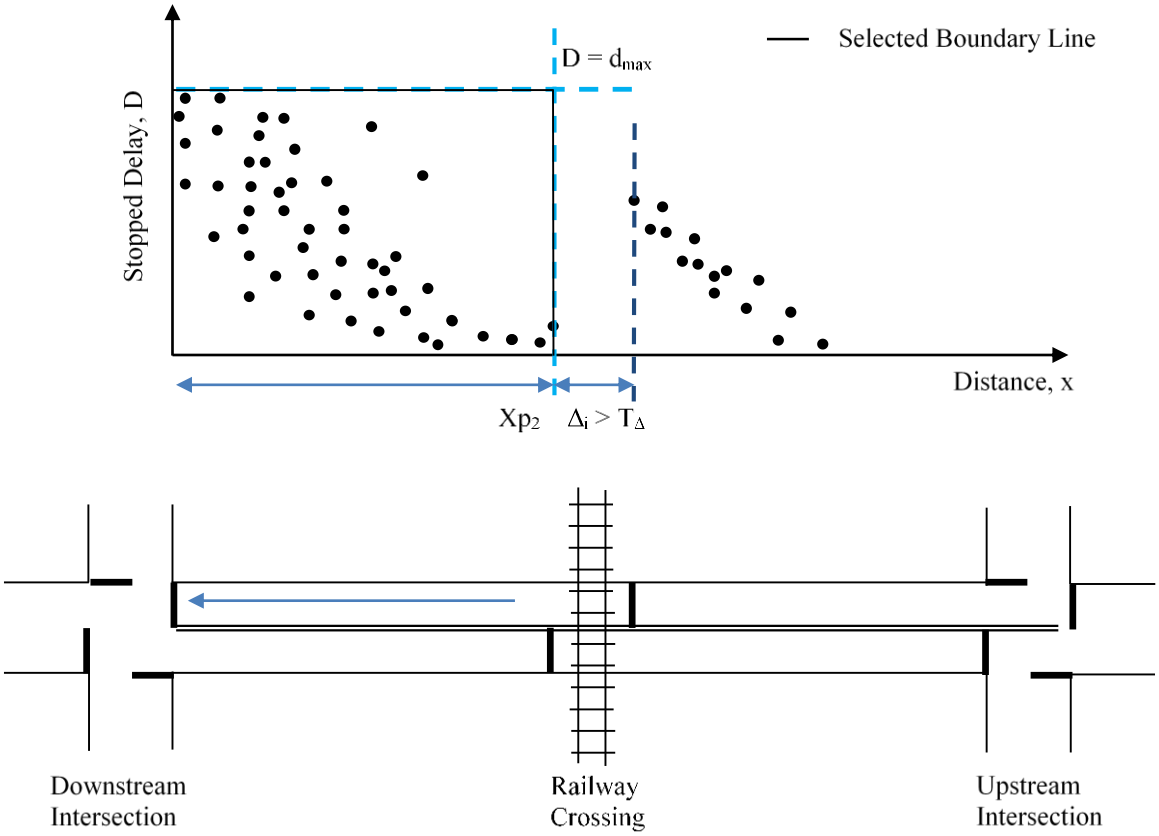

Figure 4-16: Candidate Delay Boundary Line

4.5 Delay and Maximum Queue Length Estimation

The stop observations under the boundary line are deemed as stopped delays caused by the operation of the traffic signal. The performance measures of an intersection are estimated based on these observations. However, estimating stopped delay per vehicle trip is of interest, not per stop event. Consequently, for transit trips with multiple stopped delay observations, the multiple observations are summed to provide a single observation representing the total stopped delay experienced by that transit vehicle at that signalized intersection. Some transit trips do not experience any stopped delays so for these trips a total stopped delay value of zero is considered.

The result is a single value of total stopped delay observation for each of the transit trips, N_T, that were observed to traverse this intersection during the period of interest.

The average stopped delay per vehicle is calculated as the summation of the total stopped delay associated with all N_T trips divided by the total number of transit trips.

Measures of variability (e.g. standard deviation, and 95th percentile) are also computed from these data. The maximum queue length is determined by the x-intercept of the boundary line, $X_{p2.}$

4.6 Proposed Index for Ranking Intersections

According to the HCM, control delay is considered as the primary measure to rank the performance of signalized intersections. The 90th percentile of delay can also be used to provide a sense of the cumulative distribution of the magnitude of delay

However, it is important to consider the number of road users that are inconvenienced by poorly performing intersections. When considering two intersections with equal average delays, it is intuitive to first improve the performance of the intersection for which the largest number of travelers will benefit. The number of transit trips that experienced delay is used as a proxy for the number of travelers that are inconvenienced at a particular intersection.

It is important to know when the queue spills back into the upstream intersection and impairs its operations. However, as the lengths of the segments are not constant, setting a fixed maximum queue length criteria is not appropriate. For example, the distance between two consecutive intersections could be long (e.g. 1000m) and therefore, a maximum queue of 250 meters would be inconsequential. On the other hand, for short segments a maximum queue length of 250 meters could mean the queue has spilled over into the upstream intersection.

Based on the above rationale, average stopped delay, 90th percentile of delay, ratio of maximum queue length to segment length and percentage of transit trips that experience delay at a given intersection approach are used to prioritize the operational quality of signalized intersection

approaches. When multiple bus routes traverse a given intersection approach, it is possible for the buses servicing the different routes to make different turning movements at the intersection. Within the context of this work, no special provision is given to the different turning movements – although this could be an area for additional research.

The value of the factors used for ranking are aggregated by weighting the values based on the number of trips traversing a given intersection approach.

The proposed index takes a value between 0 and 1, where 1 indicates the worst performing intersection. The ranking index is calculated as:

$$WT_j = \frac{\sum_{i=1}^{nr} T_{ij}(NTrip_{ij})}{\sum_{i=1}^{nr} NTrip_{ij}} \quad \textbf{(31)}$$

$$WSD_j = \frac{\sum_{i=1}^{nr} D_{ij}(NTrip_{ij})}{\sum_{i=1}^{nr} NTrip_{ij}} \quad \textbf{(32)}$$

$$WND_j = \frac{\sum_{i=1}^{nr} \psi_{ij}(NTrip_{ij})}{\sum_{i=1}^{nr} NTrip_{ij}} \quad \textbf{(33)}$$

$$RI = W_{WT}\left(\frac{WT_j}{WT_{MAX}}\right) + W_{WSD}\left(\frac{WSD_j}{WSD_{MAX}}\right) + W_{WND}\left(\frac{WND_j}{WND_{MAX}}\right) + W_Q\left(\frac{Q_j}{Q_{MAX}}\right) \quad \textbf{(34)}$$

where

RI = Ranking index for intersection approach *j*

WT_j = Weighted percentage of transit trips incurred delay at intersection approach j

WSD_j = Weighted average stopped delay for intersection approach *j* (seconds/trip)

WND_j = Weighted 90th percentile stopped delay for intersection approach *j* (seconds/trip)

D_{ij} = Average stopped delay for route *i* on approach *j*, seconds

$NTrip_i$ = Number of transit trip for a given route
nr = Total number of routes traversing the intersection approach j
T_{ij} = Percentage of transit trips on route i incurred delay at intersection approach j
ψ_{ij} = 90th percentile delay for route i on approach j, seconds

WT_{MAX} = max{WT_j, j = 1,2,3,…,N}
WSD_{MAX} = max{WSD_j, j = 1,2,3,…,N}
WND_{MAX} = max{WND_j, j = 1,2,3,…,N}
Q_j = Queue length for intersection approach j

Q_{MAX} = Max{Q_j, j = 1,2,3,…,N}
W_{WT} = Weighting factor for percentage of transit trips incurred delay
W_{WSD} = Weighting factor for weighted average stopped delay
W_{WND} = Weighting factor for weighted 90th percentile stopped delay
W_Q = Weighting factor for queue length
i = Index of the routes
j = Index of the intersections approach being ranked
N = Number of Intersection approaches

The value of the weighting factors are dependent on the objective that the agency is trying to achieve. For example, if the objective is to improve transit performance and reduce transit operation cost, then more weight should be given to intersection approaches that are traversed by the greatest number of transit vehicles. Each weighting factor must have a value between 0 and 1 and the sum of the three weighting factors must be equal to 1.

Chapter 5
Evaluation of the Proposed Methodology

In this chapter the proposed methodology is calibrated and evaluated using field data and simulation. Specifically the scheduled and unscheduled stop observations reported by the AVL/APC data are used to calibrate the parameters of the proposed dwell time and red interval estimation models. Furthermore, the stop location of the unscheduled stop observations are used to calibrate the boundary line algorithm. Then the estimates of average delay and maximum queue length obtained from the proposed methodology are validated against field measurements and simulation.

5.1 Model Calibration and Evaluation using Monte Carlo Simulation

The GRT's AVL/APC data is used to calibrate and evaluate the proposed methodology. Using AVL/APC data from the field permits a more accurate representation of the error and variability existing in the real world and specifically the variability in dwell time that cannot be explained by the dwell time estimation model.

In the proposed methodology, the red interval of an intersection is estimated based on the 95^{th} percentile of the difference between the total stop time and the estimated dwell times of the bus. The dwell time of the bus is estimated stochastically to account for the variability in dwell time data not explained by the passenger activity variables. Therefore, the error associated with the dwell time estimation model becomes inherent into the red interval estimation.

Furthermore, the estimation of red interval duration is dependent on observing the scenario in which the transit vehicle arrives at the near-sided station during the green interval, serves the station and as it's about to clear the station the signal turns red. Only in this scenario is the red interval equal to the difference between the bus total stop time and dwell time. To be able to

estimate the red interval, this particular scenario should be available within the dataset. It is assumed that with a large dataset of scheduled observations this scenario is available.

This chapter endeavours to answer the following questions:

1. What is the accuracy of the dwell time estimation model?
2. How many scheduled observations are needed for accurate red interval estimation?
3. How accurate is the estimated red interval?

To answer these questions we conduct a Monte Carlo simulation using AVL/APC data for which the actual dwell time and red interval are known.

In the next section we describe how the AVL/APC data are used to generate scenarios that are then used to calibrate and evaluate the dwell time and red interval estimation models (described in Sections 5.1.2 and 5.1.3, respectively).

5.1.1 Scenario Generation

The AVL/APC data from the same 14 transit stations presented in Table 4-3 are used. These stations are far-sided transit stations with no bus bay or layover times scheduled and were not influenced by any traffic control or other geometric features. Therefore, we can reasonably assume that the dwell time is equal to the total stopped time as recorded in the AVL/APC data. In the MCS we assume that the observed AVL/APC data were obtained from near-sided transit stations and therefore we treat these data as *scheduled stops*. However, as depicted in Figure 5-1, for these near-sided transit stations the duration of the total stop time, *TS*, is a function of the dwell time (*DW*) and the impact of the traffic signal. From the observed AVL/APC we know the dwell time but we must simulate the effect of the traffic signal in order to determine the value of *TS*.

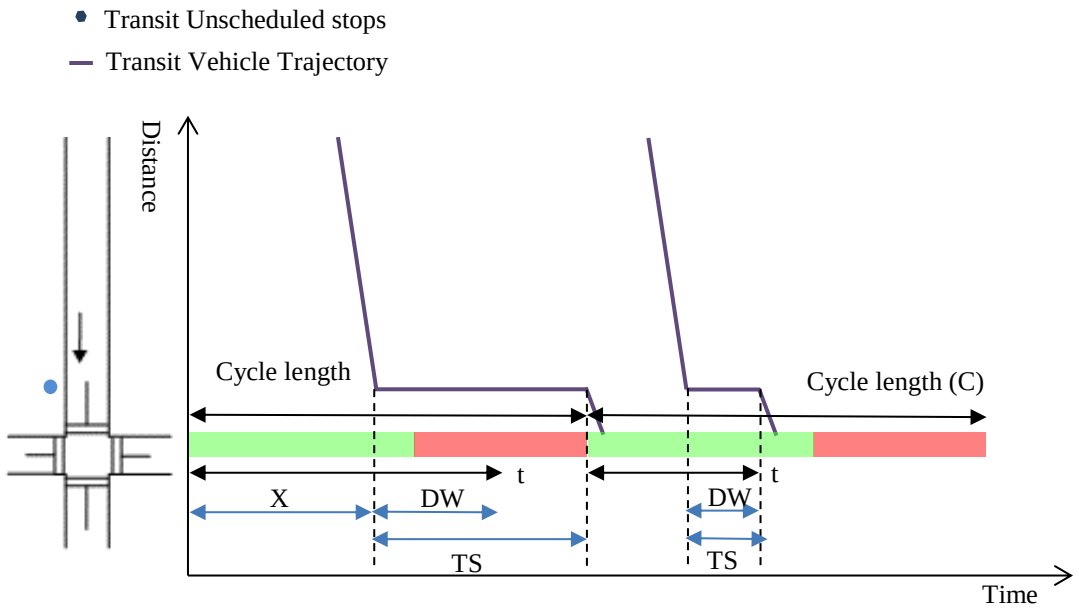

Figure 5-1: The Schematic for Generating Total Stop Time of the Bus.

As indicated in Figure 5-1, if the bus arrives at the intersection during the green interval and finishes serving the station before the start of the red interval, then *TS* will be equal to dwell time. However, if the bus arrives at the intersection during the green interval and the signal turns red before the end of the dwell time, then *TS* will be equal to the time the bus arrived at the intersection until the end of the red interval.

Thus *TS* is a function of the arrival time of the bus relative to the signal timing and the duration of the red interval, both of which are treated within the MCS as random variables as described below.

A variable *t* is defined as the time from the beginning of the green interval until the end of the dwell time. A value for *t* is randomly generated based on the uniform distribution with the constraint that $DW \leq t \leq C$ (C = cycle length). Variable $t_{arr,i}$, represents the time the transit vehicle, *i*, arrived at the intersection and is computed as:

$$t_{arr,i} = t - DW_i \quad \textbf{(35)}$$

The green interval is calculated as the difference between the cycle length and red interval; where the cycle length, *C*, is a known fixed value and the red interval is randomly generated based on the range defined in Table 5-1.

The scenario generation simulation is carried out for a set of cycle times with a defined range of red interval, as presented in Table 5-1. Since the analysis is conducted for the peak period, it is expected that the traffic volume and the signal timings stay relatively constant. For this reason a small variation of 5 seconds in the red interval duration is selected.

Table 5-1: Cycle Length and Red Interval Duration

Cycle Length (Seconds)	Minimum Red Interval (Seconds)	Maximum Red Interval (Seconds)
60	30	35
70	35	40
90	45	50
105	50	55
120	55	60

Figure 5-2, demonstrates the scenario generation process. For each simulation trial, one AVL/APC data is selected randomly from the database then the scenario that describes the arrival of the bus at the signalized intersection relative to the signal timing is generated. The steps taken for each observation *i*, are as follows:

1. One of the available scheduled stop observations is randomly selected based on the uniform distribution. The passenger activity (B_i, A_i) and the actual dwell time (DW_i) of the bus are obtained.
2. The duration of the red interval, R_i, is randomly chosen between the predetermined ranges (obtained from Table 5-1), based on the uniform distribution.
3. The green interval is calculated as, $G_i = C - R_i$
4. A number between dwell time (DW_i) and the cycle length is randomly selected to represent variable t_i.

5. The time at which the transit vehicle arrives at the station, $t_{arr,i}$, is computed as $t_{arr,i} = t_i - DW_i$
6. The total stop time can be calculated as follows:

$$TSi = \begin{cases} C - t_{arr,i} & if \quad t_i > G_i \; and \; t_i \geq DW_i \\ DW_i & if \quad t_i < G_i \end{cases} \qquad \textbf{(36)}$$

7. The passenger activity (B_i, A_i) and total stop time (TS_i) are used as input in Sections 5.1.2 and 5.1.3 to estimate the dwell time and the red interval respectively. The actual dwell time (DW_i) and red interval (R_i) are used to evaluate the proposed methodology.

Once the scenario is generated, the passenger activity information (B_i, A_i) and the generated total stop time (TS_i) are used to estimate dwell time ($\hat{DW}_i$) as described in section 4.2.2. The red interval is estimated based on the 95th percentile of the difference between *TS* and *n* dwell time estimated trials for all the considered observations. Section 5.1.2 evaluates the accuracy of dwell time estimation model and Section 5.1.3 examines the accuracy of the red interval estimation.

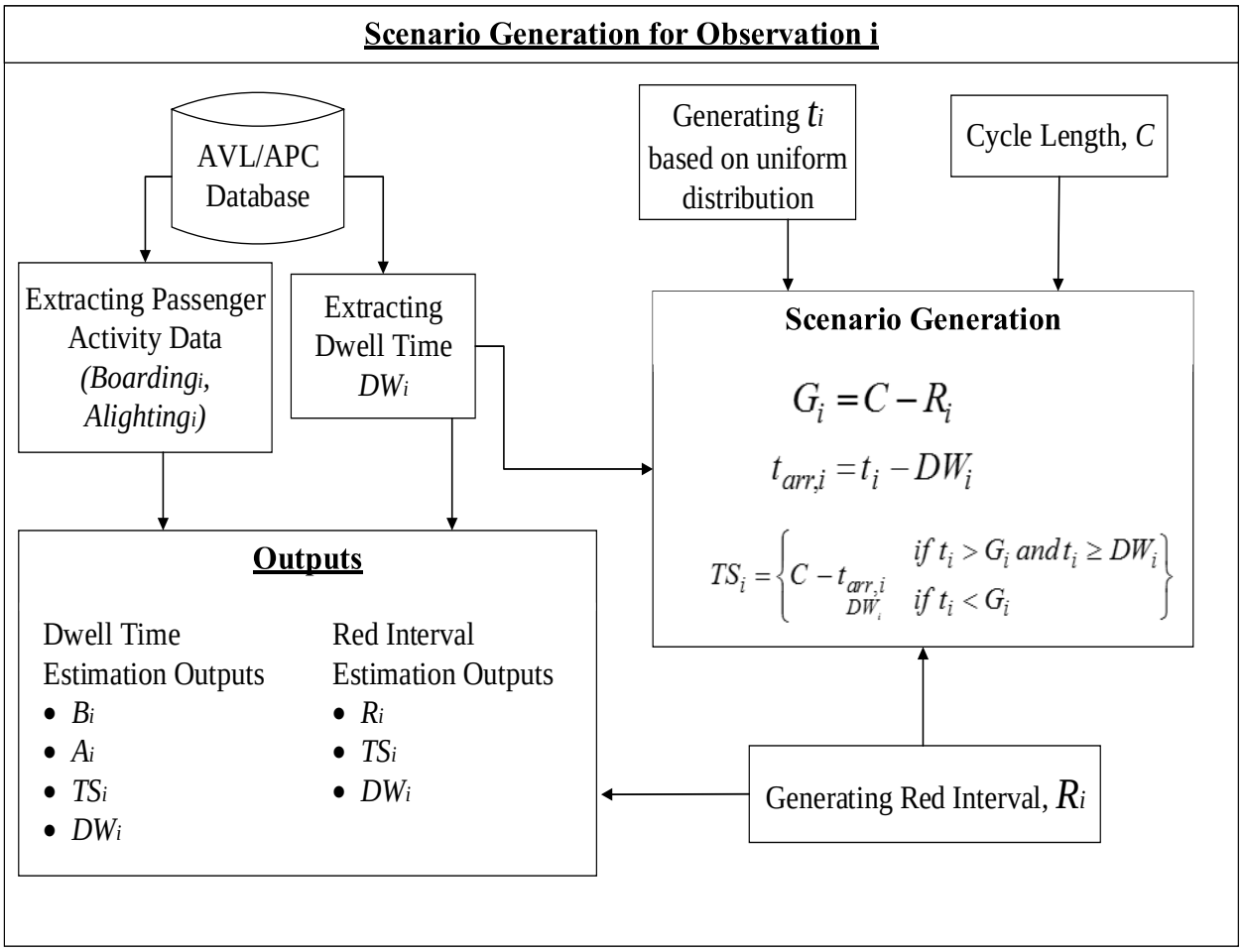

Figure 5-2: Schematic of the Scenario Generation Process Conducted for Each Observation

5.1.2 Evaluating the Dwell time Estimation Model

The stochastic form of the dwell time estimation model was hypothesized to account for more of the variability in dwell time in comparison to linear and non-linear regression models. However, due to the stochastic nature of the model, dwell time can take a range of values. Therefore, a certain number of MCS trials, *n*, is carried out to converge dwell time to its mean value.

To determine the number of MCS trials (*n*) required to accurately estimate dwell time the following steps are carried out:

1. For a randomly selected scheduled observation i, Nb_i, Na_i, TS_i, DW_i, information are obtained from the scenario generation process described in section 5.1.1. The passenger activity information is used to estimate $\overline{DW}$ in order to construct the appropriate Poisson distribution for the observation. TS_i is used to update the distribution, as described in section 4.2.2.

2. n MCS trials are carried out to obtain n estimates of dwell time(where n starts from 5 and increases in increments of 5). The notation $DW_{i,j}$ represents the dwell time estimated for observation i in MCS trail j of n trials.

3. The n number of dwell times are averaged , $DW_{i,\,estimate} = \frac{1}{n}\sum_{j=1}^{n} DW_{i,\,j}$

4. Absolute error of dwell time is calculated as:

$$Absolute\ \ Error_i = \left| DW_{i,\,actual} - DW_{i,\,estimate} \right|$$

5. The steps from 1 to 4 are repeated for all the available observations from the 14 stations.

6. The Root Mean Square Error (RMSE) is calculated using:

$$RMSE = \sqrt{\frac{1}{Num}\sum_{i=1}^{Num}(P_i - O_i)^2} \qquad \textbf{(37)}$$

where

P_i = Predicted value of dwell time for observation i
O_i = Observed value of dwell time for observation i
Num = Number of observations

7. The number of MCS trials, n, is increased by 5 and the process (Steps 1-6) is repeated.

RMSE measures the average error of the predicted values. The values of RMSE can range from 0 to infinity where 0 indicates a perfect match between predicted and observed values. The RMSE results from the analysis are presented in Table 5-2. From these results it can be observed that the improvement (reduction) in RMSE is marginal for *n* greater than 20 and consequently *n* = 20 was chosen.

Table 5-2: The RMSE Associated With Each of the Number of MCS Trials

Number of MCS, *n*	5	10	15	20	25	30
RMSE	8.37	7.45	7.19	4.69	4.68	4.67

Figure 5-3, presents the estimated vs. observed dwell time plots for the stochastic model proposed (using 20 MCS trials) and the deterministic ordinary least square (OLS) regression model. The trend-line of the OLS model has a R^2 of 0.29, while the R^2 of the proposed stochastic model is 0.50. The proposed model can explain 50 percent of the variability in dwell time data - a significant improvement over the dwell time regression model suggested by the literature.

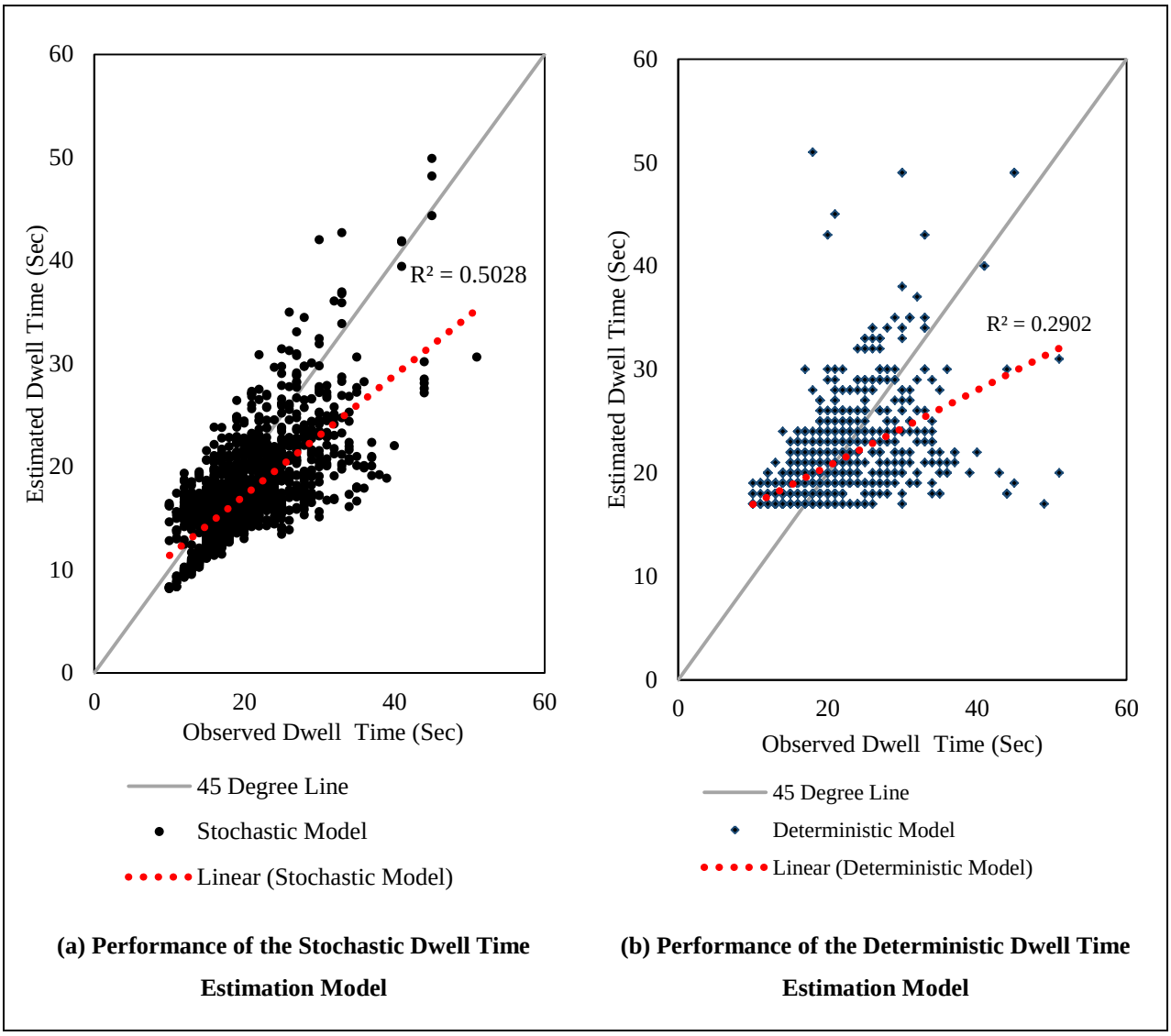

(a) Performance of the Stochastic Dwell Time Estimation Model

(b) Performance of the Deterministic Dwell Time Estimation Model

Figure 5-3: Comparison of Estimated vs. Observed Plots of Stochastic and Deterministic Dwell Time Estimation Models

5.1.3 Evaluating the Red interval Estimation Model

To answer the questions: (1) how many scheduled stop observations are needed to estimate the red interval and (2) what is the associated error with the red interval estimation, another MCS is conducted.

The simulation process, which consists of two modules, is depicted in Figure 5-4. Module 1 estimates the dwell time as described in the previous section. Module 2 calculates the red interval. As indicated in Figure 5-4, the red interval is estimated on the basis of N scheduled stop observations (i = 1, N). We first determine how the red interval duration estimation error varies as a function of N.

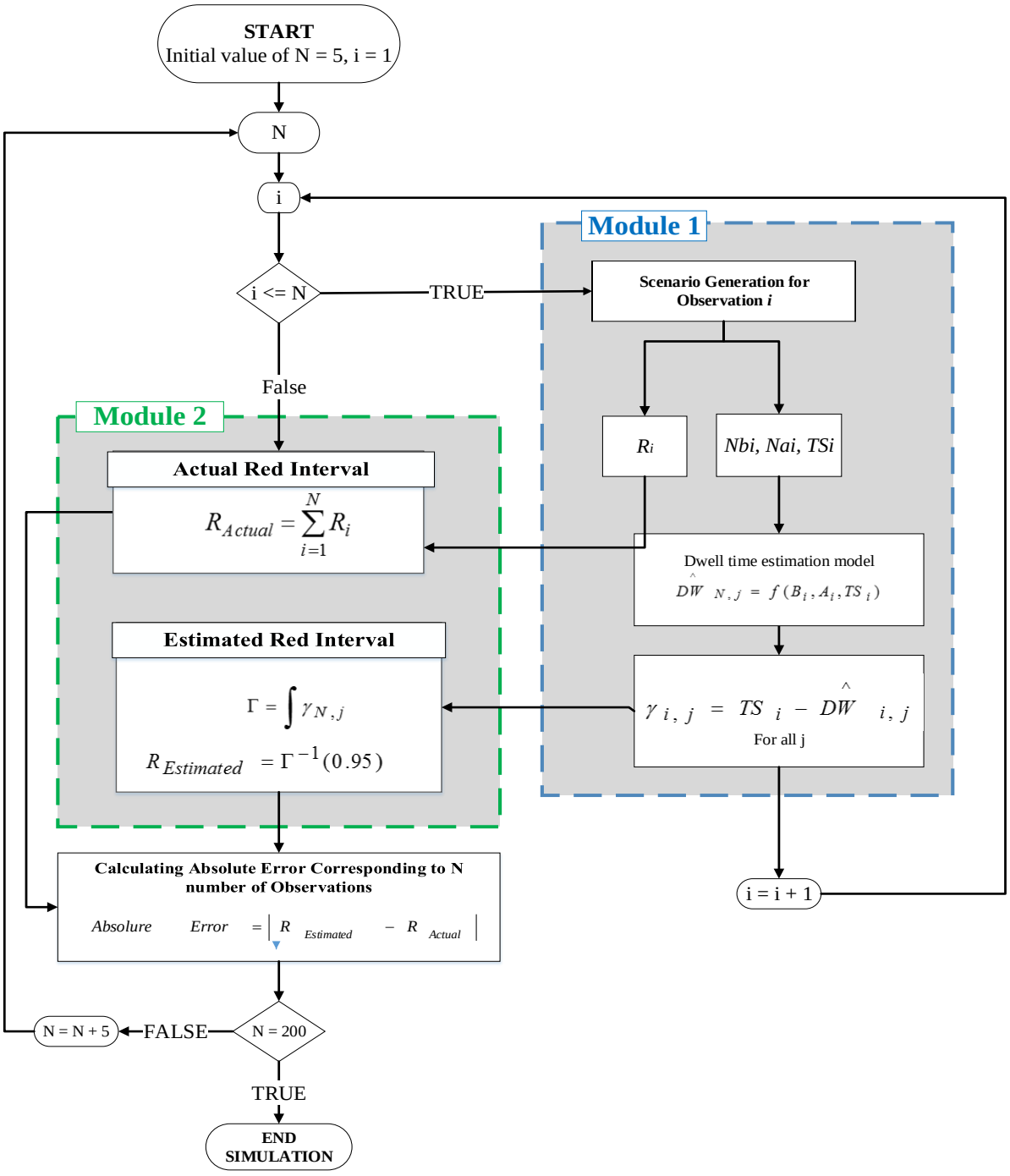

Figure 5-4: Flow Chart of Absolute Error Simulation

The simulation process is summarized below:

Module 1

a. For a randomly selected scheduled observation *i*, Nb_i, Na_i, TS_i, R_i, information is obtained from the scenario generation process described in section 5.1.1.

b. R_i, is the input in Module 2 for the actual red interval calculation.

c. The passenger activity information is used to estimate $\overline{DW}$ in order to construct the appropriate Poisson distribution for the observation. TS_i is used to update the distribution, as described in section 4.2.2.

d. Conduct 20 Monte Carlo Simulation (MCS) trials (MCS trial ID = *j*) using Equation (22) ($DW_{i,j}; j = 1, n$)

e. Compute $\gamma_{i,j} = TS_i - DW_{i,j}$ for all *j*. $\gamma_{i,j}$ is the input for Module 2 in the red interval estimation calculation.

Module 2

a. The red interval is estimated for the *N* number of observations. The duration of the red interval, $R_{Estimated}$, is estimated as the 95th percentile of the difference between the total stop time and the dwell time trials for the *N* considered observations.

b. The actual red interval, R_{Actual}, is calculated as the average of the red intervals generated for the *N* considered observations.

c. The absolute error is calculated as, $Absolute\ \ Error = \left| R_{Estimated} - R_{Actual} \right|$

40 simulation trials are carried out for each cycle length. Since observations are selected randomly, the initial pattern of absolute error with respect to the number of observations is dependent on which observations and scenarios are selected first. In order to avoid this bias and converge to the average absolute error associated with each number of observations, the simulation process is repeated 10 times so that there are 10 absolute error values associated with each number of observations for a given cycle length. The absolute errors are averaged for each number of observations are presented in Figure 5-5.

The pattern observed in Figure 5-5, demonstrates that as the number of observations increases the average absolute error in the estimate of red interval decreases.

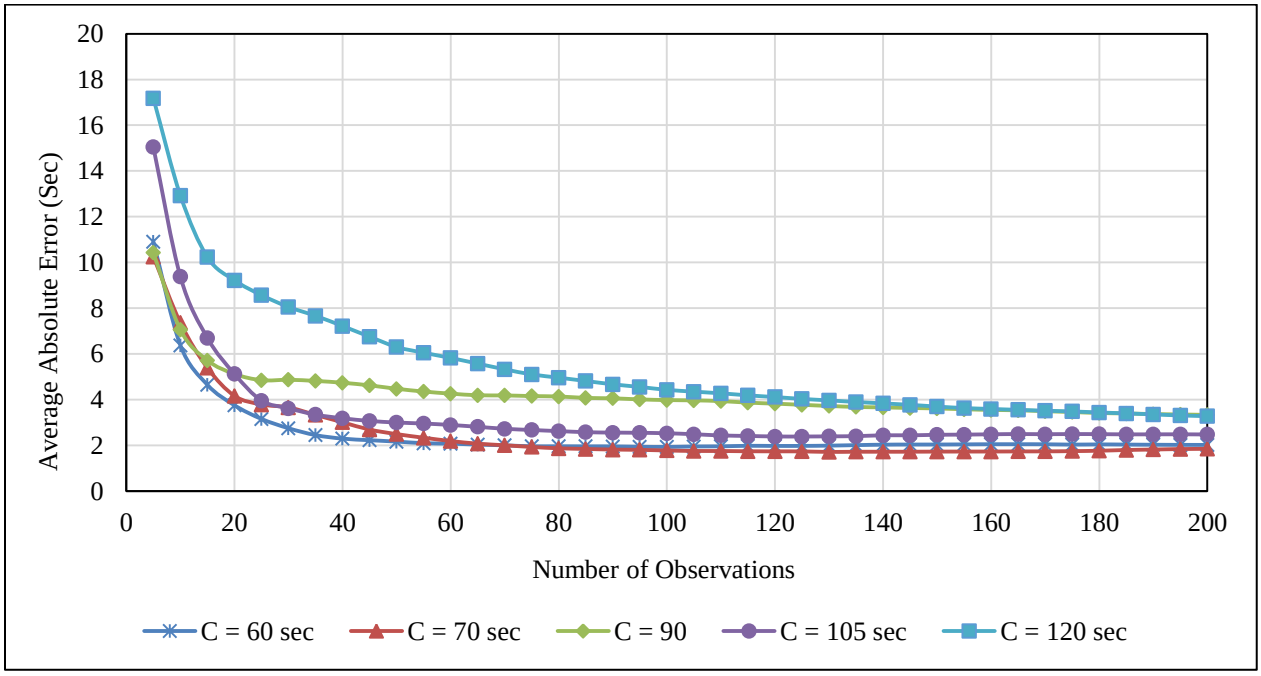

Figure 5-5: Average Absolute Error versus. Number of Observation Plot for Various Cycle Lengths

During the peak service hours GRT routes operate with the following headways: 36 routes with 30 minute headway; 12 routes with 15 minute headways; and 2 routes with 1 hour headways. The summary of the number of scheduled stop observations detected during the peak period (4:30 PM– 6 PM) at the near-sided transit stations is provided in Table 5-3. At minimum, there are 5 scheduled observations available for each headway category which from Figure 5-5 suggests absolute error for the red interval estimation ranging from 10.4 to 17.2 seconds. However, if instead of considering the minimum number of observations obtained at any of the intersections we consider the 10^{th} percentile instead (i.e. 15 observations) then, from Figure 5-5 we expect the absolute error in the red interval duration to range from 4.6 to 10 seconds

(approximately 8% of the cycle length). We assume that this level of accuracy is sufficient for estimating the stop delays. Appendix B presents histograms of the number of observations for each of the headway categories.

Table 5-3: Number of Scheduled Stop Observations Available at Near-sided Transit Stations During PM Peak Period (4:30 – 6:00 PM)

	Number of Observations			
Service Headway (minutes)	**Average**	**Minimum**	**10th Percentile**	**Maximum**
15	194	5	31	983
30	122	5	14	469
60	53	7	15	118

5.2 Validating the Model using VISSIM Simulation

The archived AVL/APC data do not contain any information about signal timing and therefore it was not possible to validate the proposed model, particularly the model for estimating the red interval duration, using the AVL/APC data. Instead, simulation was chosen as the method of validation because one of the main objectives was to validate the proposed red interval estimation methodology. Simulation also allows for the validation of the assumption that transit vehicles can be used to estimate the average delay incurred by passenger vehicles.

To this end, a hypothetical arterial segment was constructed in VISSIM, consisting of two signalized intersections and one un-signalized intersection as illustrated in Figure 5-6. The upstream intersection operates under fixed signal timing for which the through movement experiences a signal timing of: red interval = 22 seconds, green interval = 35 seconds and amber interval = 3 seconds (cycle length= 60 seconds).

The downstream intersection is a T-intersection which operates under a four-phase signal timing plan in which the protected phase for the westbound left-turn movement is actuated. An actuated timing plan is used so that the red interval duration is not fixed, but varies depending on the extensions that occur for the actuated phase. Phase one corresponds to the protected left turn on

the westbound approach (Figure 5-6 (b)), with a minimum effective green interval of 5 seconds and extends at intervals of 3 seconds in response to vehicle actuations to a maximum of 20 seconds.

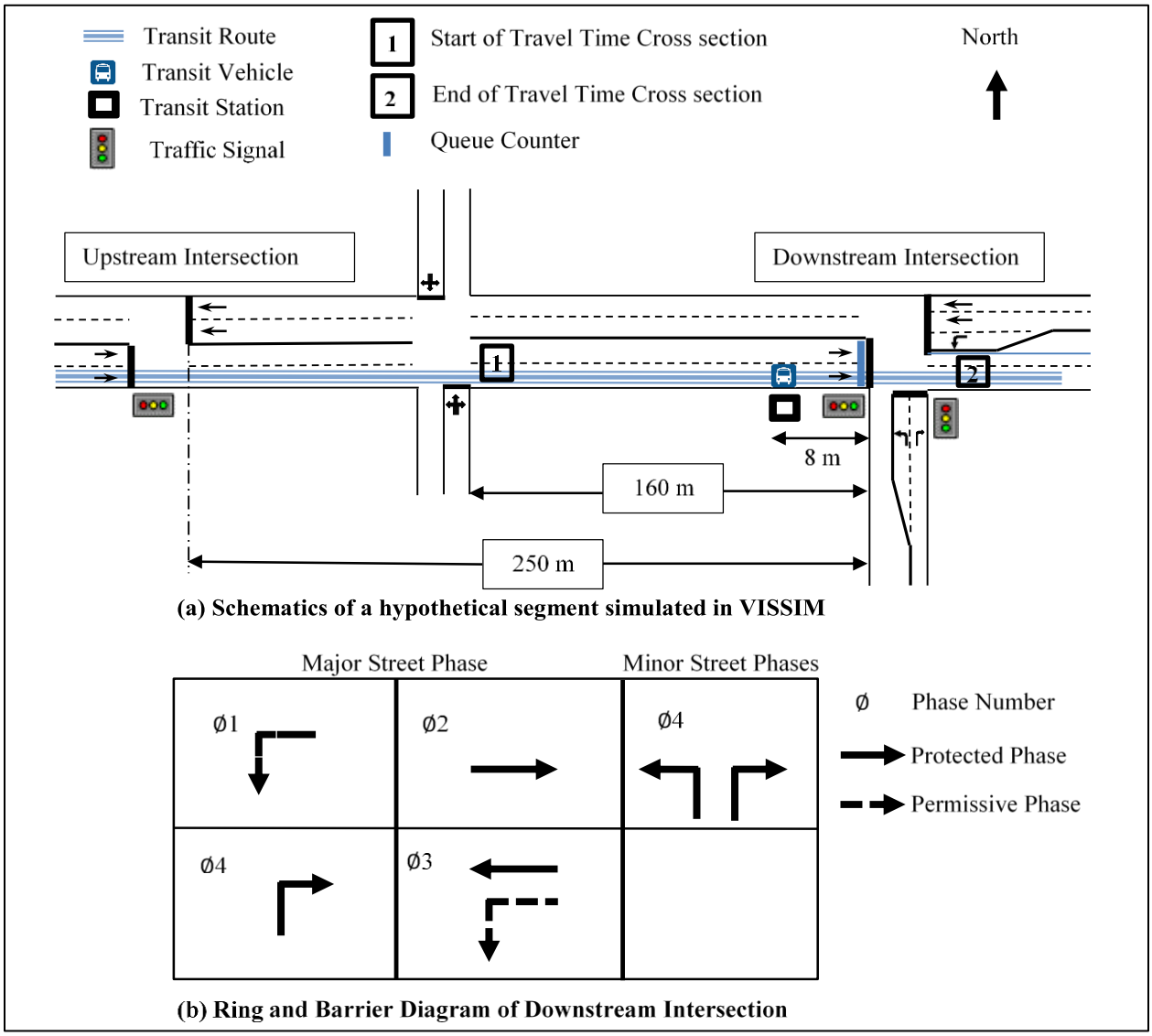

Figure 5-6: Hypothetical Arterial Segment Used for Validating the Proposed Models.

A transit route runs eastbound on the segment and serves the near-sided station at the downstream intersection. This route is served by buses which have a headway of 15 minutes corresponding to the shortest headway scheduled for GRT routes. The 15 minute headway provides the maximum expected number of observations within a month of operation. It also ensures that the interval between the buses arriving at the intersections is large enough to exclude the effects of bus bunching.

The passenger demand at the transit station is assumed to follow a Poisson distribution with the mean arrival rate equal to 20 passengers per hour. 20 passengers per hour for boarding passengers represents the average number of boarding passengers observed from GRT's AVL/APC data. Alighting demand is set to 3% of the load on the bus (the number of passengers already on the bus is set to be 10 passengers).

One long simulation run, with a duration of 35 hours, was conducted, with a 30 minute warm up period. This simulation captured 138 transit trips (equivalent to the number of transit trip observations expected in an archived AVL/APC dataset during the peak hour over a one month period). The passenger vehicle demand simulated in the network is based on constant demand rates provided in Table 5-4.

Table 5-4: Passenger Vehicle Demand Input for the Simulated Network

Input No.	Volume (veh/hr)
Eastbound Through	2000
Westbound Through	1530
Westbound Left	100
Northbound Left	170
Northbound Right	230

The travel time measurement segment was defined, as indicated in Figure 5-6, to obtain the stopped delay incurred by the vehicles due to the downstream signalized intersection. The queue length at the downstream intersection was measured by placing a queue counter at the stop line. The queue was counted from the location of the queue counter to the most upstream vehicle on

the approach having a speed less than 10 km/hr. Figure 5-7 presents the histogram of the maximum queue length outputted from VISSIM.

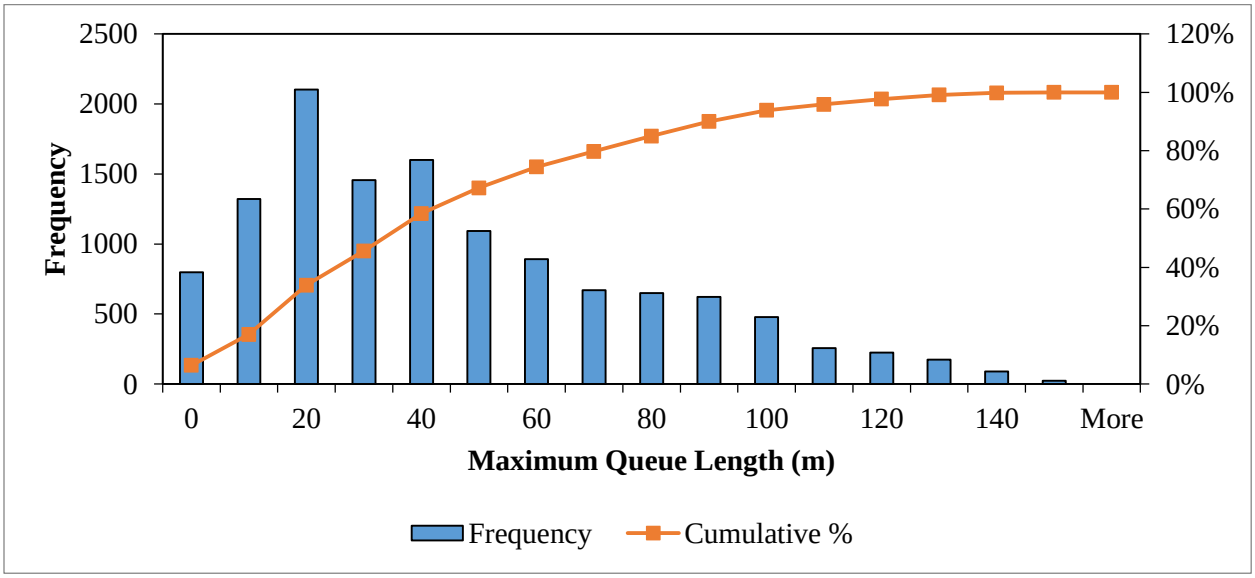

Figure 5-7: Histogram of Maximum Queue Length Obtained From the VISSIM Simulation

The signal timing was extracted from VISSIM to determine the red interval duration for the through lanes on the eastbound approach to the downstream intersection. The red interval duration, which varied as a result of the actuated protected left turn phase, ranged from 25 to 30 seconds, with a mean of 25.5 seconds. For approximately 80% of the cycles, the red interval duration was 25 seconds. The histogram of the red interval during the simulation is presented in Figure 5-8.

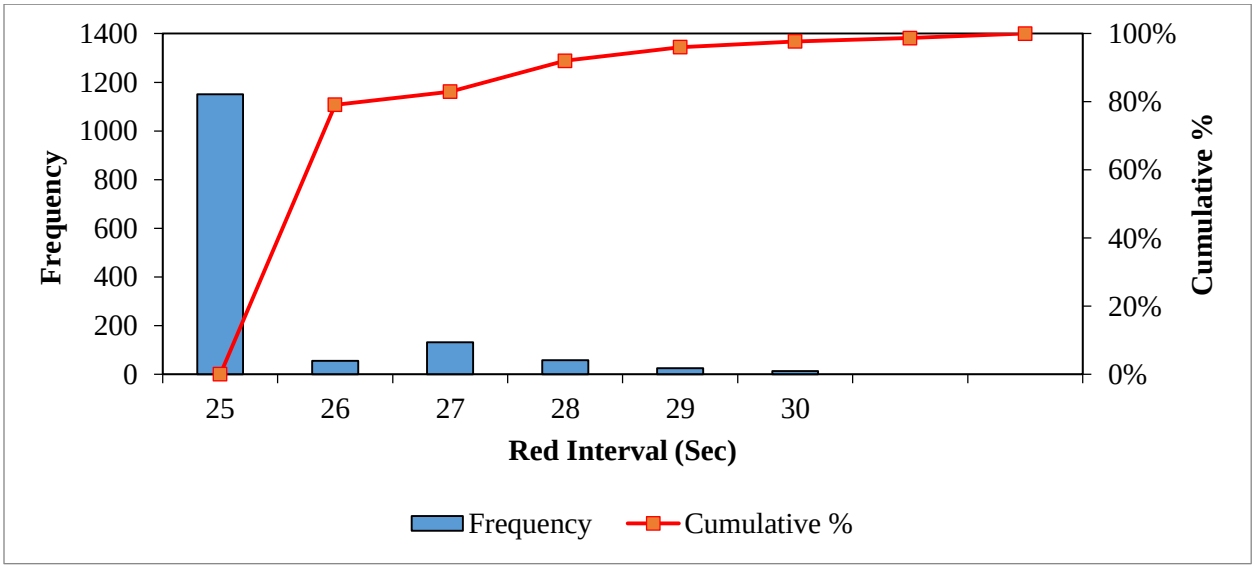

Figure 5-8: Histogram of the Red Interval Implemented in the Simulation

The transit vehicles' GPS coordinates, passenger activities, dwell times and waiting times (defined as the events that the transit vehicle stopped for reasons other than to allow passenger activity at the stop (PTV, 2011), i.e. it represents the *unscheduled* stop observations) were obtained from VISSIM. The stop events occurring within 10 meters of the transit station were labelled as *scheduled stops* and their corresponding dwell time was added to their waiting time. All other stop events were labeled as *unscheduled stops*. For each stop event, the total stopped time was recorded. For scheduled stop events, the total stopped time included dwell time and any additional waiting time as a result of the traffic signal operation.

The original dwell time estimation model was developed using the Region of Waterloo's AVL/APC data. Considering the simulation environment as another region, the dwell time model required recalibration since passenger behavior varies for different regions. Therefore, the dwell time estimation model was recalibrated based on passenger activity data obtained from VISSIM.

The number of boardings (*Nb*) and number of alightings (*Na*) from the simulation ranged from 1 to 19 and from 1 to 3, respectively. The distributions of transit vehicle dwell times as a function

of *Nb* and *Na* are shown in Figure 5-9(a) and (b) respectively. It can be observed that there is a substantially smaller variation in the simulated dwell times than in the field data (i.e. Figure 5-9).

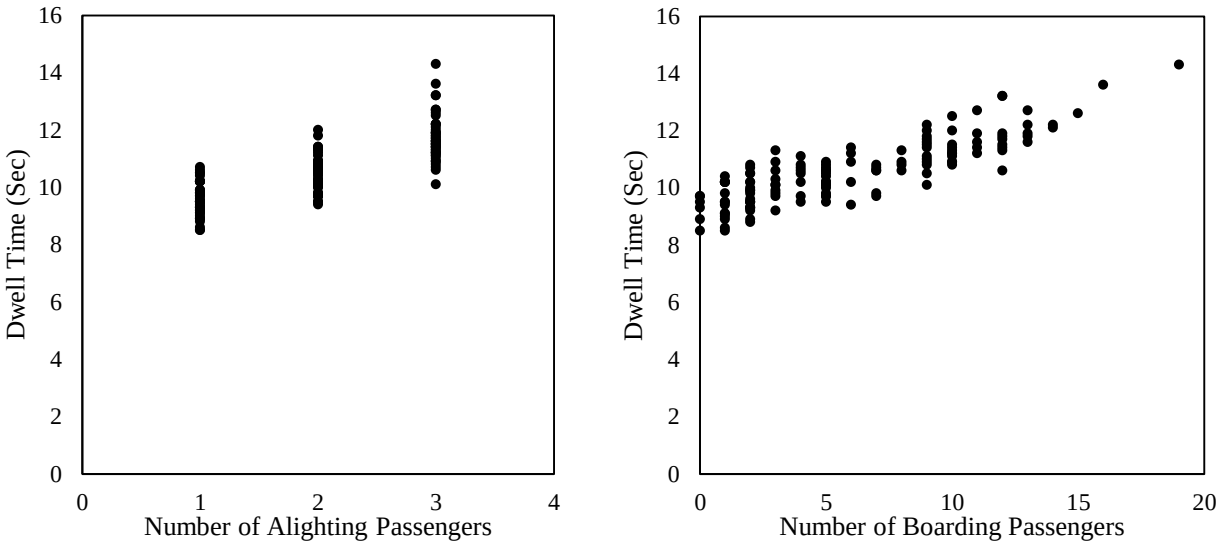

(a) Dwell Time as a Function of Number of Boarding Passengers

(b) Dwell Time as a Function of Number of Alighting Passengers

Figure 5-9: Variation of Simulated Dwell Time and Passenger Activity Data

Equation (38) presents the linear regression model developed for estimating the dwell time as a function of the number of boarding passengers (*Nb*). The number of alighting passengers was not statistically significant, likely as a result of the small range of values for *Na*, and was excluded from the model. The constant and intercept values were statistically significant and the model demonstrated a good fit to the data with $R^2 = 0.72$ as illustrated in Table 5-5.

$$\hat{DW} = 9.3 + 0.22Nb \quad \textbf{(38)}$$

Table 5-5: Dwell Time Estimation Regression Results Based on VISSIM Data

Regression Statistics					
Multiple R	0.85				
R Square	0.72				
Adjusted R Square	0.72				
Standard Error	0.57				
Observations	139.00				
Analysis of Variance (ANOVA)					
Source	*Degree of Freedom (df)*	*Sum of Squares (SS)*	*Mean Square (MS)*	*F-test*	*Significance F*
Regression	1.00	117.52	117.52	357.83	0.00
Residual	137.00	44.99	0.33		
Total	138.00	162.51			
	Coefficients	***Standard Error***	***t Stat***	***P-value***	
Intercept	9.30	0.08	110.53	0.00	
Nb	0.22	0.01	18.92	0.00	

Equation (38) is used to estimate the dwell time of each scheduled observation. Next the red interval duration is estimated based on the 95^{th} percentile of the difference between total stop time of the transit vehicles and the dwell time (estimated by Equation (38)).

Then all the near-sided scheduled observations were classified into one of the aforementioned 3 scenarios and their corresponding stopped delays were estimated. The stopped delay was estimated for all scheduled and unscheduled observations. The proposed BL was calibrated to the stop observations, presented in Figure 5-10. The observations under the BL were used to estimate the intersection's average delay and maximum queue length.

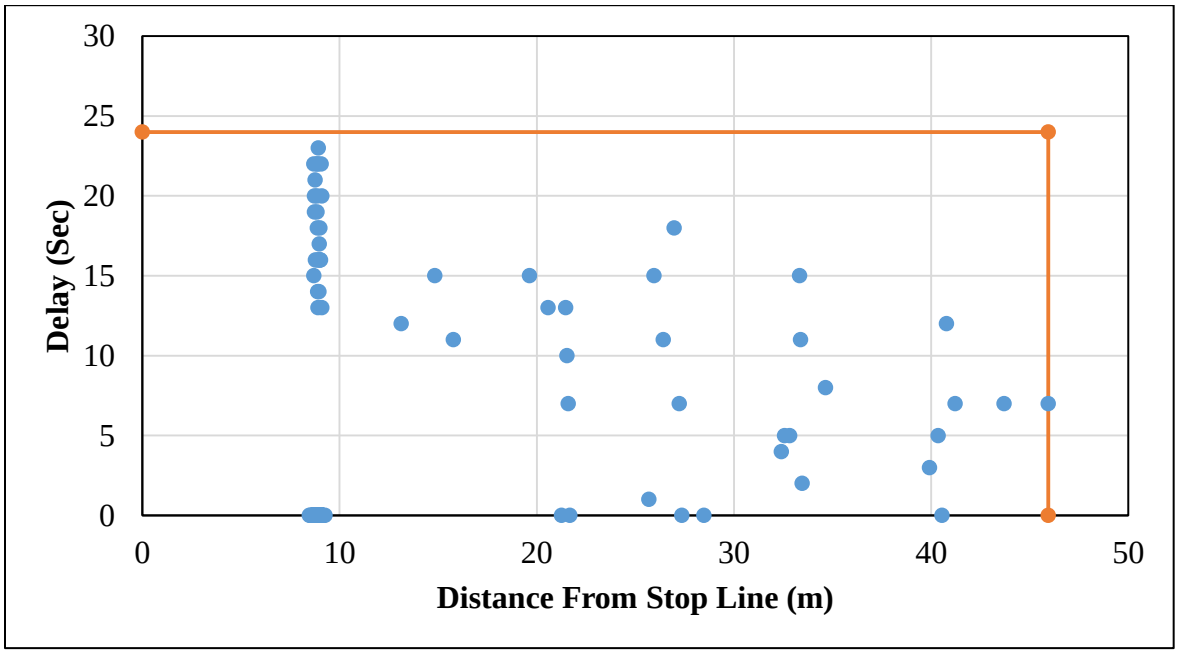

Figure 5-10: The Boundary Line Calibrated to the Simulated Scheduled and Unscheduled Stop Observations

The delay and queue length estimated by the proposed methodology were compared to the measurements extracted from VISSIM (Table 5-6).

Table 5-6: Comparison of Performance Measurements Obtained From VISSIM and Estimated By the Proposed Methodology.

Measure of Performance		Observed (VISSIM Output)	Estimated Using Proposed Method
Red Interval Duration* (seconds)	**Minimum**	25	--
	Mean	25.5	--
	Maximum	30	--
	95th percentile	28	24
Stopped Delay (seconds)	**Average**	3.70	3.8
	Standard Deviation	6.60	7.4
Queue Length (meters)	**Maximum**	47.9	45.9
Number of Trips (Vehicle)	**Total**	67368	138

* *Red interval duration for the through lanes on the eastbound approach to the downstream intersection*

The 95th percentile of the red interval durations was extracted from VISSIM. These data show that the simulated red interval durations ranged from 25 to 30 seconds with a 95th percentile of 28 seconds. The 95th percentile red interval duration estimated by the proposed method was 24 seconds representing a relative error of 14% compared to the 95th percentile red interval duration from the simulation.

A 2-tailed *t*- test at 95% confidence level was used to determine if the average stopped delay estimated by the proposed methodology was statically different from that measured in the simulation environment. The results indicate there is no evidence to conclude that the observed and estimated average stopped delays are different.

The t-test cannot be used to compare the observed and estimated queue length as the queue lengths are not a mean. Instead the relative error was used to evaluate the accuracy of the maximum queue estimation. The relative error of maximum queue length was found to be 4%. These results demonstrate that the proposed methodology could accurately estimate the downstream intersection's average stopped delay and maximum queue length.

These results indicate that, at least within the simulation environment, the proposed methodology can accurately estimate average stopped delay and maximum queue length. We recognize that the level of variation encountered within the real world may be larger than the variation exhibited by the simulation data and therefore these performance results should be interpreted as indicative rather than conclusive. In the next section, we examine the performance using field data.

5.3 Validation of the Maximum Queue length estimated by the Boundary Line Algorithm

Ten intersections were selected for which Yang and Hellinga's (2012) boundary line fitting method provided poor results and as a result, the performance measurements were erroneously estimated. The new proposed boundary line algorithm was applied to the data of these segments. Figure 5-11 shows for a sample intersection approach (for University at Hazel) a comparison of (A) the boundary line calibrated using Yang and Hellinga's (2012) BL algorithm, and (B) the boundary line calibrated using the BL fitting algorithm proposed in this thesis.

As mentioned previously there is a parking lot entrance 75m from the stop-line of University at Hazel intersection, as shown in Figure 5-12. The proposed BL algorithm correctly distinguished the stop observations that are caused by the traffic signal operations from those that are caused by other factors (e.g. buses having to stop as a result of vehicles entering or existing the parking lot) and estimates the maximum queue length as 35 meters. It should be noted that an independent measure of the maximum queue length was not available. Consequently, the ability to validate the accuracy of the proposed boundary line fitting algorithm was limited to a qualitative assessment of quality of the fit of the boundary line and the estimated queue length with respect to the plot of the stopped delay observations within a GIS. Despite these limitations, it appears that the proposed fitting algorithm is more robust than the algorithm from Yang and Hellinga (2012). The results from the remaining selected segments show similar improvements. The remaining plots are presented in Appendix C.

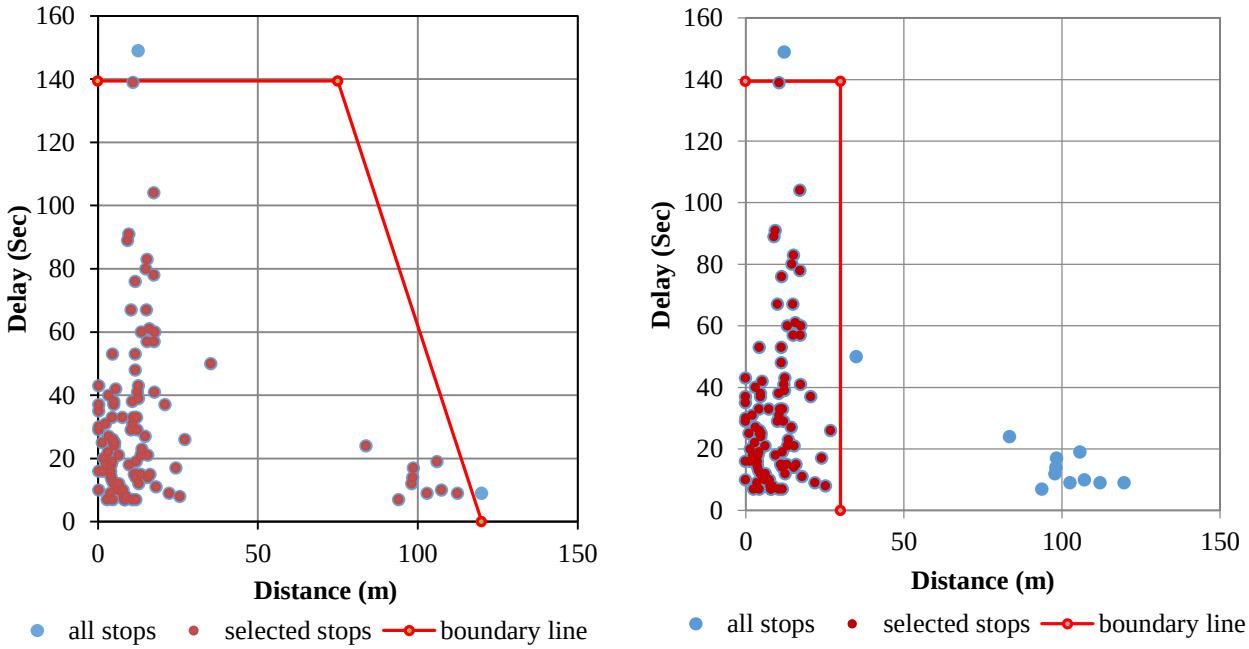

(A) Yang and Hellinga's Algorithm **(B) Proposed Algorithm**

Figure 5-11: Comparison of the BL Fitted to Stop Observations of University at Hazel Intersection

Figure 5-12: The Unscheduled Stop Observations Superimposed on Google Maps for University at Hazel Intersection [Source: Google Maps]

5.4 Validation using field data

The proposed methodology is applied to 5 intersections that are traversed by one transit route serving the far-sided transit station while another route serves the near-sided transit station. This permits a direct comparison of the performance measures obtained from buses that service a near-sided stop with performance measures obtained from buses that do not service the stop.

The results illustrate the ability of the proposed methodology to accurately estimate the average stopped delay and maximum queue length of the intersections.

The proposed model addresses the unique challenges of intersection approaches with near-sided transit stations and therefore AVL/APC data were extracted for intersections which were traversed by at least one transit route servicing a near-sided transit station and at least one transit route that did not service a near-sided transit station. Data were obtained for a total of five intersections that met these criteria. The boundary line fitting algorithm proposed in this thesis was used to fit a boundary line to the stopped delay of the *unscheduled* stop observations

obtained from the transit routes which did not service the near-sided transit station. The stop observations under the boundary line were used to estimate the average stopped delay and maximum queue length (essentially Yang and Hellinga's methodology is carried out with the boundary line fitting algorithm proposed in Section 4.3). These estimates are considered as the benchmark.

The methodology proposed in this study scheduled stop observations was applied to the AVL/APC data obtained from the transit routes which did service the near-sided transit station. Both transit routes traverse the same intersection approach and therefore we expect the estimates of stopped delay and queue length (which are intended to be an estimate of the delays and queue lengths experienced by general purpose vehicles) obtained from the proposed method to be similar to the benchmark estimates.

Table 5-7 provides the average stopped delay, HCM Level of Service[6], standard deviation of stopped delay, maximum queue length and number of transit trips from the benchmark method and from the proposed method for all five intersection approaches. The benchmark results indicate that average stopped delays range from approximately 1 second to 25 seconds representing a range in LOS from A to C. The results from the proposed method provide a range of stopped delays from 1 to 16 seconds and provide the same LOS for each intersection as the benchmark method. A paired *t*-test (at 95% confidence level) was conducted to determine if the average stopped delays estimated by the two methods were statistically different. For all five intersections, the calculated t-value is less than the critical value of 1.96 indicating that there is not enough evidence to suggest that the two methods provide statistically different estimates of average delay.

[6] The Highway Capacity Manual defines LOS on the basis of the average vehicle control delay. Control delay is generally considered to be 1.3 times greater than stopped delay and this is the conversion used to establish the LOS in Table 2.

Relative error was used to measure the accuracy of the queue length estimated. The maximum queue lengths calculated are based on a single value and unlike the mean that represents the whole distribution, they are prone to extreme variations. This explains the significant differences between the maximum queue lengths of some segments estimated from the two methods which ranges from 3% to 33%.

Table 5-7: Comparison of Estimates from Proposed Method With Benchmark Estimates

		Charles at Benton	Charles at Cedar	Columbia at Albert	Columbia at Hagey	Courtland at Stirling
Benchmark	**Avg Stopped Delay (Sec)**	7.16	2.10	8.45	10.64	19.77
	LOS	A	A	B	B	C
	Std of Delay (Sec)	11.92	5.80	9.84	16.4	24.89
	Max. Queue (m)	53.00	30.00	112.00	90.00	56.00
	Number of trips	390	390	142	457	194
Proposed Method	**Avg Stopped Delay (Sec)**	7.22	4.33	9.58	14.64	15.54
	LOS	A	A	B	B	C
	Std of Delay (Sec)	13.11	8.10	18.92	23.37	22.28
	Max. Queue (m)	48.00	40.00	115.00	98.00	58.00
	Number of Trips	244	295	142	457	244
	t_{calc} for Delay	0.02	0.90	0.32	0.96	0.81
	$t_{critical}$ for Delay	1.96	1.96	1.96	1.96	1.96
	Relative Error of Queue Length	9%	33%	3%	9%	4%

Chapter 6
Ranking Signalized Intersections

The real world application of ranking signalized intersections on the basis of the performance measures estimated from the proposed methodology is demonstrated in this Chapter. Three months of AVL/APC data were obtained from the Grand River Transit (GRT) agency (2013/9-2013/11). The data were filtered to only include the pm peak period (4:30 pm to 6:00 pm) for non-holiday weekdays from in-service transit trips. The proposed methodology was used to estimate intersection operational performance measures on the basis of the archived AVL/APC for the signalized intersections within the road network in the Region of Waterloo. Then the intersections are prioritized based on the estimated average stopped delay, 90^{th} percentile of stopped delay, percentage of trips that incur delay and maximum queue length.

The portions of transit routes containing far-sided transit stations have been segmented as part of previous work. There are 800 far-sided segments available for analysis. However, due to time constraints only 20 intersections with near-sided transit stations have been segmented. The proposed methodology is applied to all the available near-side and far-side segments.

The ranking process is a subjective process. Agencies may define different criteria and weighting factors to prioritize intersections based on the objectives they want to achieve. Here intersection approaches are ranked using the procedure described in Section 4.6. Equal weights (1/4) have been assigned to each factor (i.e. average stopped delay, 90^{th} percentile of stopped delay, percentage of trips that incur delay and maximum queue length). Equation (39) is used to rank the intersection approaches.

The worst 20 (worst performing) intersection approaches are identified in Table 6-1. The complete list of ranked intersection approaches is provided in Appendix D.

$$RI = \frac{1}{4}\left(\frac{WT_j}{WT_{MAX}}\right) + \frac{1}{4}\left(\frac{WSD_j}{WSD_{MAX}}\right) + \frac{1}{4}\left(\frac{WND_j}{WND_{MAX}}\right) + \frac{1}{4}\left(\frac{Q_j}{Q_{MAX}}\right) \quad \textbf{(39)}$$

where

RI = Ranking index for intersection approach j

WT_j = Weighted percentage of transit trips incurred delay at intersection approach j

WSD_j = Weighted average stopped delay for intersection approach j (seconds/trip)

WND_j = Weighted 90th percentile stopped delay for intersection approach j (seconds/trip)

WT_{MAX} = max{WT_j, j = 1,2,3,…,N}

WSD_{MAX} = max{WSD_j, j = 1,2,3,…,N}

WND_{MAX} = max{WND_j, j = 1,2,3,…,N}

Q_j = Maximum Queue length for intersection approach j

Q_{MAX} = Max{Q_j, j = 1,2,3,…,N}

i = Index of the routes

j = Index of the intersections approach being ranked

N = Number of Intersection approaches

Table 6-1: Worst 20 Signalized Intersection Approaches in Waterloo Region Ranked Based on Equation (39)

Downstream Intersection Name	Count of Route	Total Number of Trips	Weighted Average Stopped Delay (Sec)	Weighted 90th Percentile Delay (Sec)	Weighted Percentage of Trips with Delay	Max of Queue Length (m)	Index	LOS
HESPELER_AT_Eagle_And_Pinebush	3	687	42.94	79.76	0.67	349	0.90	E
HOMER_WATSON_AT_ManitouAndDoon_Village	4	506	31.14	69.04	0.69	224	0.71	D
FOUNTAIN_AT_Shantz_Hill	3	521	27.47	51.95	0.70	266	0.68	D
FAIRWAY_AT_Lackner	1	145	31.99	96.80	0.58	99	0.66	D
VICTORIA_AT_Natchez	1	141	36.61	75.00	0.75	50	0.65	D
FRANKLIN_AT_Pinebush	3	393	17.70	52.51	0.50	370	0.64	C
KING_AT_Fountain	1	142	19.84	43.20	0.76	268	0.63	C
HESPELER&WATER_AT_Coronation_And_Dundas	6	1906	27.72	77.00	0.53	170	0.62	D
COURTLANDAndFAIRWAY_AT_Manitou	1	202	24.04	54.00	0.81	157	0.62	C
WESTMOUNT_AT_Glasgow	1	296	14.76	40.00	0.54	365	0.60	B
OTTAWA_AT_Homer_Watson	6	1601	26.47	72.85	0.52	163	0.60	C
FRANKLIN_AT_Savage	1	147	31.54	73.00	0.67	45	0.59	D
WATER_AT_Main	2	282	25.90	48.58	0.73	142	0.58	C
WESTMOUNT_AT_Williamsburg	1	290	27.62	66.00	0.78	35	0.57	D
FISCHER_HALLMAN_AT_Columbia	2	743	23.86	51.96	0.68	155	0.57	C
NORTHFIELD_AT_Kraus	1	297	29.82	72.00	0.67	34	0.57	D
HOMER_WATSON_AT_Conestoga_College	5	664	22.82	65.52	0.52	176	0.57	C
HOMER_WATSON_AT_Bleams	3	557	21.86	62.05	0.57	175	0.56	C
NORTHFIELD_AT_Skylark	1	285	31.02	69.00	0.66	35	0.56	D
FRANKLIN_AT_Elgin_And_Saginaw	2	289	25.44	65.73	0.57	125	0.56	C

Note:

- The blue shaded rows represent the 7 worse performing intersection approaches that appear in the top 20 regardless of the weighting factors values.

Figure 6-1, graphs the ranking index calculated using Equation (39) versus the rank of the intersection approaches. Figure 6-1, illustrates that the relationship between the ranking index and intersection's ranking is not a linear relationship. In fact merely a handful of intersection approaches are clearly ranking higher than the proceeding intersection approach.

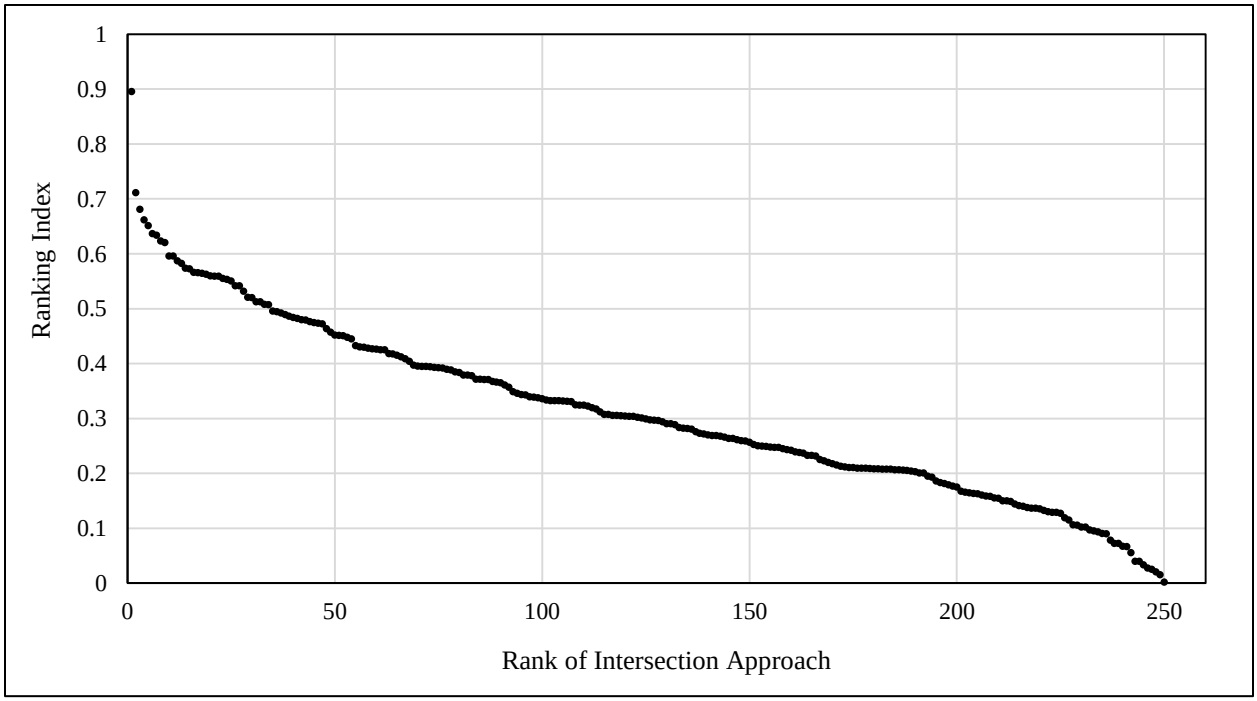

Figure 6-1: Ranking Index vs. Rank of Intersection Approaches

In order to acquire a better understanding of the sensitivity of the ranking results to the weighting factors, intersection approaches are ranked based on each factor separately. Table 6-2 to Table 6-4 summarizes the top 20 worse performing intersection approaches based on average stopped delay, 90^{th} percentile of stopped delay, and percentage of trips that incurred stopped delay, respectively.

The survey of the 4 tables (Table 6-1-Table 6-4) reveal that 7 intersections consistently appear in the worse 20 intersection approaches. The 7 intersections are shaded in blue in the following tables and are listed below:

1. Hespeler at Eagle and Pinebush
2. Homer-Watson at Manitou and Doon Village
3. Victoria at Natchez
4. Franklin at Savage
5. Westmount at Williamsburg
6. Northfield at Kraus
7. Northfield at Skylark

These 7 intersections will be identified as within the top 20 worst performing intersection approaches regardless of the value of the weighting factors used. The unscheduled stop observations of the buses from these intersections are superimposed on Google maps in Appendix E. The figures in Appendix E provide a visual verification of the performance of these intersection approaches.

Table 6-2: Worst 20 Signalized Intersection Approaches in Waterloo Region Ranked Based on Weighted Average Stopped Delay

Downstream Intersection Name	Count of Route	Total Number of Trips	Weighted Average Stopped Delay (Sec)	Weighted 90th Percentile Delay (Sec)	Weighted Percentage of Trips with Delay	Max of Queue Length (m)	Index	LOS
HESPELER_AT_Eagle_And_Pinebush	3	687	42.9	79.8	0.7	349	1.0	E
VICTORIA_AT_Natchez	1	141	36.6	75.0	0.8	50	0.9	D
FAIRWAY_AT_Lackner	1	145	32.0	96.8	0.6	99	0.7	D
FRANKLIN_AT_Savage	1	147	31.5	73.0	0.7	45	0.7	D
HOMER_WATSON_AT_Manitou&DoonVillage	4	506	31.1	69.0	0.7	224	0.7	D
NORTHFIELD_AT_Skylark	1	285	31.0	69.0	0.7	35	0.7	D
NORTHFIELD_AT_Kraus	1	297	29.8	72.0	0.7	34	0.7	D
KING_AT_Farmers_MarketHwy_85_SB_Ramp	1	148	28.2	68.3	0.7	39	0.7	D
HESPELER &WATER_AT_Coronation&Dundas	6	1906	27.7	77.0	0.5	170	0.6	D
WESTMOUNT_AT_Williamsburg	1	290	27.6	66.0	0.8	35	0.6	D
FOUNTAIN_AT_Shantz_Hill	3	521	27.5	52.0	0.7	266	0.6	D
OTTAWA_AT_Homer_Watson	6	1601	26.5	72.8	0.5	163	0.6	C
WATER_AT_Main	2	282	25.9	48.6	0.7	142	0.6	C
FRANKLIN_AT_Elgin_And_Saginaw	2	289	25.4	65.7	0.6	125	0.6	C
FAIRWAY_AT_Wilson	4	842	24.4	62.9	0.6	130	0.6	C
COURTLANDAndFAIRWAY_AT_Manitou	1	202	24.0	54.0	0.8	157	0.6	C
FISCHER_HALLMAN_AT_Columbia	2	743	23.9	52.0	0.7	155	0.5	C
FRANKLIN_AT_Can_Amera	1	147	23.8	46.0	0.8	93	0.5	C
KING_AT_Weber_Wool	1	148	23.4	57.0	0.7	81	0.5	C
DUNDAS_AT_Beverly	1	246	22.9	60.0	0.6	88	0.5	C

Table 6-3: Worst 20 Signalized Intersection Approaches in Waterloo Region Ranked Based on 90th Percentile Stopped Delay

Downstream Intersection Name	Count of Route	Total Number of Trips	Weighted Average Stopped Delay (Sec)	Weighted 90th Percentile Delay (Sec)	Weighted Percentage of Trips with Delay	Max of Queue Length (m)	Index	LOS
FAIRWAY_AT_Lackner	1	145	31.99	96.80	0.58	99	1.0	D
KING_AT_Tu_Lane	1	245	21.10	83.00	0.35	158	0.9	C
HESPELER_AT_Eagle_And_Pinebush	3	687	42.94	79.76	0.67	349	0.8	E
HESPELER_&_WATER @Coronation_&_Dundas	6	1906	27.72	77.00	0.53	170	0.8	D
VICTORIA_AT_Natchez	1	141	36.61	75.00	0.75	50	0.8	D
FRANKLIN_AT_Savage	1	147	31.54	73.00	0.67	45	0.8	D
OTTAWA_AT_Homer_Watson	6	1601	26.47	72.85	0.52	163	0.8	C
NORTHFIELD_AT_Kraus	1	297	29.82	72.00	0.67	34	0.7	D
HOMER_WATSON_AT_ManitouAndDoon_Village	4	506	31.14	69.04	0.69	224	0.7	D
NORTHFIELD_AT_Skylark	1	285	31.02	69.00	0.66	35	0.7	D
KING_AT_Farmers_MarketAndHwy_85_SB_Ramp	1	148	28.22	68.30	0.67	39	0.7	D
WESTMOUNT_AT_Williamsburg	1	290	27.62	66.00	0.78	35	0.7	D
FRANKLIN_AT_Elgin_And_Saginaw	2	289	25.44	65.73	0.57	125	0.7	C
HOMER_WATSON_AT_Conestoga_College	5	664	22.82	65.52	0.52	176	0.7	C
LANCASTER_AT_Guelph	1	144	22.83	64.20	0.50	44	0.7	C
FAIRWAY_AT_Wilson	4	842	24.43	62.87	0.58	130	0.6	C
HOMER_WATSON_AT_Bleams	3	557	21.86	62.05	0.57	175	0.6	C
UNIVERSITY_AT_Lincoln	1	296	17.78	61.00	0.45	256	0.6	C
DUNDAS_AT_Beverly	1	246	22.85	60.00	0.59	88	0.6	C
WEBER_AT_Columbia	1	142	13.70	59.90	0.26	33	0.6	B

Table 6-4: Worst 20 Signalized Intersection Approaches in Waterloo Region Ranked Based on Weighted Percentage of Transit Trips with Delay

Downstream Intersection Name	Count of Route	Total Number of Trips	Weighted Average Stopped Delay (Sec)	Weighted 90th Percentile Delay (Sec)	Weighted Percentage of Trips with Delay	Max of Queue Length (m)	Index	LOS
COURTLANDAndFAIRWAY_AT_Manitou	1	202	24.0	54.0	0.8	157	1.0	C
ERBSVILLE_AT_Laurelwood	1	286	22.2	42.0	0.8	64	1.0	C
WESTMOUNT_AT_Williamsburg	1	290	27.6	66.0	0.8	35	1.0	D
FRANKLIN_AT_Can_Amera	1	147	23.8	46.0	0.8	93	1.0	C
KING_AT_Fountain	1	142	19.8	43.2	0.8	268	0.9	C
VICTORIA_AT_Natchez	1	141	36.6	75.0	0.8	50	0.9	D
WATER_AT_Main	2	282	25.9	48.6	0.7	142	0.9	C
COURTLAND_AT_Benton	1	290	18.9	38.0	0.7	63	0.9	C
VICTORIA_AT_Edna	1	141	14.5	32.0	0.7	47	0.9	B
FOUNTAIN_AT_Shantz_Hill	3	521	27.5	52.0	0.7	266	0.9	D
HOMER_WATSON_AT_ManitouAndDoon_Village	4	506	31.1	69.0	0.7	224	0.8	D
FISCHER_HALLMAN_AT_Columbia	2	743	23.9	52.0	0.7	155	0.8	C
HESPELER_AT_Eagle_And_Pinebush	3	687	42.9	79.8	0.7	349	0.8	E
FRANKLIN_AT_Savage	1	147	31.5	73.0	0.7	45	0.8	D
NORTHFIELD_AT_Kraus	1	297	29.8	72.0	0.7	34	0.8	D
KING_AT_Farmers_MarketAndHwy_85_SB_Ramp	1	148	28.2	68.3	0.7	39	0.8	D
PARKHILL_AT_George	1	97	17.4	38.0	0.7	145	0.8	C
NORTHFIELD_AT_Skylark	1	285	31.0	69.0	0.7	35	0.8	D
KING_AT_Weber_Wool	1	148	23.4	57.0	0.7	81	0.8	C
HIGHLAND_AT_Highland_Cres	1	139	20.3	40.0	0.7	30	0.8	C

Chapter 7
Conclusion and Recommendations

In this thesis a methodology is proposed to estimate the average stopped delay and maximum queue length at signalized intersections with near-sided transit stations using archived AVL/APC data.

The performance of the proposed methodology was evaluated through a simulation study which demonstrated that the proposed methodology has the ability to estimate intersection performance measures with accuracy comparable to microscopic simulation. The proposed model was also applied to field data for five signalized intersections. The results confirm that the proposed model is able to effectively estimate average delay and queue length for signalized approaches containing near-side transit stations. Lastly, the amendment to the boundary line algorithm proved to perform better in detecting the extent of the predominant queue. The algorithm is able to distinguish between stopped delays caused by the traffic signal and other causes. Furthermore, the proposed method appears to be more robust than the method proposed by Yang and Hellinga (2012).

The proposed methodology has only been validated for transit routes making through movements. Transit vehicles making turning movements at the intersections may experience additional delays as a result of yielding to pedestrians or opposing traffic (e.g. when making left turns during a permitted phase). The applicability of the proposed method to intersections where transit vehicles make turning movements requires further investigation.

The methodology assumes that no layover time is scheduled at the near-sided transit stations. If layover time is scheduled and is not explicitly labeled in the AVL/APC data, this may introduce errors in the model estimates. Consequently, it is recommended that the proposed method not be applied to intersections with near-sided transit stations for which layover time is scheduled.

The proposed method has the potential to be implemented completely automatically. Currently processing of data through GIS involves manual work. This proves to be very time consuming when evaluating the entire network. As part of future work, it is suggested the process be automated.

The proposed ranking index evaluated the performance of intersection approaches with no special provision given to the different turning movements made at a given intersection approach when multiple bus routes traverse that approach. However different turning maneuvers have disproportional impacts on the delay experienced at the intersection. The ranking and impacts of various turning movements at a given intersection need to be further researched.

References

Adamski, A., Probabilistic Model of Passenger Service Processes at Bus Stops. Transportation Research, Vol. 26B, No. 4, 1992, pp. 253-259.

Almohanna,I. Application of Transit AVL/APC Data for Network Wide Monitoring of the Performance of Signalized Intersections. University of Waterloo, 2014.

Benekohal R.F., Y.M. Elzohairy and J.E. Saak. A comparison of Delay from HCS, Synchro, PASSER II, PASSER IV and CORSIM for an Urban Arterial. Presented at 81th Annual Meeting of the Transportation Research Board, Washington, D.C., 2002.

Benekohal, R. F., Zhao, W., Lu, Y., and Wang, L. _1992_. "Real-time delay measurement and intersection analysis system." 4th Int. Conf. on Microcomputers in Transportation, ASCE, New York, 285–296.

Click, S.M. (2003) "Variables Affecting the Stopped to Control Delay at Signalized Intersection". Compendium of papers of the 82nd Annual TRB Conference held Jan. 12 – 16, 2003 in Washington, DC.

Dueker, K. J., T. J. Kimpel, and J. G. Strathman. Determinants of Bus Dwell Time. Journal of Public Transportation, Vol. 7, No. 1, 2004, pp. 21-40.

Farhan, A., A. Shalaby, and T. Sayed. Bus Travel Time Prediction Using AVL and APC. Applications of Advanced Technologies in Transportation, ASCE, 2002, pp. 616-623.

Ferna´ndez, R., del Campo, M., and Swett, C., 2009. Data collection and calibration of passenger service time models for the Transantiago system. European Transport Conference, The Netherlands, 6–8 October

Furth, P. G., B. Hemily, T. H. J. Muller, and J. G. Strathman. Uses of Archived AVL-APC Data to Improve Transit Performance and Management: Review and Potential. TCRP Web Document 23, Project H-28, 2003.

Grand River Transit. Fast Facts, 2011, http://www.grt.ca/en/aboutus/fastfacts.asp. Accessed Jan. 2013.

Golani, H. Use of Archived bus location, dispatch, and ridership data for transit analysis. In Transportation Research Record Journal of the Transportation Research Board, No. 1992, TRB of the National Acedemies, Washington, D.C., 2007, pp. 101–112.

Highway Capacity Manual 2010. TRB, National Research Council, Washington D.C., 2010.

Hunter, M., Nachtsheim, C., Neter, J., & Li, W. (2005). Applied Linear Statistical Models.McGraw-Hill Irwin.

Kim, W. An Improved Bus Signal Priority System for Netwroks with Nearside Bus Stops. Texas A&M university, 2004.

Ko, J., H. Micheal and G. Randall. (2008) "Measuring control delay components using second-by-second GPS speed data" Journal of Transportation Engineering, Vol. 134, Issue 8, 2008, pp. 338-346

Kraft, W. and T. Bergen. Evaluation of Passenger Service Times for Street Transit Systems. In Transportation Research Board 505, TRB, National Research Council, Washington, D.C., 1974, pp. 13-20

Kwong, K., R. Kavaler, R. Rajagopal, and P. Varaiya. Arterial Travel Time Estimation Based on Vehicle Reidentification Using Wireless Sensors. Transportation Research, Part C, forthcoming.

Kittelson & Associates, United States. Federal Transit Administration, Transit Cooperative Research Program, & Transit Development Corporation. (2013). Transit Capacity and Quality of Service Manual, 3rd edition, Ch. 6, pp.66-69. Transportation Research Board.

Liao, C., and H. Liu. Development of Data-Processing Framework for Transit Performance Analysis. In Transportation Research Record Journal of the Transportation Research Board, No. 2143, TRB of the National Acedemies, Washington, D.C., 2010, pp. 34–43.

Lin, W. Quantifying delay reduction to buses with signal priority treatment in mixed mode operation. In Transportation Research Record Journal of the Transportation Research Board, No. 1811, TRB of the National Acedemies, Washington, D.C., 2002, pp.100–106.

Lin, T. M., and N. H. M. Wilson. Dwell Time Relationships for Light Rail Systems. In Transportation Research Record 1361, TRB, National Research Council, Washington, D.C., 1992, pp. 287–295.

Liu, H., W. Lin, and C. Tan. Operational Strategy for Advanced Vehicle Location System–Based Transit Signal Priority. Journal of Transportation Engineering: ASCE, Vol. 133, No. 9, pp. 513-522.

Mandelzys, M. and B. Hellinga (2010) "Automatically identifying the causes of bus transit schedule adherence performance issues using AVL/APC archived data" Transportation Research Record 2143: Journal of the Transportation Research Board, Transportation Research Board of the National Academies, Washington, D.C. 2010, pp. 9 – 15.

Marshall, L. F., H. S. Levinson, L. C. Lennon, and C. Cheng. Bus Service Times and Capacities in Manhattan. In Transportation Research Record 1266, TRB, National Research Council, Washington, D.C., 1990, pp. 189–196.

Mazloumi, E., S. Moridpour and H. Mohsenian (2010) "Delay function for signalized intersections in traffic assignment models" Journal of Urban Planning and Development, Vol.136, Issue 1, 2010, pp. 67-74.

Mousa, R. Analysis and Modeling of Measured Delays at Isolated Signalized Intersections." Journal of Transportation Engineering-ASCE, Vol.128, No. 4, 2002, pp. 347 – 354.

Mulandi, J., A. Stevanovic, and P. T. Martin. Cross-Evaluation of Signal Timing Optimized by Various Traffic Simulation and Signal Optimization Tools. In Transportation Research Record Journal of the Transportation Research Board, No. 2192, TRB of the National Acedemies, Washington, D.C., 2010, pp.147–155.

Olszewski, P. Overall Delay, Stopped Delay, and Stops at Signalized Intersections. Journal of Transportation Engineering-ASCE, Vol.119, No. 6, 1993, pp. 835 – 852.

Powell, W. and Y. Sheffi. A Probabilistic Model of Bus Route Performance. Transportation Science, Vol. 17, No. 4, 1983, pp. 376-404.

PTV, A. (2011) VISSIM 5.30-05 User Manual. Kurlsruhe, Germany, pp.249-256.

Quiroga, C., and Bullock, D. _1999_. "Measuring control delay at signalizedintersections." J. Transp. Eng., 125_4_, 271–280.

Rajbhandari, R., S. I. Chien, and J. R. Daniel. Estimation of Bus Dwell Times With Automatic Passenger Counter Information. In Transportation Research Record 1841, TRB, National Research Council, Washington, D.C., 2003, pp. 120–127.

Seneviratne, P. N. Simulation of Fixed Route Bus Travel Time. Journal of Advanced Transportation Engineering, Vol. 22, No. 1, 1998, pp. 39–53.
Sharma, A., D. M. Bullock, and J. A. Bonneson. Input-Output and Hybrid Techniques for Real-Time Prediction of Delay and Maximum Queue Length at Signalized Intersections. In Transportation Research Record Journal of the Transportation Research Board, No. 2035, TRB of the National Acedemies, Washington, D.C., 2007, pp.69–80.

Skabardonis, A., and N. Geroliminis. Real-Time Estimation of Travel Times on Signalized Arterials. 16th International Symposium on Transportation and Traffic Theory, University of Maryland, College Park, 2005, pp. 387–406.

Washburn, S. S., and N. Larson. Signalized intersection delay estimation: Case study comparison of TRANSYT-7F, synchro and HCS. Institute of Transportation Engineers. ITE Journal, Vol. 72, No. 3, 2002, pp. 30-35.

Alejandro Tirachini, Bus dwell time: the effect of different fare collection systems, bus floor level and age of passengers. Transportmetrica A: Transport Science, Vol. 9, Issue. 1, 2013

Yang, F., and B. Hellinga. Estimating intersection delays to transit vehicles using archived AVL/APC data. . Presented at 91th Annual Meeting of the Transportation Research Board, Washington, D.C., 2012.

Yang, F. Estimating Bus Delay at Signalized Intersections from Archived AVL/APC Data. University of Waterloo, 2012.

York, I.O., 1993. Factors affecting bus-stop times. Transport Research Laboratory, Project Report 2, Crowthorne.

Appendix A- Model Development

Investigation of the data revealed that dwell time follows a Poisson distribution, when the passenger activities are grouped based on the number of passengers boarding and alighting. Easy Fit software was used to determine which distribution best fit the data. Easy Fit uses the Kolmogorov-Smirnov test and the Anderson Darling test to evaluate the goodness of fit of a distribution to the data. For all the passenger activity groups, the Poisson distribution was ranked as first or second best fit to the data. The result obtained from Easy Fit is presented below.

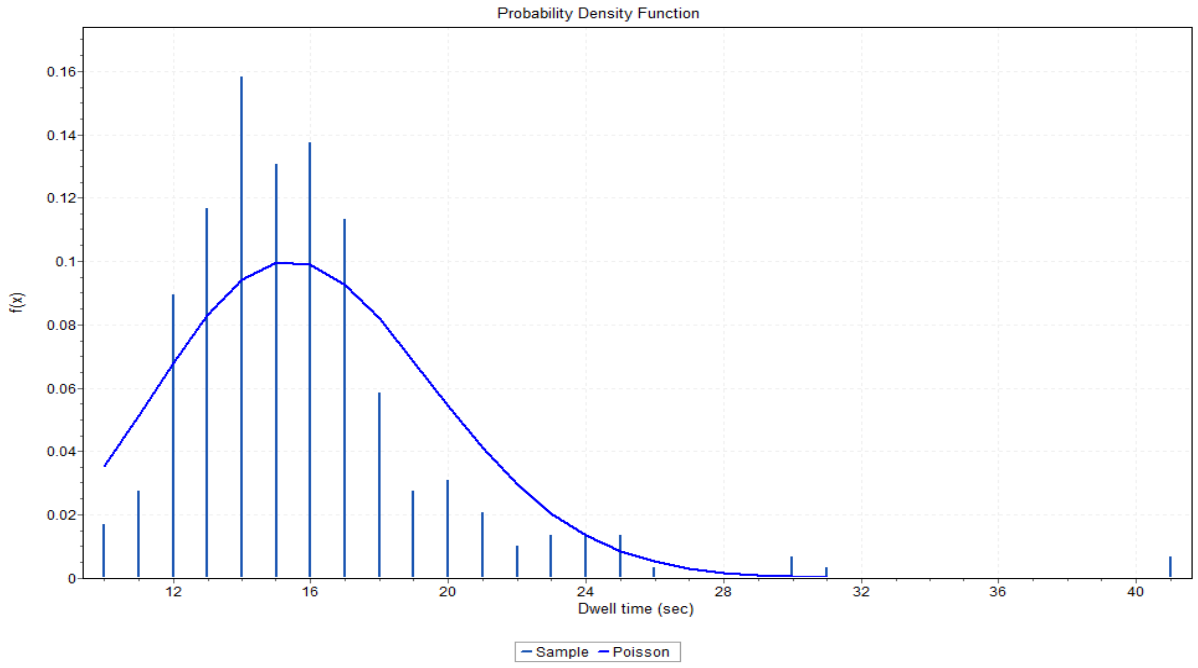

Figure A-1: Poisson distribution Fitted to the Dataset including only Observations with 1 passenger alighting

#	Distribution	Kolmogorov Smirnov		Anderson Darling	
		Statistic	Rank	Statistic	Rank
5	Poisson	0.15582	1	9.4749	1
4	Neg. Binomial	0.15642	2	9.5292	2
1	D. Uniform	0.24104	3	88.397	3
2	Geometric	0.50303	4	91.396	4
3	Logarithmic	0.66143	5	161.33	5
6	Bernoulli	No fit (data max > 1)			
7	Binomial	No fit			
8	Hypergeometric	No fit			

Figure A-2: Goodness of Fit of the Distributions Fitted to the Dataset including only Observations with 1 passenger lighting

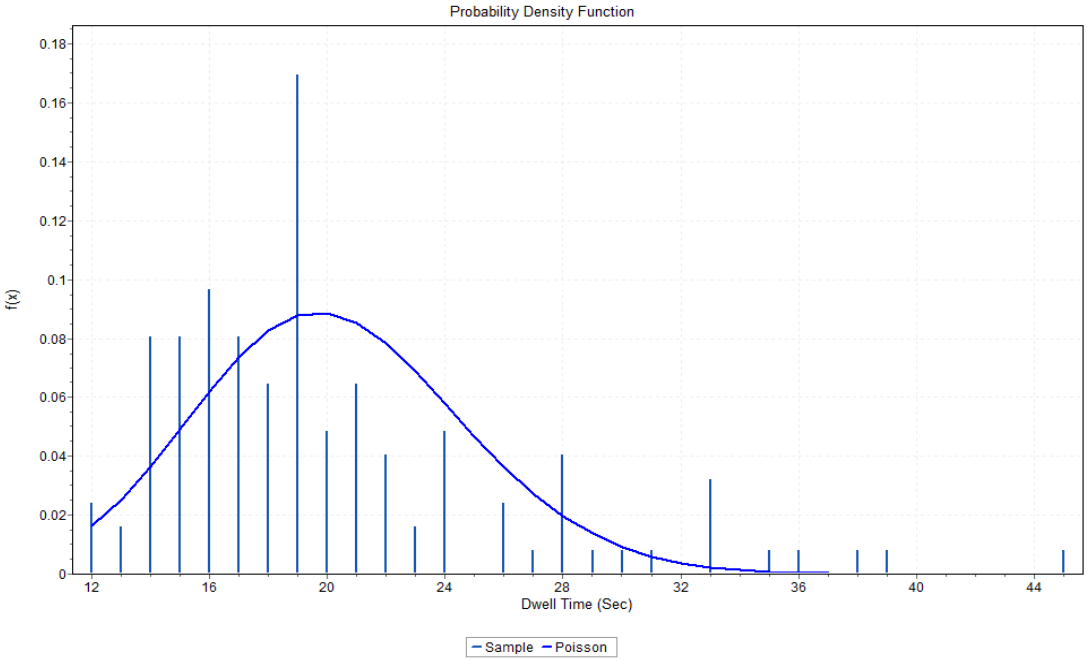

Figure A-3: Poisson distribution Fitted to the Dataset including only Observations with 2 passenger lighting

#	Distribution	Kolmogorov Smirnov		Anderson Darling	
		Statistic	Rank	Statistic	Rank
5	Poisson	0.16046	1	4.7647	2
4	Neg. Binomial	0.17175	2	4.6961	1
1	D. Uniform	0.19777	3	42.598	4
2	Geometric	0.47522	4	33.425	3
3	Logarithmic	0.6577	5	66.63	5
6	Bernoulli	No fit (data max > 1)			
7	Binomial	No fit			
8	Hypergeometric	No fit			

Figure A-4 Goodness of Fit of the Distributions Fitted to the Dataset including only Observations with 2 passenger lighting

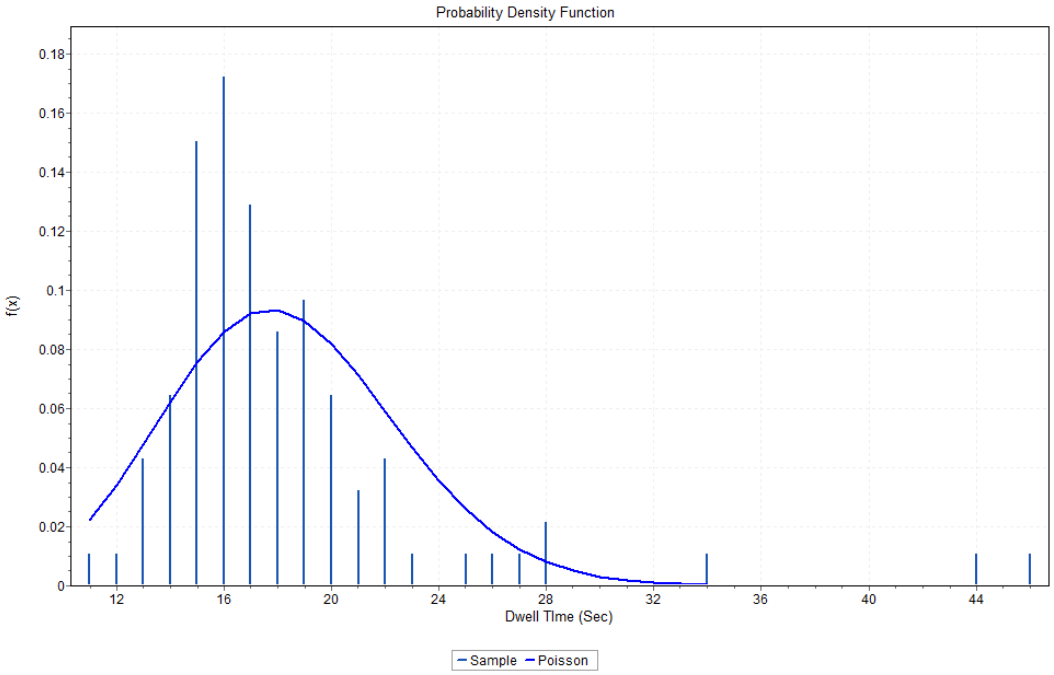

Figure A-5: Poisson distribution Fitted to the Dataset including only Observations with 3 Passenger Alighting

#	Distribution	Kolmogorov Smirnov		Anderson Darling	
		Statistic	Rank	Statistic	Rank
5	Poisson	0.1394	1	3.7451	1
4	Neg. Binomial	0.22609	2	6.032	2
1	D. Uniform	0.25127	3	28.38	3
2	Geometric	0.50489	4	28.383	4
3	Logarithmic	0.66668	5	51.713	5
6	Bernoulli	No fit (data max > 1)			
7	Binomial	No fit			
8	Hypergeometric	No fit			

Figure A-6: Goodness of Fit of the Distributions Fitted to the Dataset including only Observations with 3 Passenger Alighting

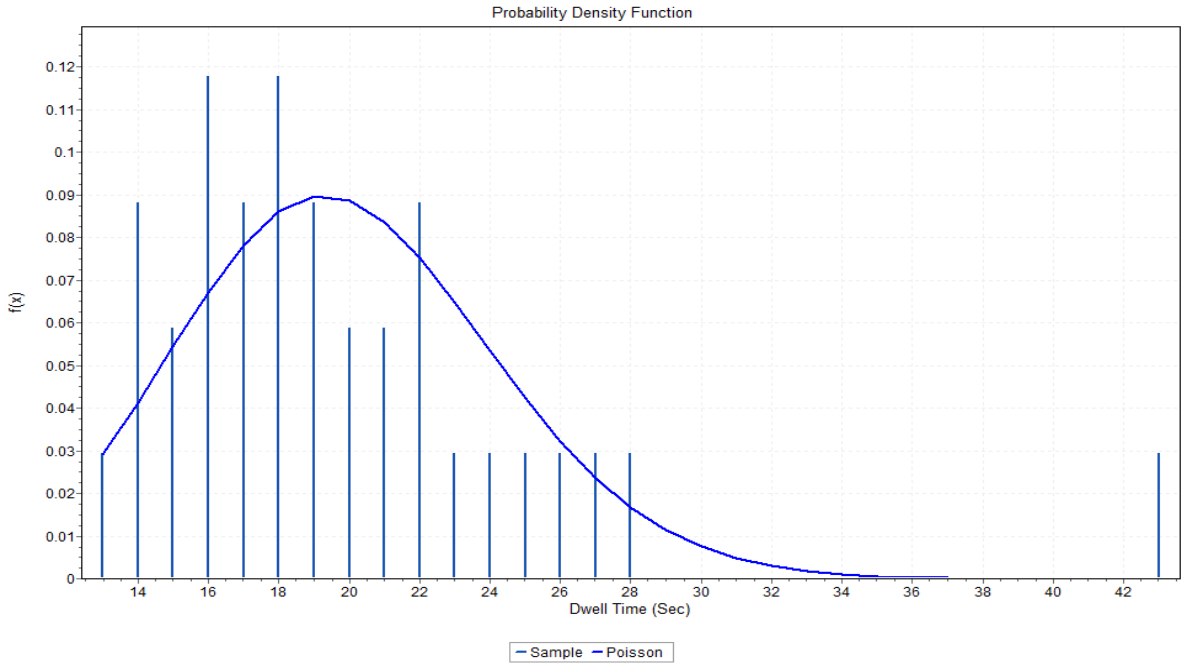

Figure A-7: Poisson distribution Fitted to the Dataset including only Observations with 4 Passenger Alighting

#	Distribution	Kolmogorov Smirnov		Anderson Darling	
		Statistic	Rank	Statistic	Rank
5	Poisson	0.10103	1	0.62869	1
4	Neg. Binomial	0.15917	2	1.0533	2
1	D. Uniform	0.18111	3	5.3626	3
2	Geometric	0.49842	4	9.8557	4
3	Logarithmic	0.67555	5	18.757	5
6	Bernoulli	No fit (data max > 1)			
7	Binomial	No fit			
8	Hypergeometric	No fit			

Figure A-8: Goodness of Fit of the Distributions Fitted to the Dataset including only Observations with 4 Passenger Alighting

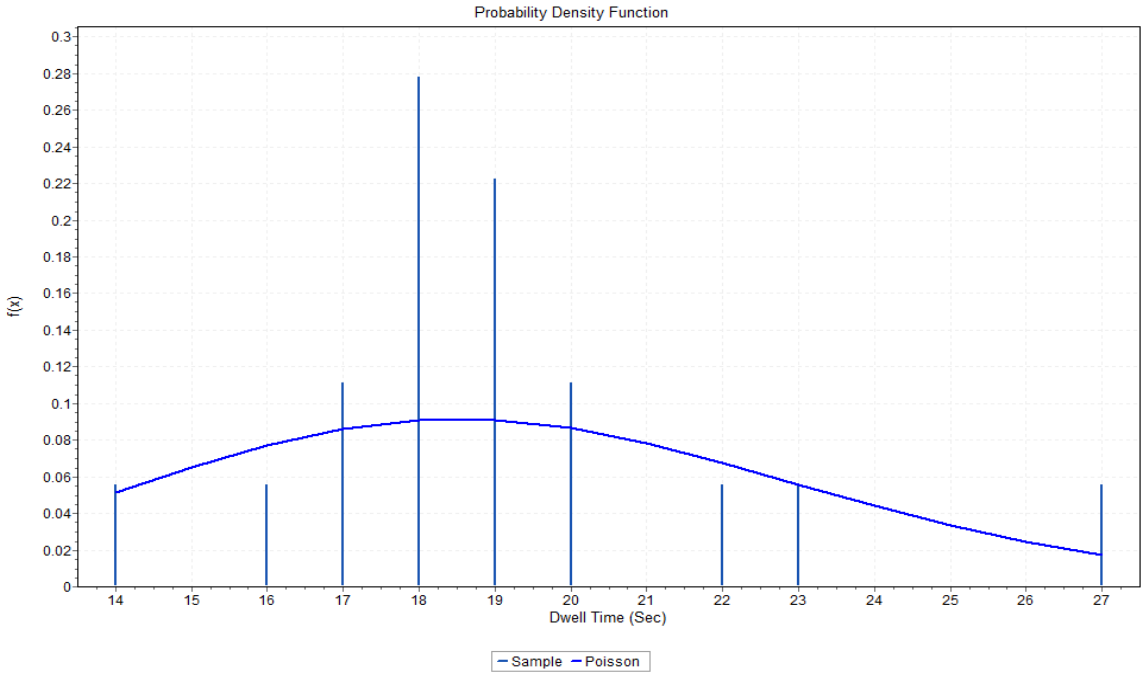

Figure A-9: Poisson distribution Fitted to the Dataset including only Observations with 5 Passenger Alighting

#	Distribution	Kolmogorov Smirnov		Anderson Darling	
		Statistic	Rank	Statistic	Rank
2	D. Uniform	0.22222	1	6.2113	3
5	Poisson	0.26725	2	1.6461	2
1	Binomial	0.27429	3	1.5497	1
3	Geometric	0.53671	4	6.5928	4
4	Logarithmic	0.69544	5	10.906	5
6	Bernoulli	No fit (data max > 1)			
7	Hypergeometric	No fit			
8	Neg. Binomial	No fit			

Figure A-10: Goodness of Fit of the Distributions Fitted to the Dataset including only Observations with 5 Passenger Alighting

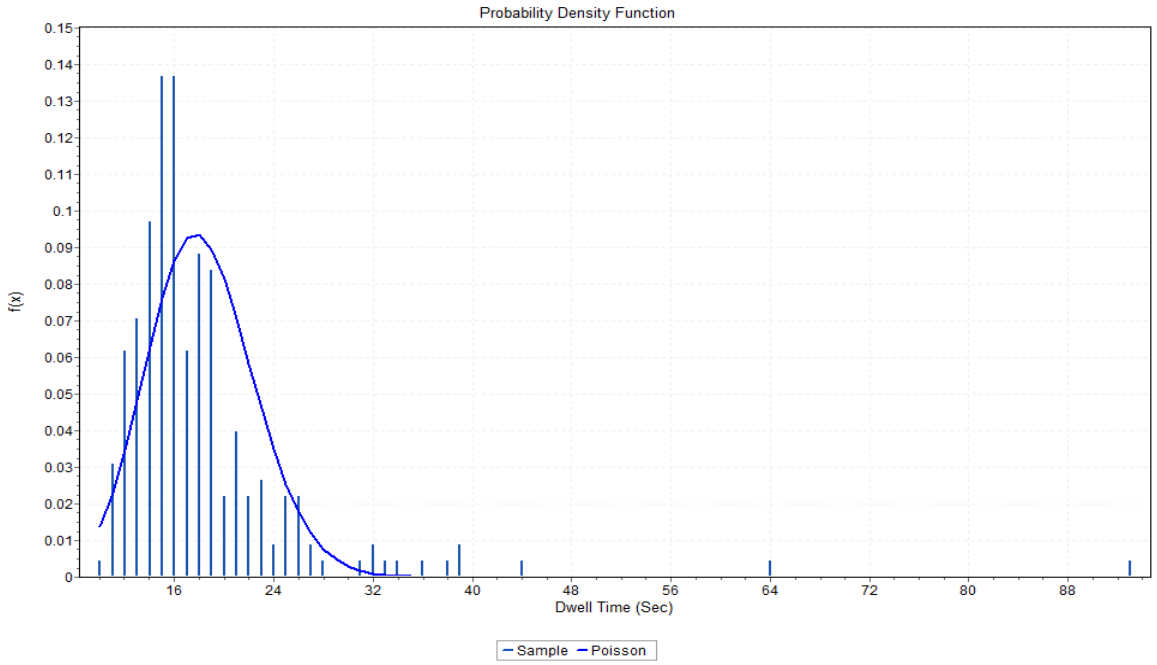

Figure A-11: Poisson distribution Fitted to the Dataset including only Observations with 1 Passenger Boarding

#	Distribution	Kolmogorov Smirnov		Anderson Darling	
		Statistic	Rank	Statistic	Rank
5	Poisson	0.17858	1	12.95	1
4	Neg. Binomial	0.25375	2	19.317	2
1	D. Uniform	0.26105	3	65.263	4
2	Geometric	0.46956	4	59.92	3
3	Logarithmic	0.65299	5	118.18	5
6	Bernoulli	No fit (data max > 1)			
7	Binomial	No fit			
8	Hypergeometric	No fit			

Figure A-12: Goodness of Fit of the Distributions Fitted to the Dataset including only Observations with 1 Passenger Boarding

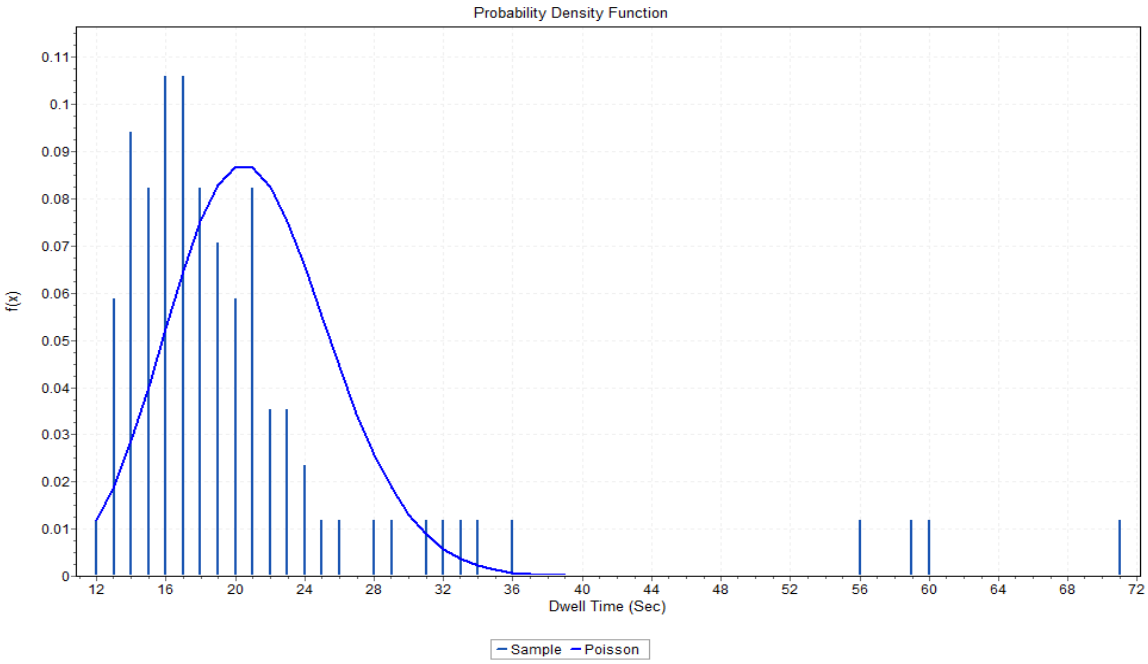

Figure A-13: Poisson distribution Fitted to the Dataset including only Observations with 1 Passenger Boarding and 2 Passenger Alighting

#	Distribution	Kolmogorov Smirnov		Anderson Darling	
		Statistic	Rank	Statistic	Rank
5	Poisson	0.14838	1	1.3689	1
4	Neg. Binomial	0.17695	2	1.4831	2
1	D. Uniform	0.2465	3	16.024	4
2	Geometric	0.5111	4	12.883	3
3	Logarithmic	0.67318	5	23.827	5
6	Bernoulli	No fit (data max > 1)			
7	Binomial	No fit			
8	Hypergeometric	No fit			

Figure A-14: Goodness of Fit of the Distributions Fitted to the Dataset including only Observations with 1 Passenger Boarding and 2 Passenger Alighting

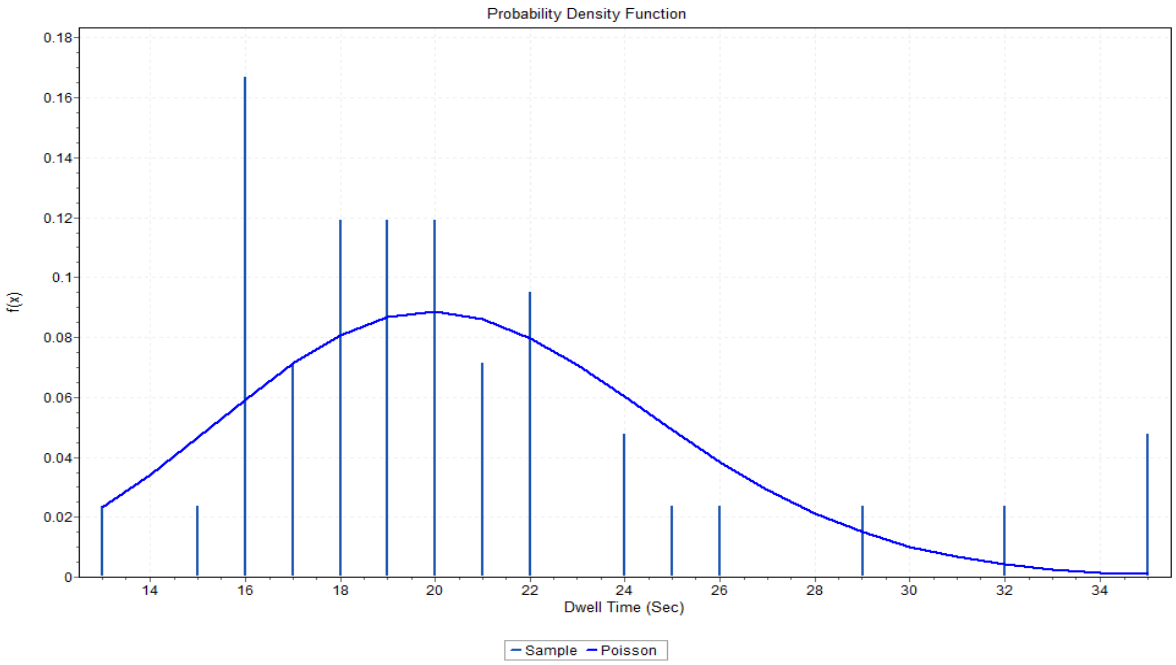

Figure A-15: Poisson distribution Fitted to the Dataset including only Observations with 1 Passenger Boarding and 3 Passengers Alighting

#	Distribution	Kolmogorov Smirnov		Anderson Darling	
		Statistic	Rank	Statistic	Rank
5	Poisson	0.14838	1	1.3689	1
4	Neg. Binomial	0.17695	2	1.4831	2
1	D. Uniform	0.2465	3	16.024	4
2	Geometric	0.5111	4	12.883	3
3	Logarithmic	0.67318	5	23.827	5
6	Bernoulli	No fit (data max > 1)			
7	Binomial	No fit			
8	Hypergeometric	No fit			

Figure A-16: Goodness of Fit of the Distributions Fitted to the Dataset including only Observations with 1 Passenger Boarding and 3 Passenger Alighting

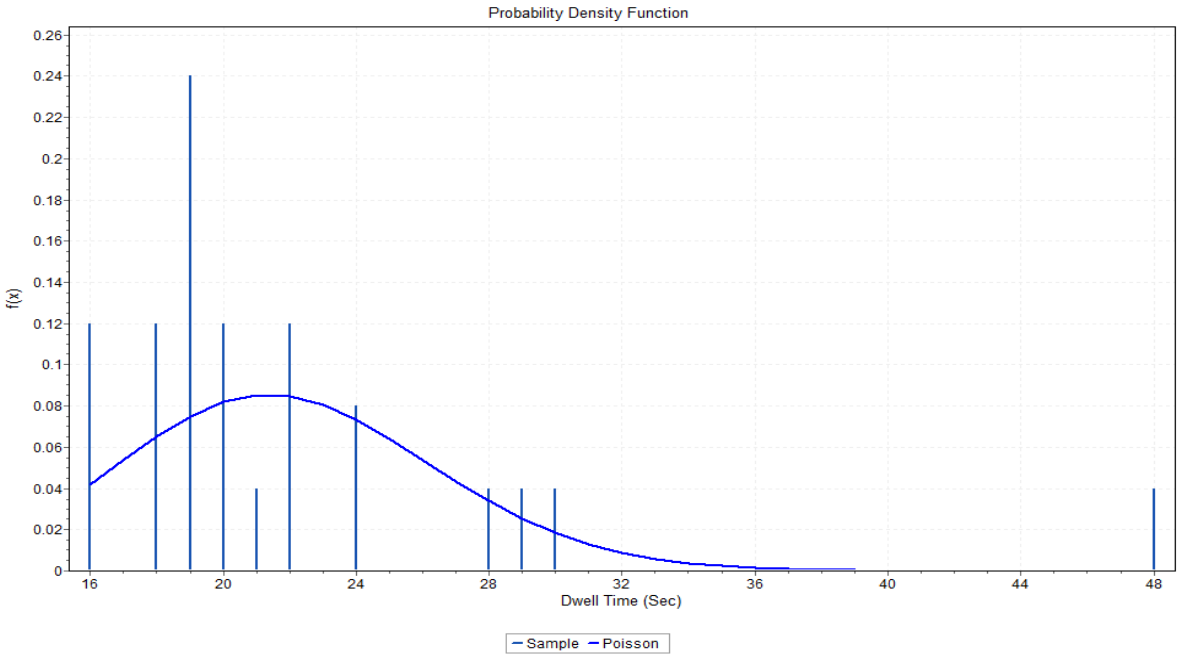

Figure A-17: Poisson distribution Fitted to the Dataset including only Observations with 1 Passenger Boarding and 4 Passengers Alighting

#	Distribution	Kolmogorov Smirnov		Anderson Darling	
		Statistic	Rank	Statistic	Rank
5	Poisson	0.20006	1	1.5913	1
4	Neg. Binomial	0.22881	2	1.8415	2
1	D. Uniform	0.26087	3	6.1125	3
2	Geometric	0.53284	4	7.5986	4
3	Logarithmic	0.69825	5	14.194	5
6	Bernoulli	No fit (data max > 1)			
7	Binomial	No fit			
8	Hypergeometric	No fit			

Figure A-18: Goodness of Fit of the Distributions Fitted to the Dataset including only Observations with 1 Passenger Boarding and 4 Passenger Alighting

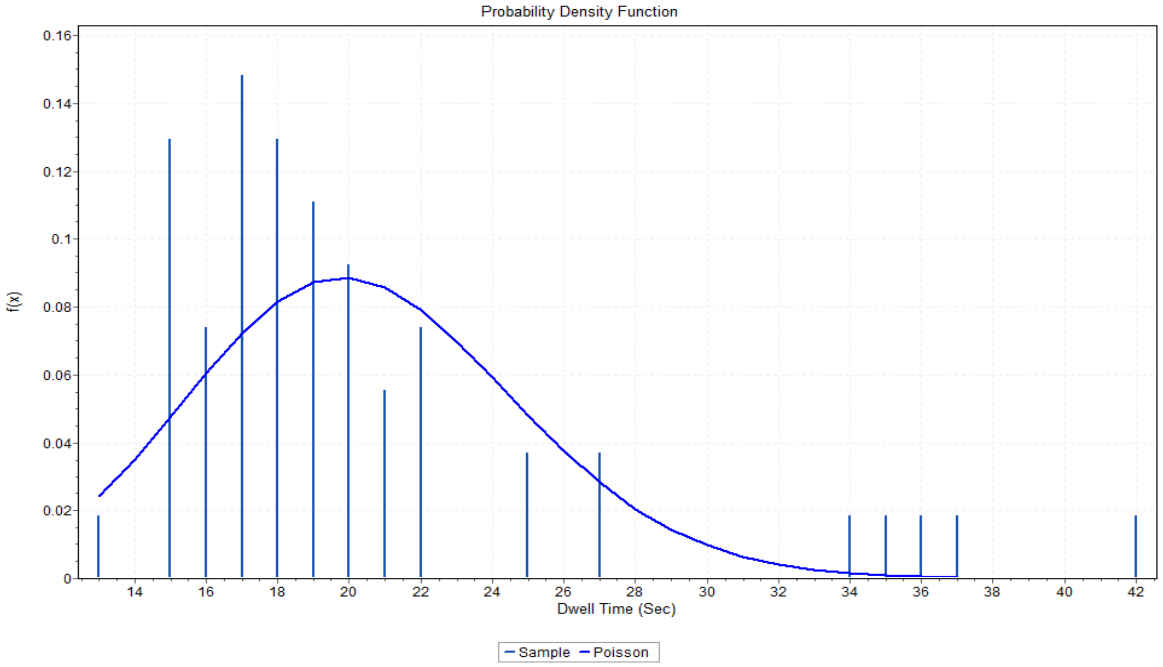

Figure A-19: Poisson distribution Fitted to the Dataset including only Observations with 2 Passengers Boarding and 1 Passenger Alighting

#	Distribution	Kolmogorov Smirnov		Anderson Darling	
		Statistic	Rank	Statistic	Rank
5	Poisson	0.17255	1	3.4428	2
4	Neg. Binomial	0.22527	2	3.2997	1
1	D. Uniform	0.2672	3	21.463	4
2	Geometric	0.51793	4	15.596	3
3	Logarithmic	0.67915	5	29.793	5
6	Bernoulli	No fit (data max > 1)			
7	Binomial	No fit			
8	Hypergeometric	No fit			

Figure A-20: Goodness of Fit of the Distributions Fitted to the Dataset including only Observations with 2 Passenger Boarding and 1 Passenger Alighting

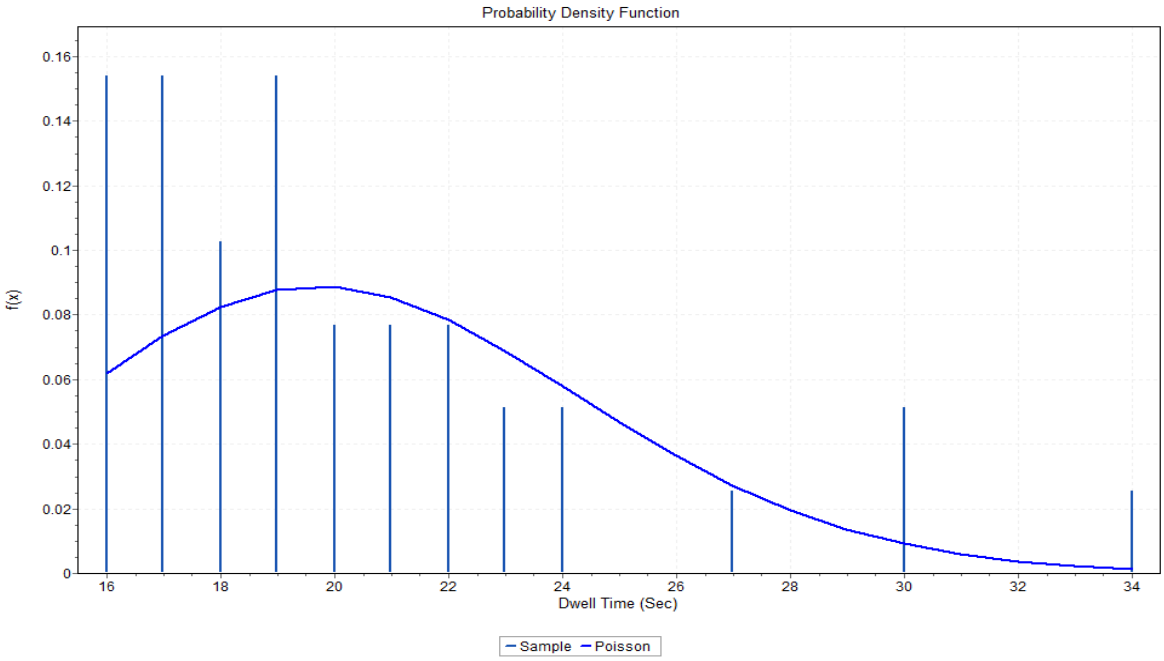

Figure A-21: Poisson distribution Fitted to the Dataset including only Observations with 2 Passengers Boarding and 2 Passenger Alighting

#	Distribution	Kolmogorov Smirnov		Anderson Darling	
		Statistic	Rank	Statistic	Rank
1	Binomial	0.19694	1	1.4901	1
5	Poisson	0.2081	2	1.5805	2
3	Geometric	0.5601	4	12.76	3
2	D. Uniform	0.26667	3	13.868	4
4	Logarithmic	0.71009	5	22.709	5
6	Bernoulli	No fit (data max > 1)			
7	Hypergeometric	No fit			
8	Neg. Binomial	No fit			

Figure A-22: Goodness of Fit of the Distributions Fitted to the Dataset including only Observations with 2 Passenger Boarding and 2 Passenger Alighting

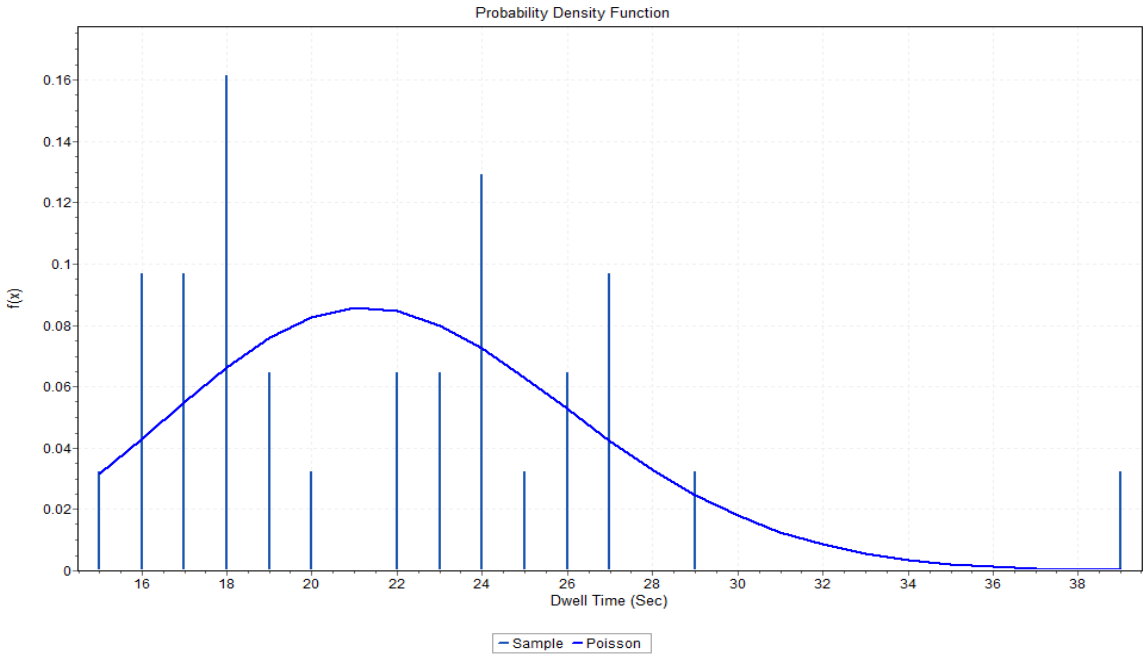

Figure A-23: Poisson distribution Fitted to the Dataset including only Observations with 2 Passengers Boarding and 3 Passengers Alighting

#	Distribution	Kolmogorov Smirnov		Anderson Darling	
		Statistic	Rank	Statistic	Rank
5	Poisson	0.13783	2	0.77833	1
4	Neg. Binomial	0.12471	1	0.78687	2
1	D. Uniform	0.18996	3	4.7575	3
2	Geometric	0.513	4	9.3015	4
3	Logarithmic	0.68738	5	17.583	5
6	Bernoulli	No fit (data max > 1)			
7	Binomial	No fit			
8	Hypergeometric	No fit			

Figure A-24: Goodness of Fit of the Distributions Fitted to the Dataset including only Observations with 2 Passenger Boarding and 3 Passenger Alighting

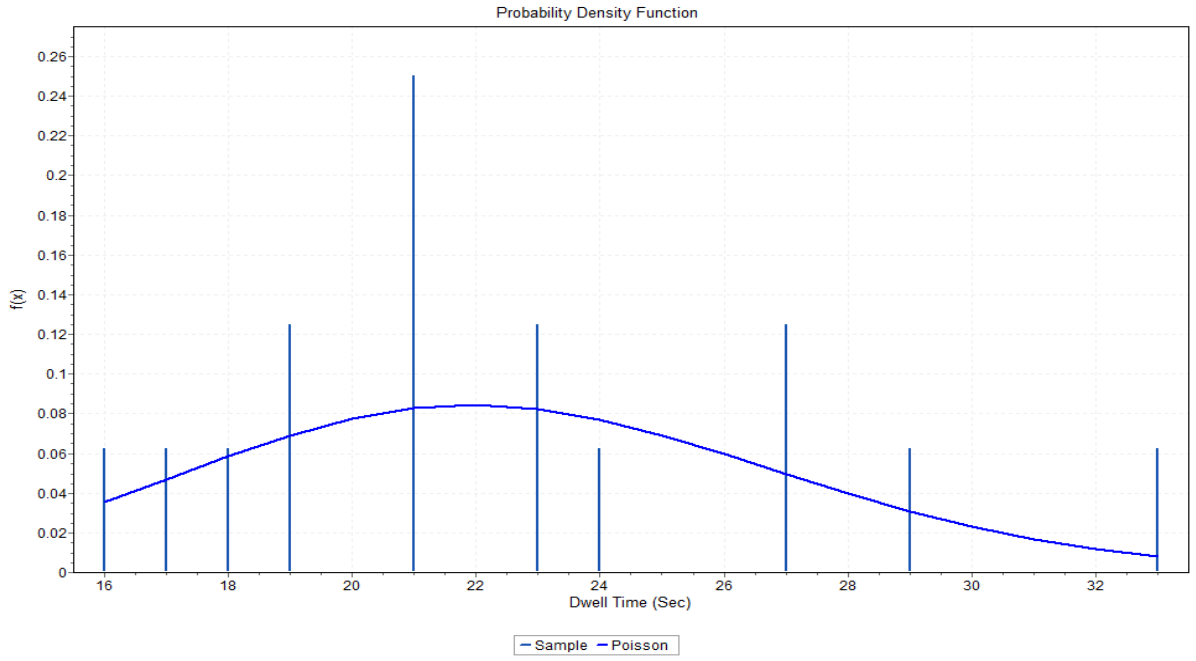

Figure A-25: Poisson distribution Fitted to the Dataset including only Observations with 2 Passengers Boarding and 4 Passengers Alighting

#	Distribution	Kolmogorov Smirnov		Anderson Darling	
		Statistic	Rank	Statistic	Rank
5	Poisson	0.12751	2	0.34782	1
1	Binomial	0.13104	3	0.35708	2
2	D. Uniform	0.125	1	4.1161	3
3	Geometric	0.52349	4	5.0694	4
4	Logarithmic	0.69421	5	9.3173	5
6	Bernoulli	No fit (data max > 1)			
7	Hypergeometric	No fit			
8	Neg. Binomial	No fit			

Figure A-26: Goodness of Fit of the Distributions Fitted to the Dataset including only Observations with 2 Passenger Boarding and 4 Passenger Alighting

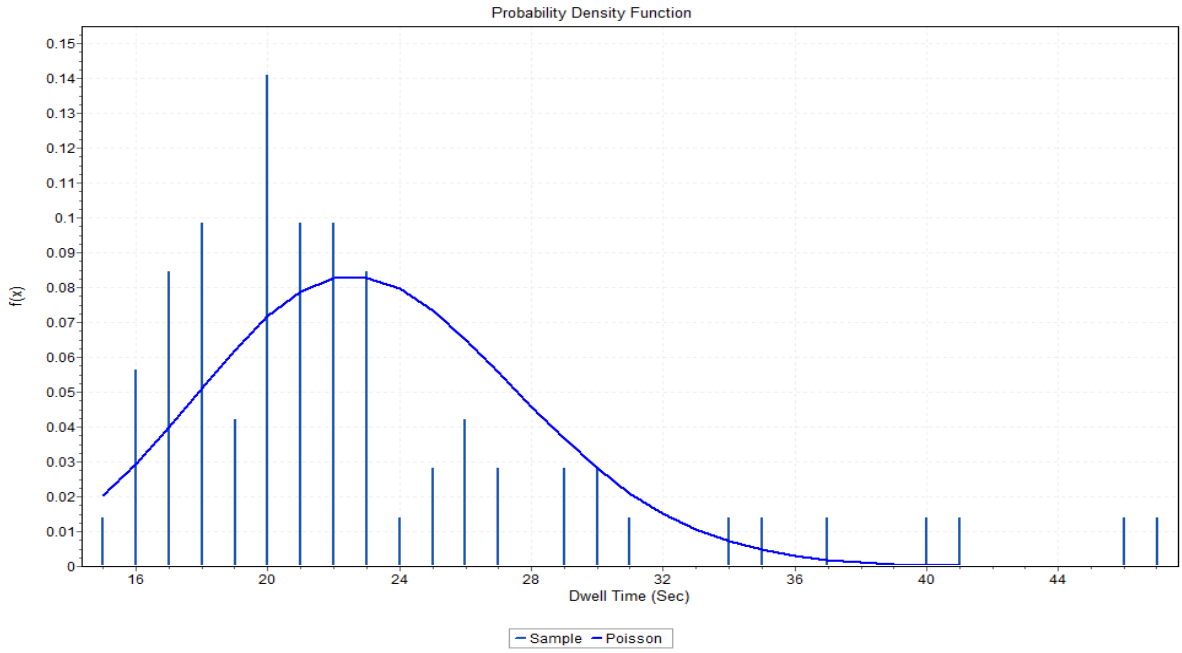

Figure A-27: Poisson distribution Fitted to the Dataset including only Observations with 3 Passengers Boarding

#	Distribution	Kolmogorov Smirnov		Anderson Darling	
		Statistic	Rank	Statistic	Rank
5	Poisson	0.169	1	3.7942	2
4	Neg. Binomial	0.17967	2	3.1838	1
1	D. Uniform	0.20331	3	26.642	4
2	Geometric	0.49982	4	19.895	3
3	Logarithmic	0.67858	5	39.42	5
6	Bernoulli	No fit (data max > 1)			
7	Binomial	No fit			
8	Hypergeometric	No fit			

Figure A-28: Goodness of Fit of the Distributions Fitted to the Dataset including only Observations with 3 Passenger Boarding

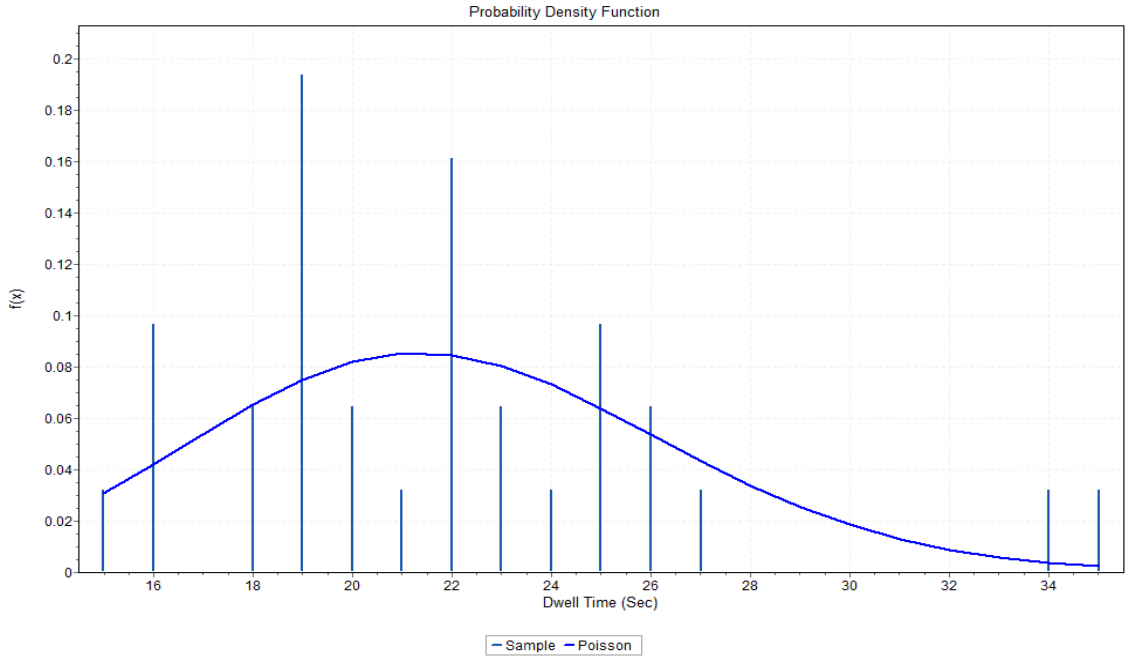

Figure A-29: Poisson distribution Fitted to the Dataset including only Observations with 3 Passengers Boarding and 1 Passenger Alighting

#	Distribution	Kolmogorov Smirnov		Anderson Darling	
		Statistic	Rank	Statistic	Rank
1	Binomial	0.1215	1	0.63077	1
5	Poisson	0.12447	2	0.64551	2
2	D. Uniform	0.18347	3	8.3402	3
3	Geometric	0.51148	4	9.7926	4
4	Logarithmic	0.68672	5	17.96	5
6	Bernoulli	No fit (data max > 1)			
7	Hypergeometric	No fit			
8	Neg. Binomial	No fit			

Figure A-30: Goodness of Fit of the Distributions Fitted to the Dataset including only Observations with 3 Passenger Boarding and 1 Passenger Alighting

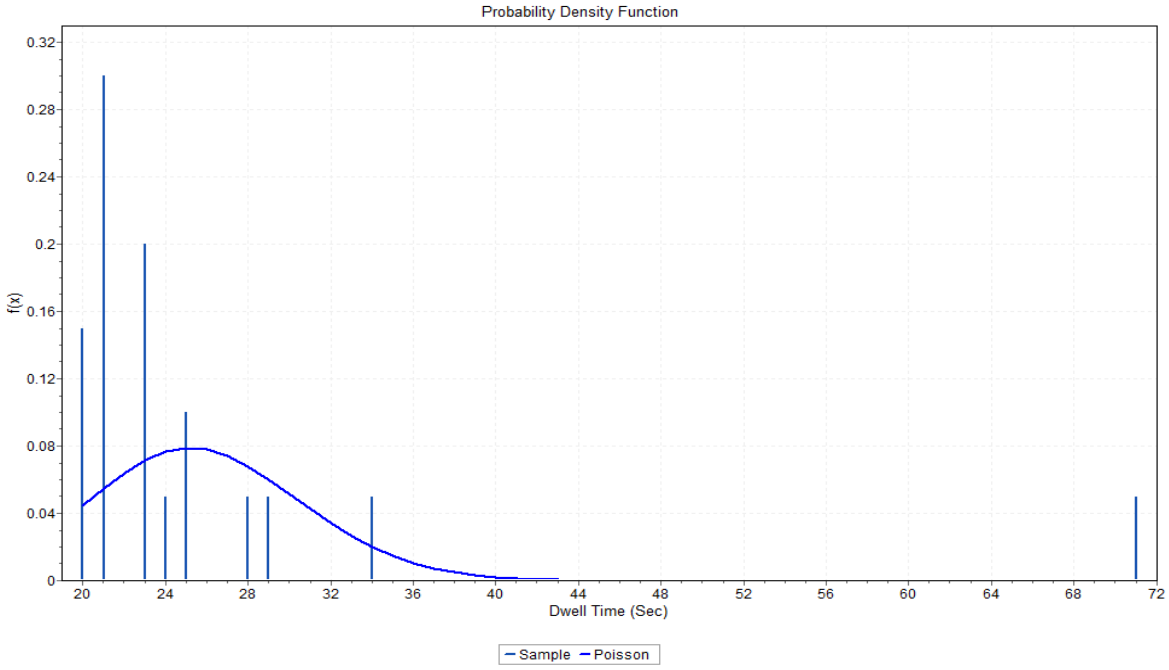

Figure A-31: Poisson distribution Fitted to the Dataset including only Observations with 3 Passengers Boarding and 2 Passengers Alighting

#	Distribution	Kolmogorov Smirnov		Anderson Darling	
		Statistic	Rank	Statistic	Rank
5	Poisson	0.30794	1	3.8013	2
4	Neg. Binomial	0.35346	2	3.0807	1
1	D. Uniform	0.36842	3	7.0791	4
2	Geometric	0.5514	4	6.048	3
3	Logarithmic	0.71311	5	11.416	5
6	Bernoulli	No fit (data max > 1)			
7	Binomial	No fit			
8	Hypergeometric	No fit			

Figure A-32: Goodness of Fit of the Distributions Fitted to the Dataset including only Observations with 3 Passenger Boarding and 2 Passenger Alighting

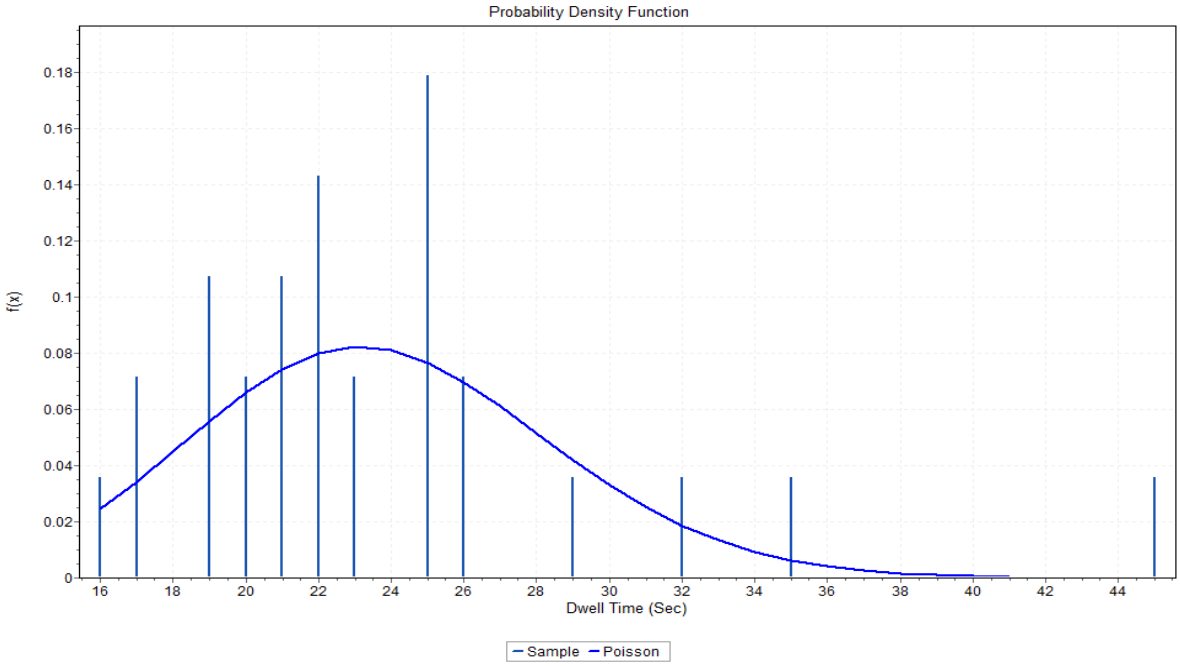

Figure A-33: Poisson distribution Fitted to the Dataset including only Observations with 3 Passengers Boarding and 3 Passengers Alighting

#	Distribution	Kolmogorov Smirnov		Anderson Darling	
		Statistic	Rank	Statistic	Rank
5	Poisson	0.12804	1	0.79722	1
4	Neg. Binomial	0.15369	2	0.96108	2
1	D. Uniform	0.20714	3	8.7947	4
2	Geometric	0.50552	4	8.5346	3
3	Logarithmic	0.68646	5	16.124	5
6	Bernoulli	No fit (data max > 1)			
7	Binomial	No fit			
8	Hypergeometric	No fit			

Figure A-34: Goodness of Fit of the Distributions Fitted to the Dataset including only Observations with 3 Passenger Boarding and 3 Passenger Alighting

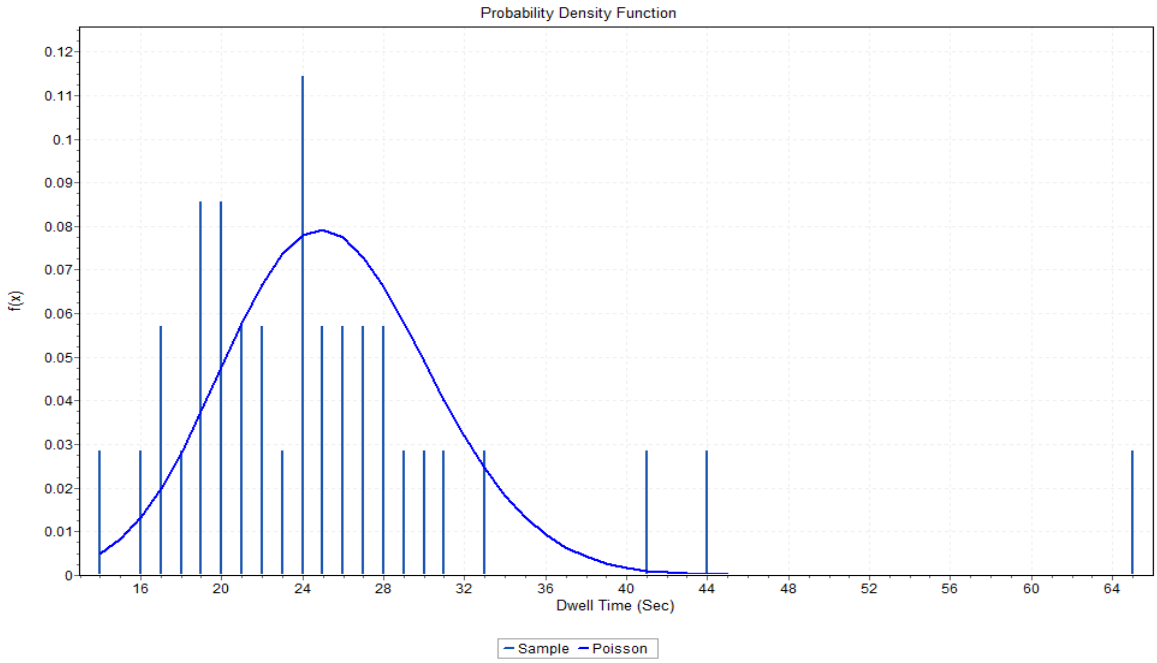

Figure A-35: Poisson distribution Fitted to the Dataset including only Observations with 4 Passengers Boarding

#	Distribution	Kolmogorov Smirnov		Anderson Darling	
		Statistic	Rank	Statistic	Rank
5	Poisson	0.14873	1	2.3093	2
4	Neg. Binomial	0.20458	2	2.1242	1
1	D. Uniform	0.20625	3	11.507	4
2	Geometric	0.45274	4	8.9556	3
3	Logarithmic	0.65239	5	18.942	5
6	Bernoulli	No fit (data max > 1)			
7	Binomial	No fit			
8	Hypergeometric	No fit			

Figure A-36: Goodness of Fit of the Distributions Fitted to the Dataset including only Observations with 4 Passenger Boarding

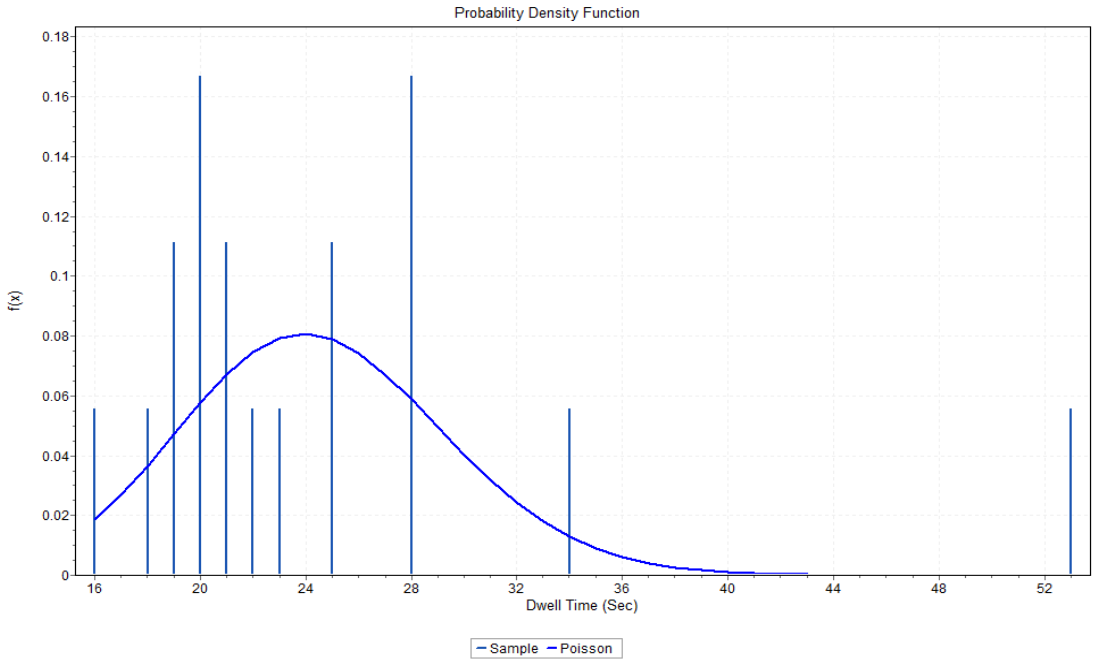

Figure A-37: Poisson distribution Fitted to the Dataset including only Observations with 4 Passengers Boarding and 1 Passengers Alighting

#	Distribution	Kolmogorov Smirnov		Anderson Darling	
		Statistic	Rank	Statistic	Rank
5	Poisson	0.21686	1	1.4703	1
1	D. Uniform	0.24603	2	5.1979	4
4	Neg. Binomial	0.2653	3	1.5278	2
2	Geometric	0.4942	4	4.9827	3
3	Logarithmic	0.68158	5	9.9874	5
6	Bernoulli	No fit (data max > 1)			
7	Binomial	No fit			
8	Hypergeometric	No fit			

Figure A-38: Goodness of Fit of the Distributions Fitted to the Dataset including only Observations with 4 Passenger Boarding and 1 Passenger Alighting

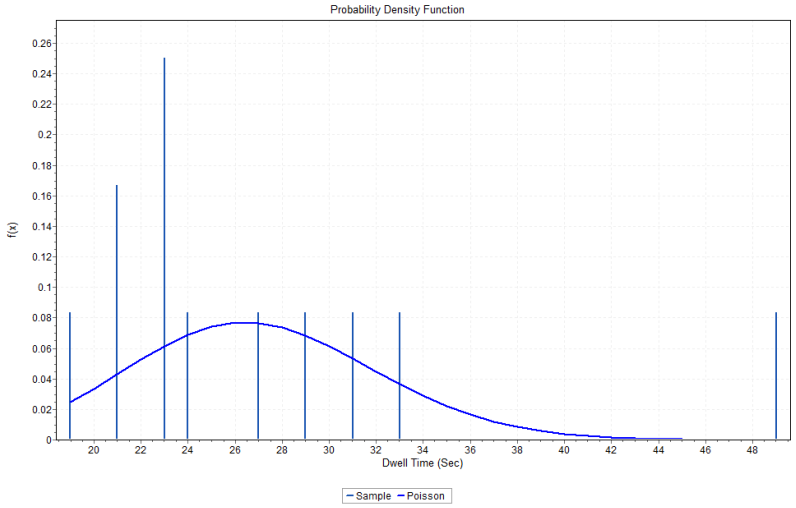

Figure A-39: Poisson distribution Fitted to the Dataset including only Observations with 4 Passengers Boarding and 2 Passengers Alighting

#	Distribution	Kolmogorov Smirnov		Anderson Darling	
		Statistic	Rank	Statistic	Rank
4	Neg. Binomial	0.18374	1	0.65417	1
5	Poisson	0.25346	3	1.0639	2
2	Geometric	0.51788	4	3.4265	3
1	D. Uniform	0.22222	2	4.4011	4
3	Logarithmic	0.69761	5	6.8387	5
6	Bernoulli	No fit (data max > 1)			
7	Binomial	No fit			
8	Hypergeometric	No fit			

Figure A-40: Goodness of Fit of the Distributions Fitted to the Dataset including only Observations with 4 Passenger Boarding and 2 Passenger Alighting

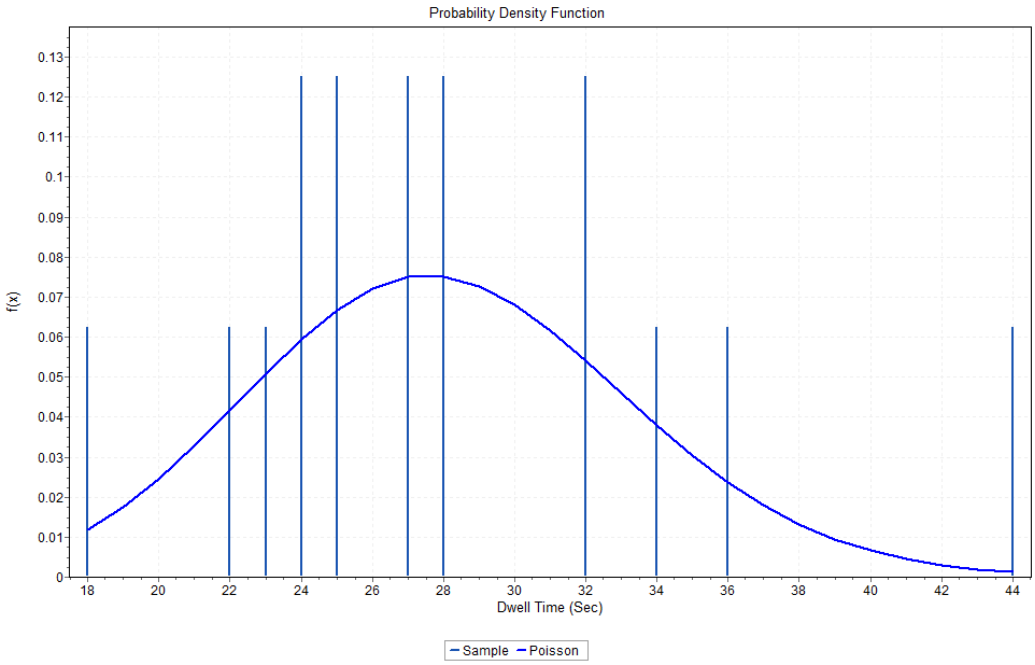

Figure A-41: Poisson distribution Fitted to the Dataset including only Observations with 5 Passengers Boarding

#	Distribution	Kolmogorov Smirnov		Anderson Darling	
		Statistic	Rank	Statistic	Rank
4	Neg. Binomial	0.13485	1	0.38068	1
5	Poisson	0.14216	2	0.39692	2
1	D. Uniform	0.1756	3	4.227	3
2	Geometric	0.49056	4	4.8915	4
3	Logarithmic	0.68236	5	9.4276	5
6	Bernoulli	No fit (data max > 1)			
7	Binomial	No fit			
8	Hypergeometric	No fit			

Figure A-42: Goodness of Fit of the Distributions Fitted to the Dataset including only Observations with 5 Passenger Boarding

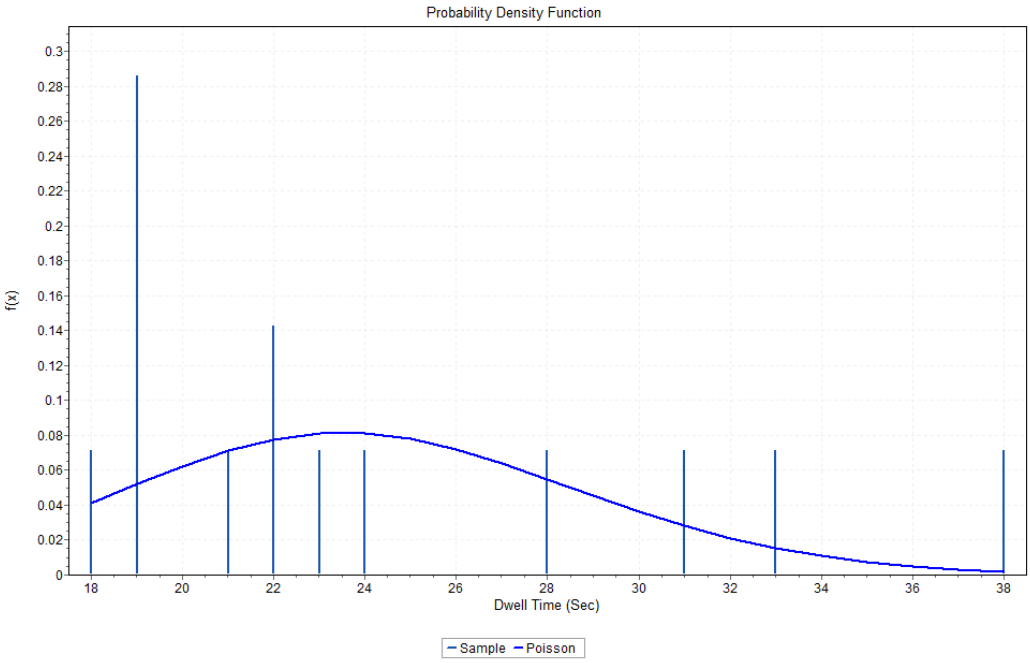

Figure A-43: Poisson distribution Fitted to the Dataset including only Observations with 5 Passengers Boarding and 1 Passengers Alighting

#	Distribution	Kolmogorov Smirnov		Anderson Darling	
		Statistic	Rank	Statistic	Rank
5	Poisson	0.17973	1	1.0217	2
4	Neg. Binomial	0.18729	2	0.71817	1
1	D. Uniform	0.2381	3	4.3326	4
2	Geometric	0.53958	4	4.1354	3
3	Logarithmic	0.70495	5	7.988	5
6	Bernoulli	No fit (data max > 1)			
7	Binomial	No fit			
8	Hypergeometric	No fit			

Figure A-44: Goodness of Fit of the Distributions Fitted to the Dataset including only Observations with 5 Passenger Boarding and 1 Passenger Alighting

Appendix B- Number of Observations Available Based on Headway Category

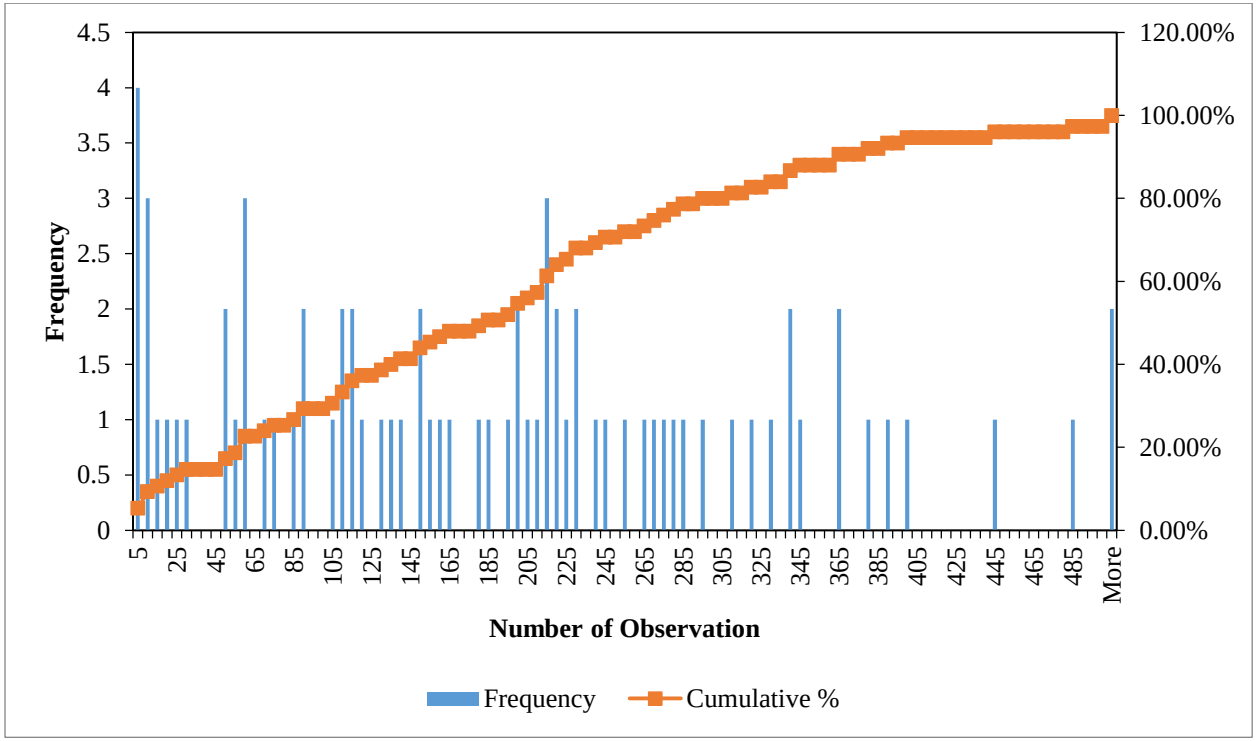

Figure B-1: Histogram of Number of Observations for Routes with 15 Minute Headway

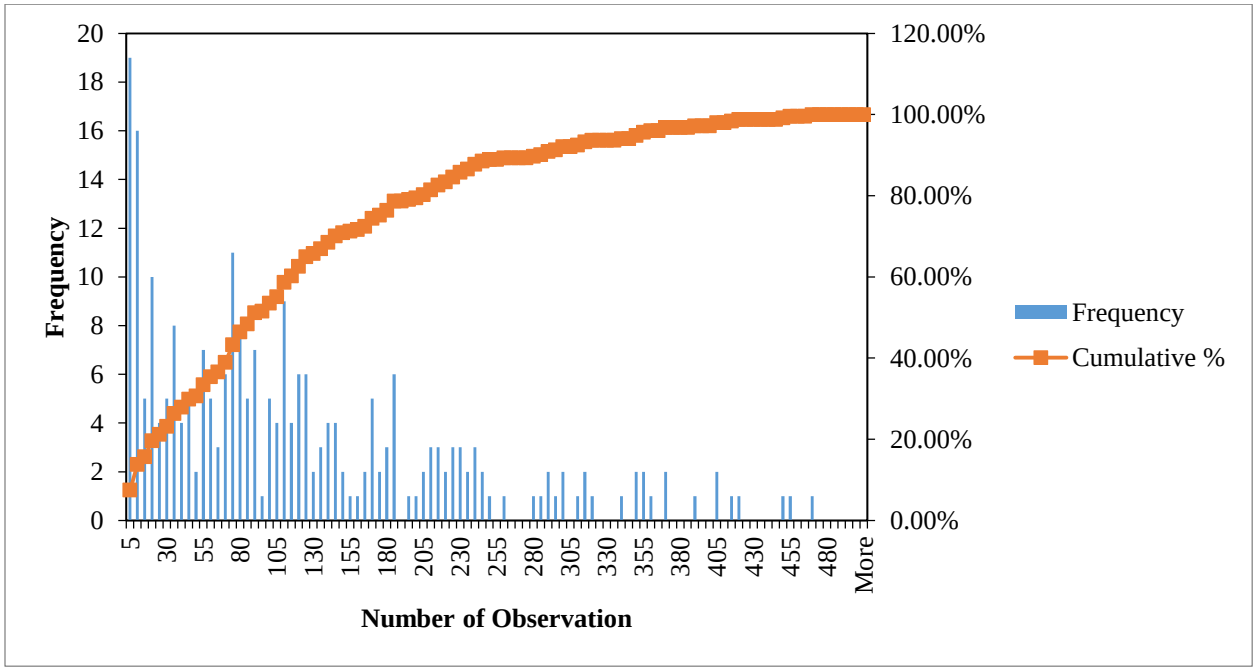

Figure B-2: Histogram of Number of Observations for Routes with 30 Minute Headway

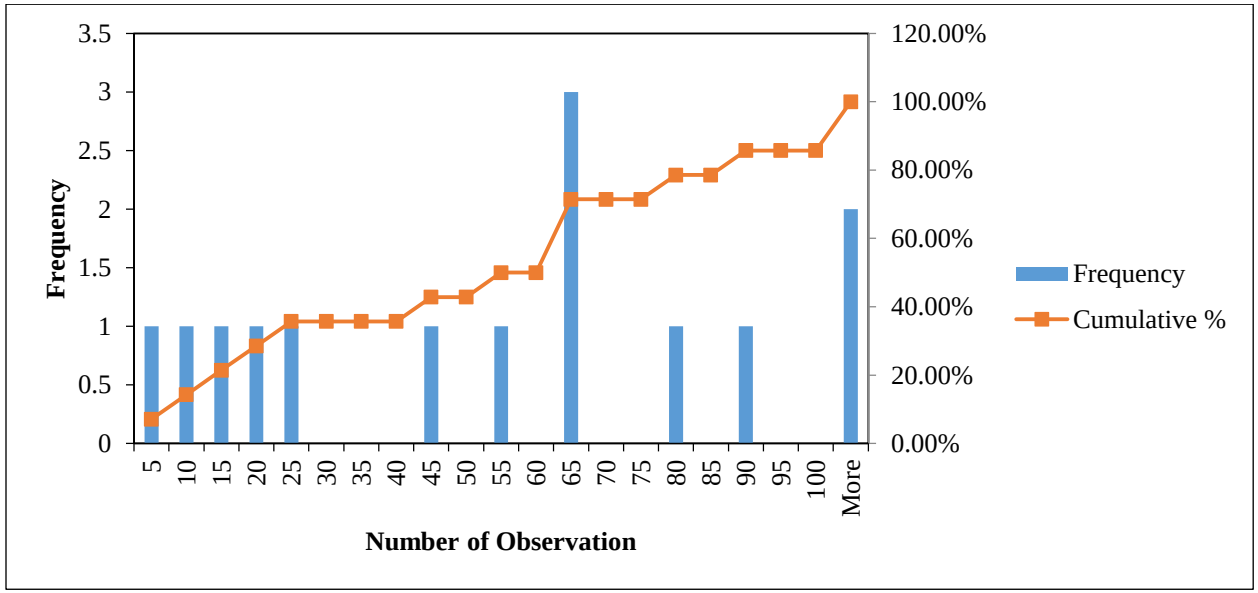

Figure B-3: Histogram of Number of Observations for Routes with 1 hour Headway

Appendix C- Queue Length Validation

This appendix presents a set of figures that highlight the differences in performance between the algorithm presented by Yang and Hellinga (2012) and the proposed boundary line algorithm. The main differences between the two algorithms are summarized below:

1. The proposed BL algorithm excludes the stopped delay observations from the adjacent road segments from the analysis.
2. In the proposed BL algorithm the distance of each observation is measured from the stop-line and not the center of the intersection as is the case in Yang's work (Yang, 2012).
3. The proposed BL algorithm defines rectangular delay envelop enclosed by maximum delay (on the y-axis) and the maximum queue length (on the x-axis).

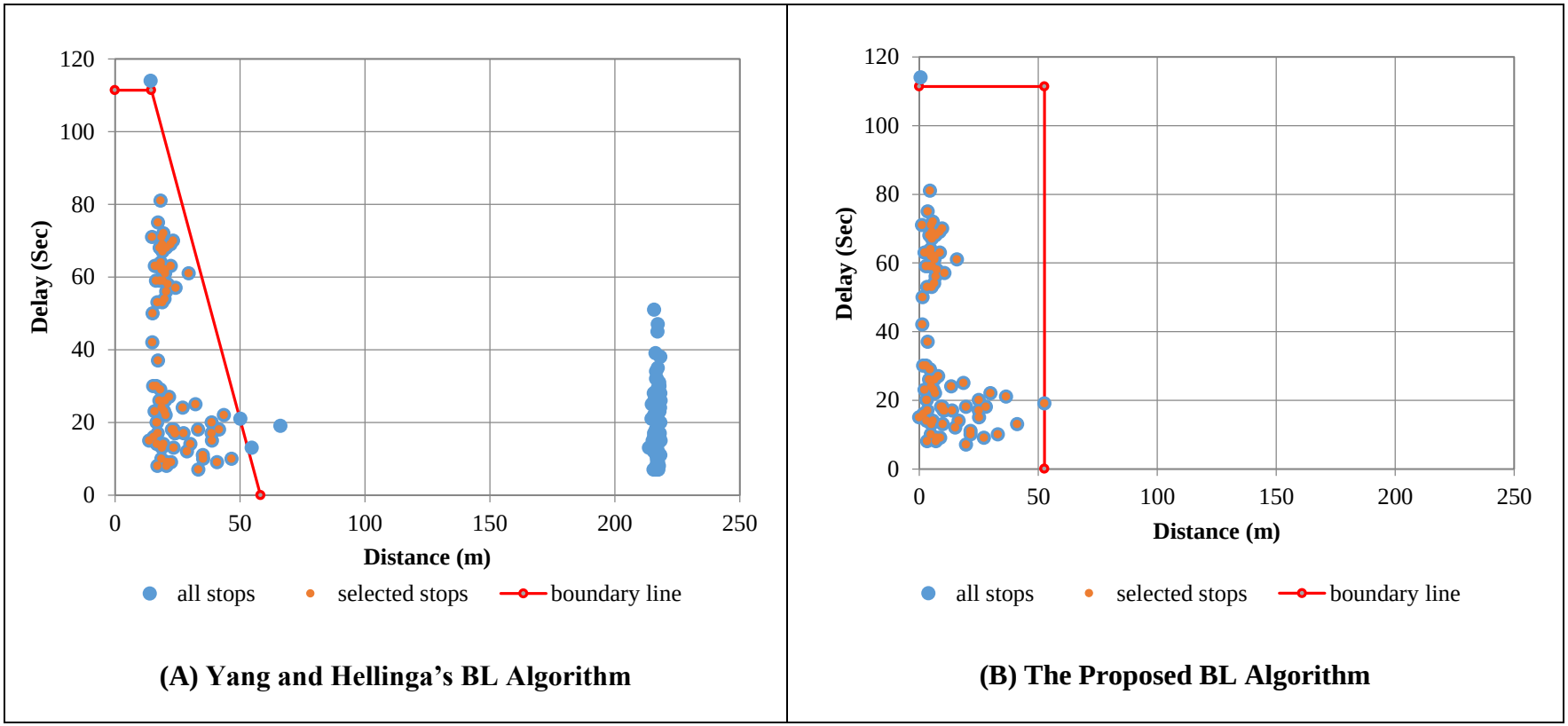

Figure C-1: Comparison of the BL Fitted to Stop Observation of Ottawa at River Intersection

Figure C-2: The unscheduled stop observations superimposed on Google Maps for Ottawa at River Intersection

The observations in Figure C-1(B) are measured from the stop line which accounts for the discrepancy between the x-values of the observations in Figure C-1(A) and (B). Also in Figure C-1(B) the observations from adjacent segments are excluded from the analysis.

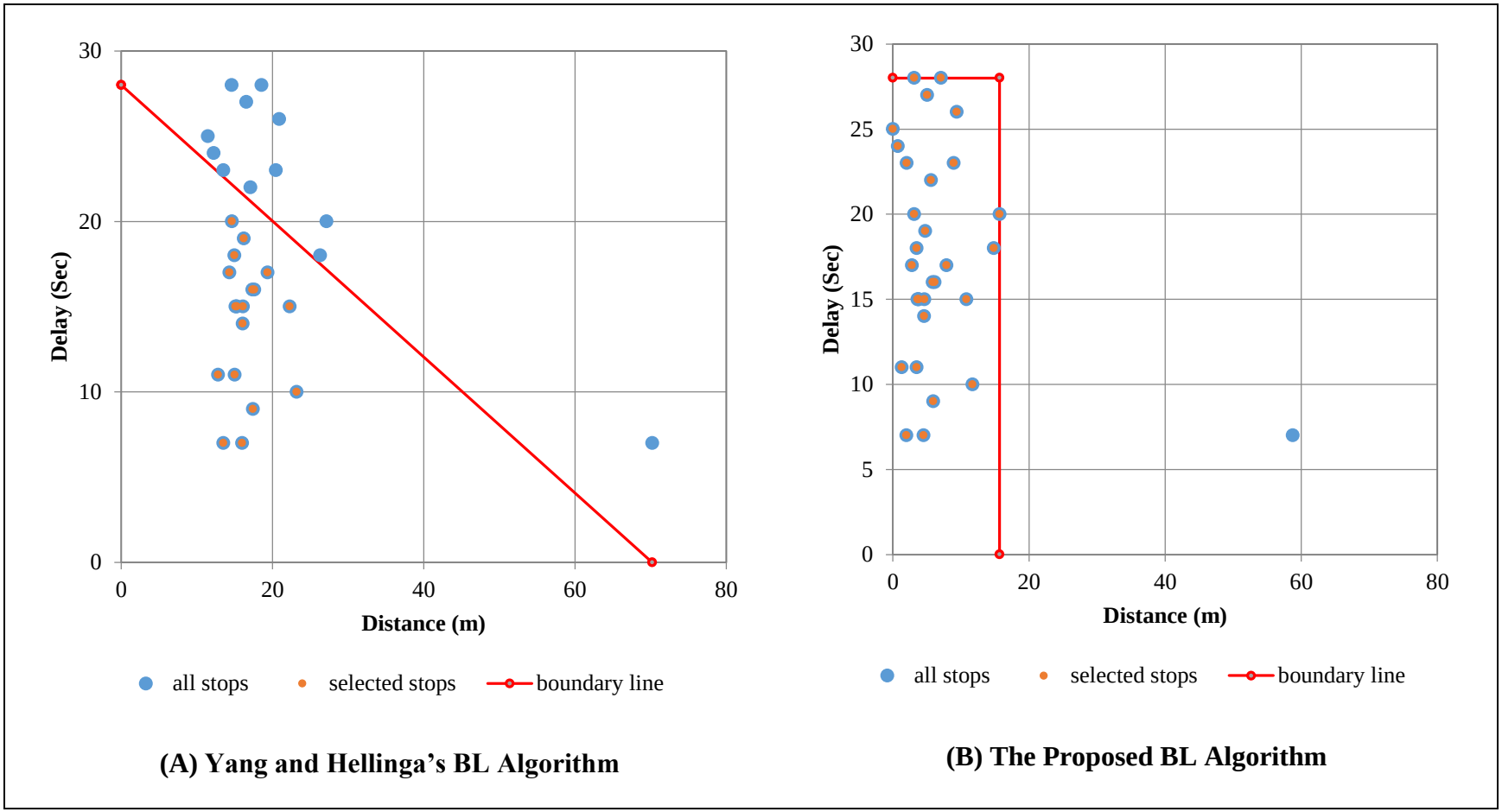

Figure C-3: Comparison of the BL Fitted to Stop Observation of Homer Watson at Stirling Ave Intersection

Figure C-4: The unscheduled stop observations superimposed on Google Maps for Homer Watson at Stirling Ave Intersection

The observations in Figure C-3(B) are measured from the stop line which accounts for the discrepancy between the x-values of the observations in Figure C-3 (A) and (B).

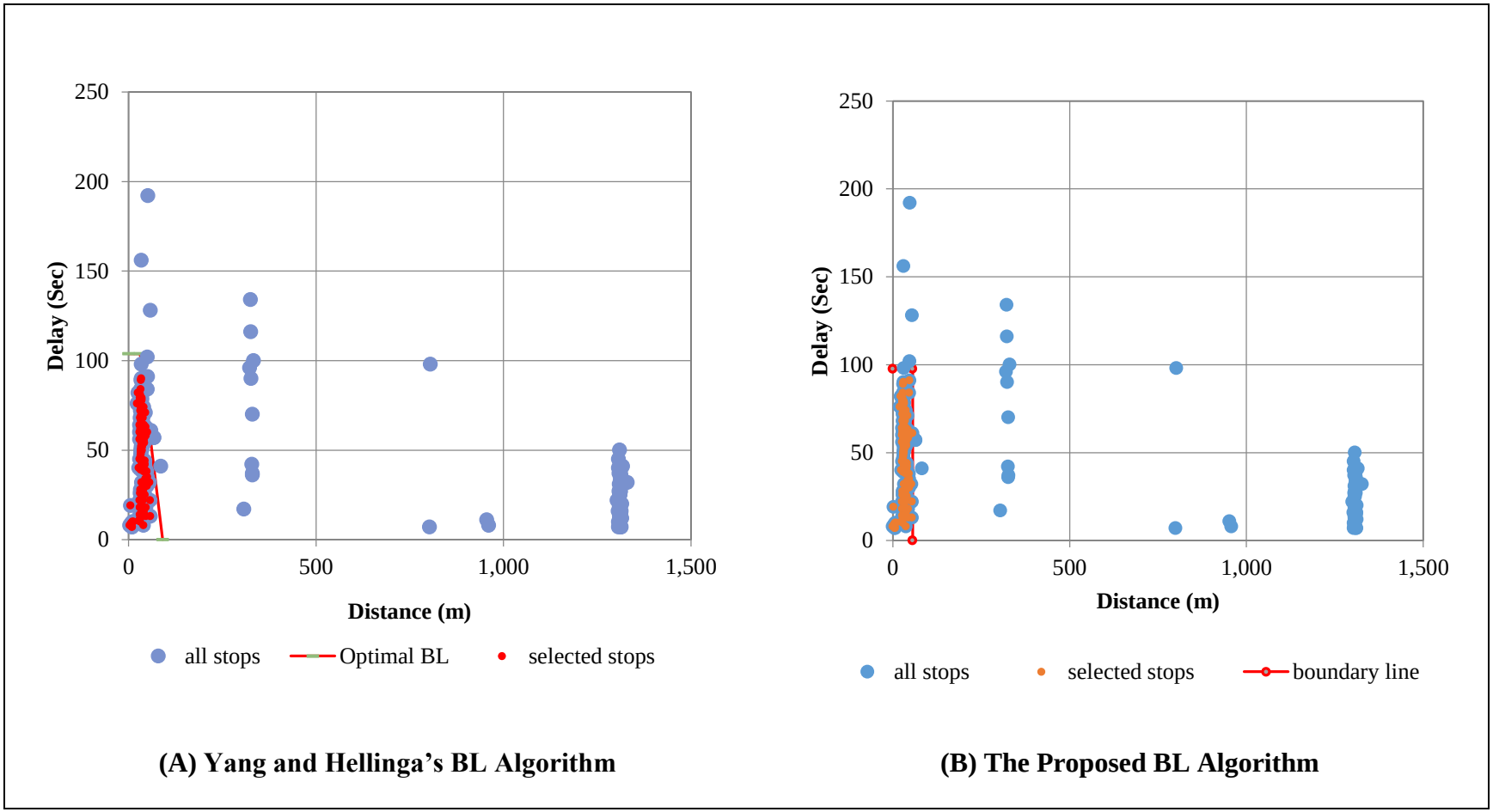

(A) Yang and Hellinga's BL Algorithm

(B) The Proposed BL Algorithm

Figure C-5: Comparison of the BL Fitted to Stop Observation of Ottawa at Strasburg Intersection

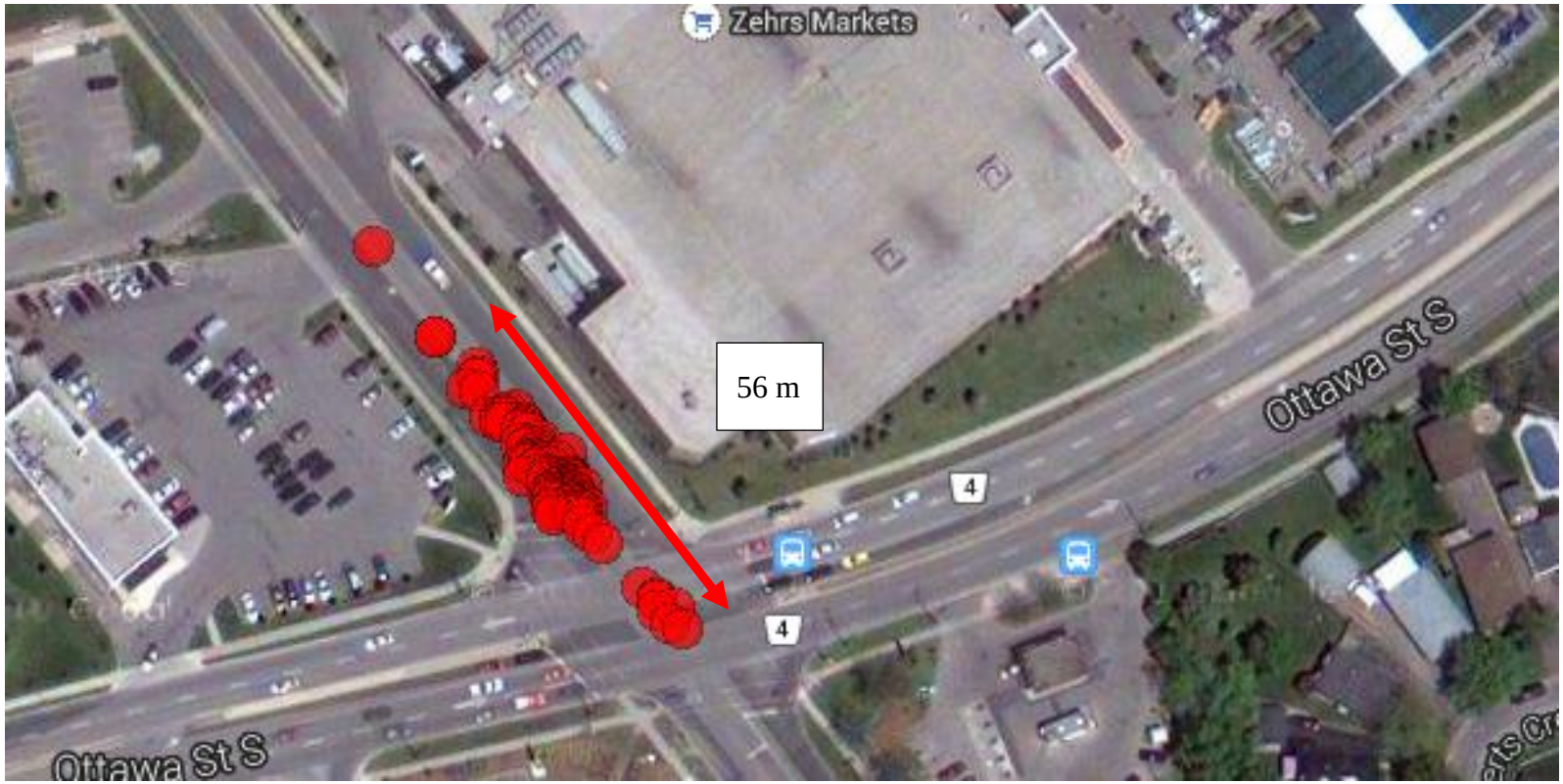

Figure C-6: The unscheduled stop observations superimposed on Google Maps for Ottawa at Strasburg Intersection.

Figure C-6 captures the left turn movement of route 3 buses at this intersection. As the result of the left turn maneuver a number of stop observations have occurred in the middle of the intersection.

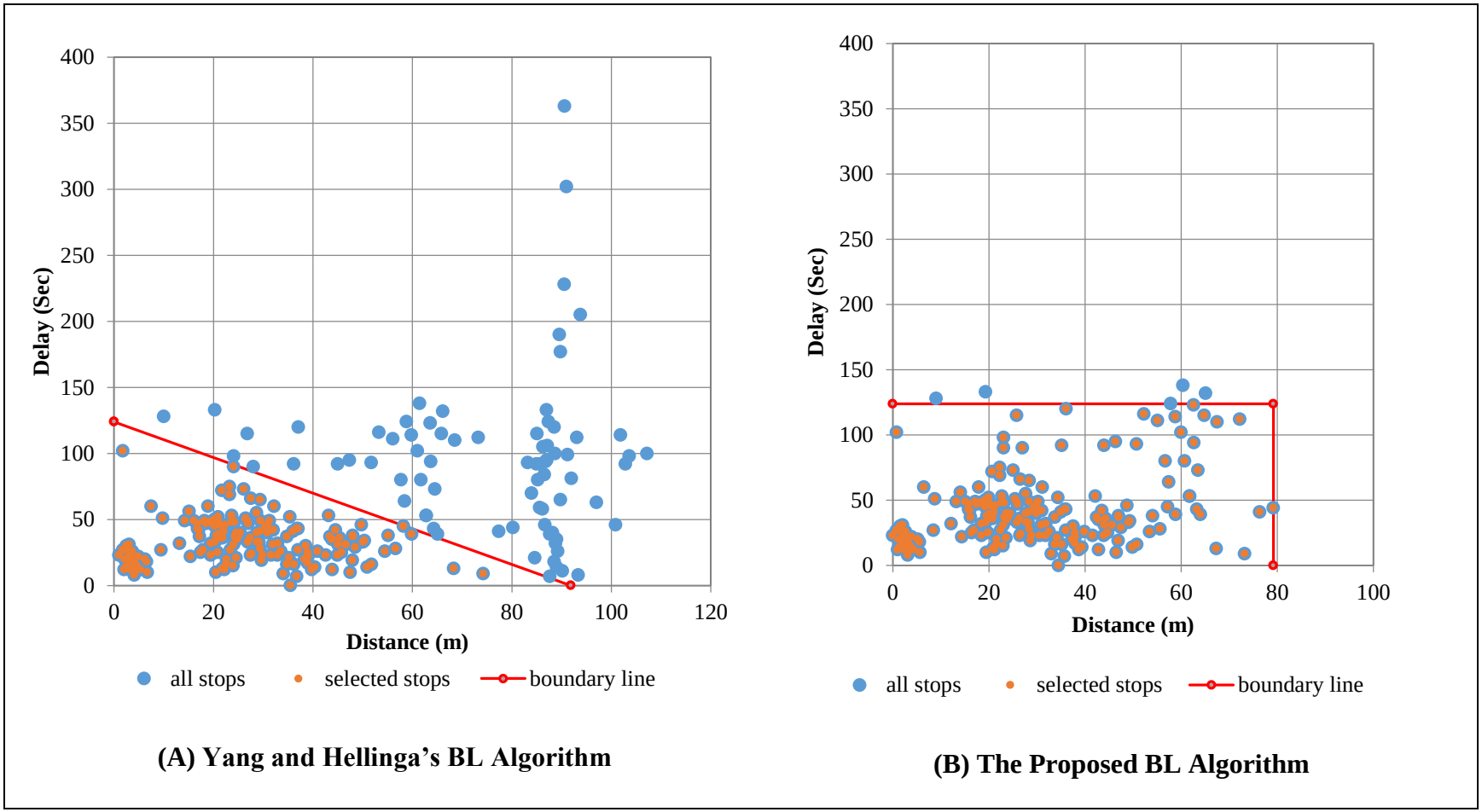

Figure C-7: Comparison of the BL Fitted to Stop Observation of Charles and Ontario Intersection

Figure C-8: The unscheduled stop observations superimposed on Google Maps for Charles an Ontario Intersection

In Figure C-7(B) the observations from adjacent segments are excluded from the analysis.

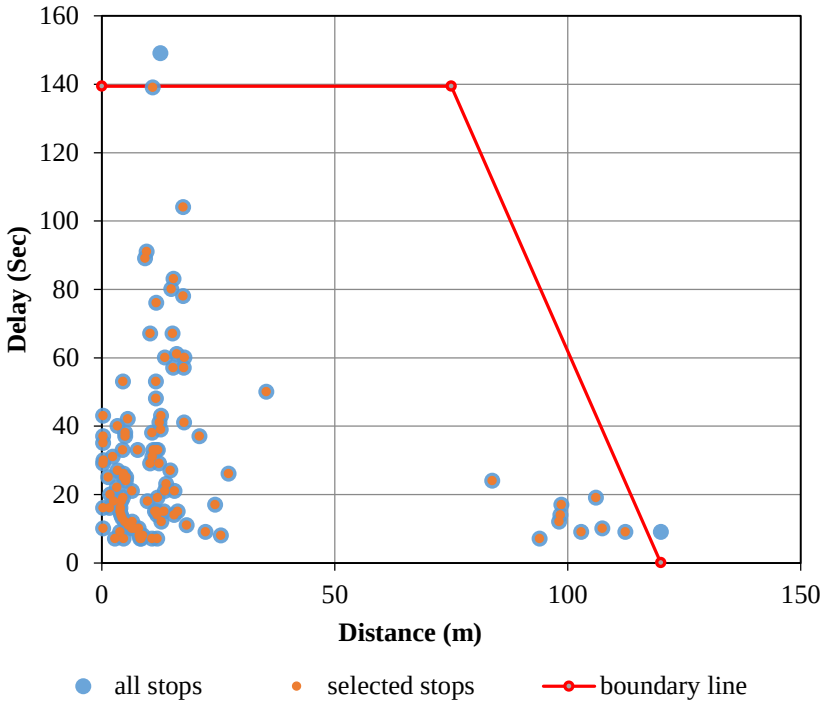

(A) Yang and Hellinga's BL Algorithm

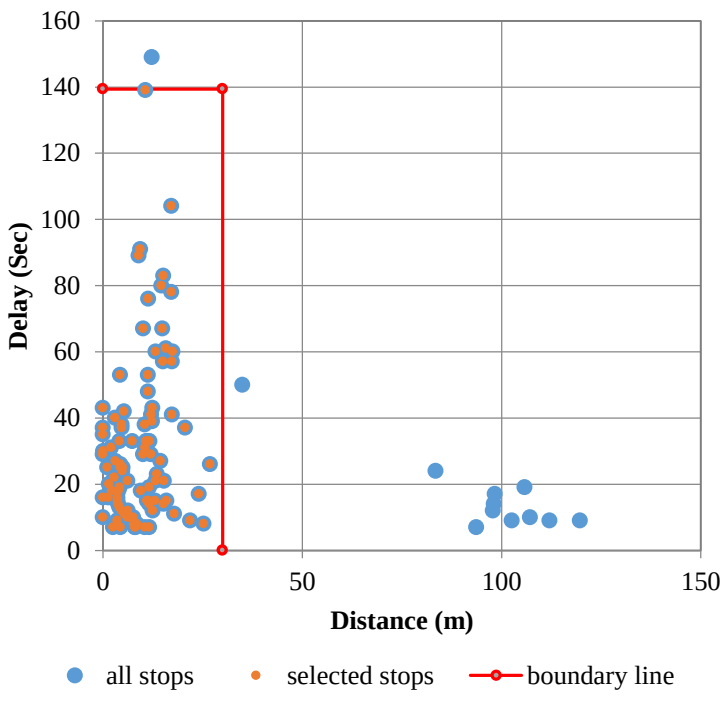

(B) The Proposed BL Algorithm

Figure C-9: Comparison of the BL Fitted to Stop Observation of University at Hazel Intersection

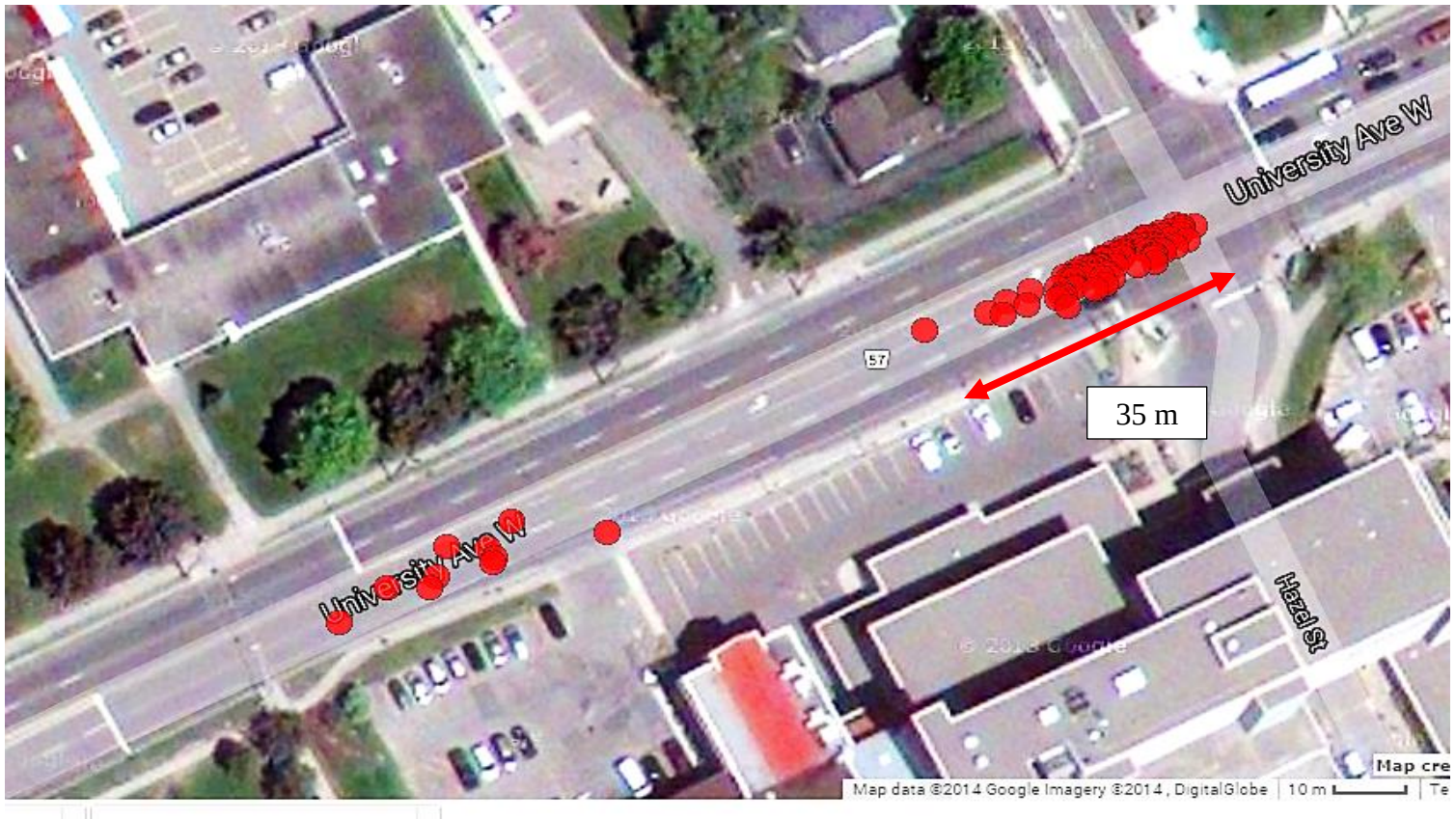

Figure C-10: The unscheduled stop observations superimposed on Google Maps for University at Hazel intersection

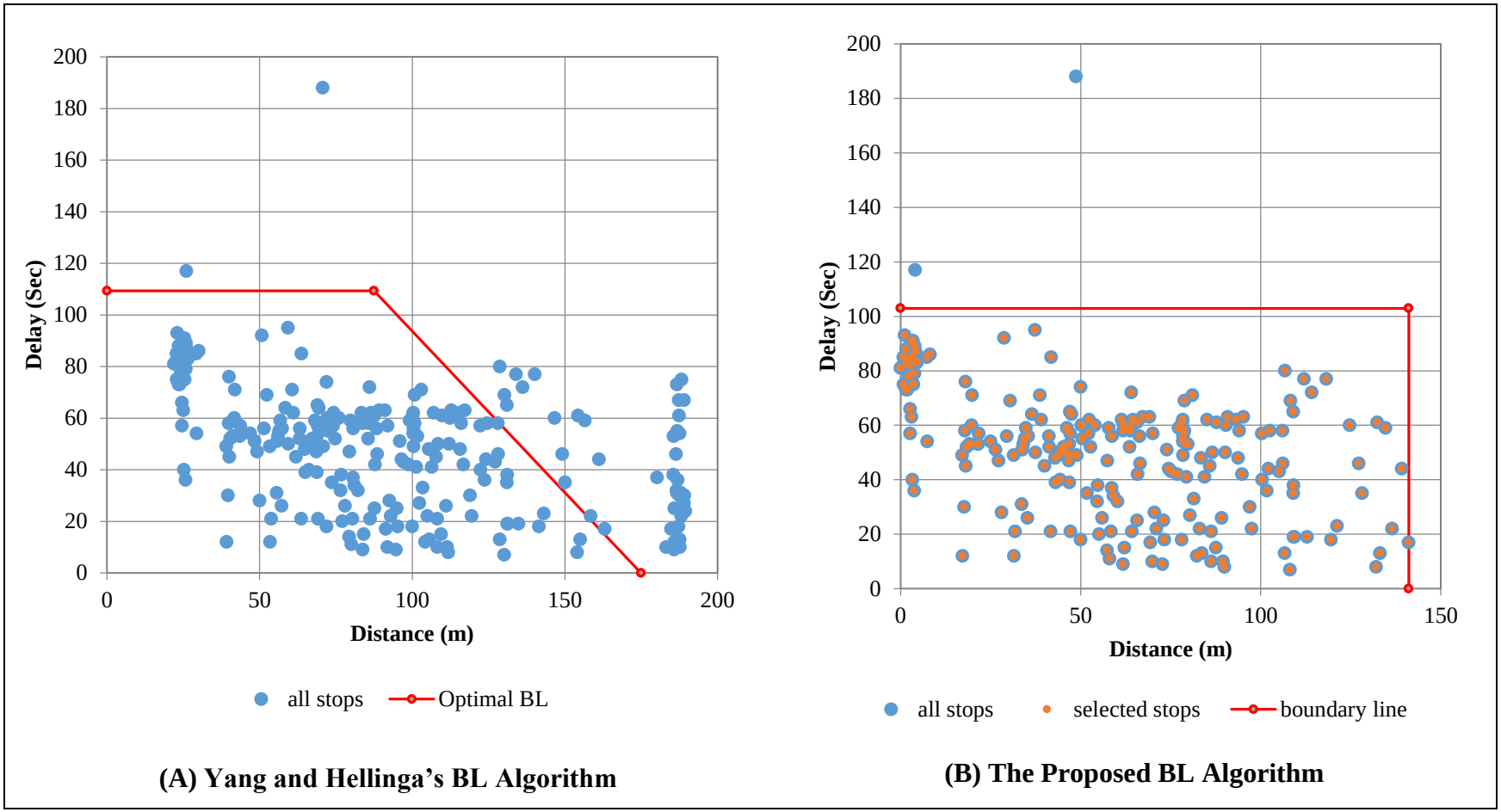

Figure C-11: Comparison of the BL Fitted to Stop Observation of Homer Watson at Ottawa Intersection (Route 11 IB)

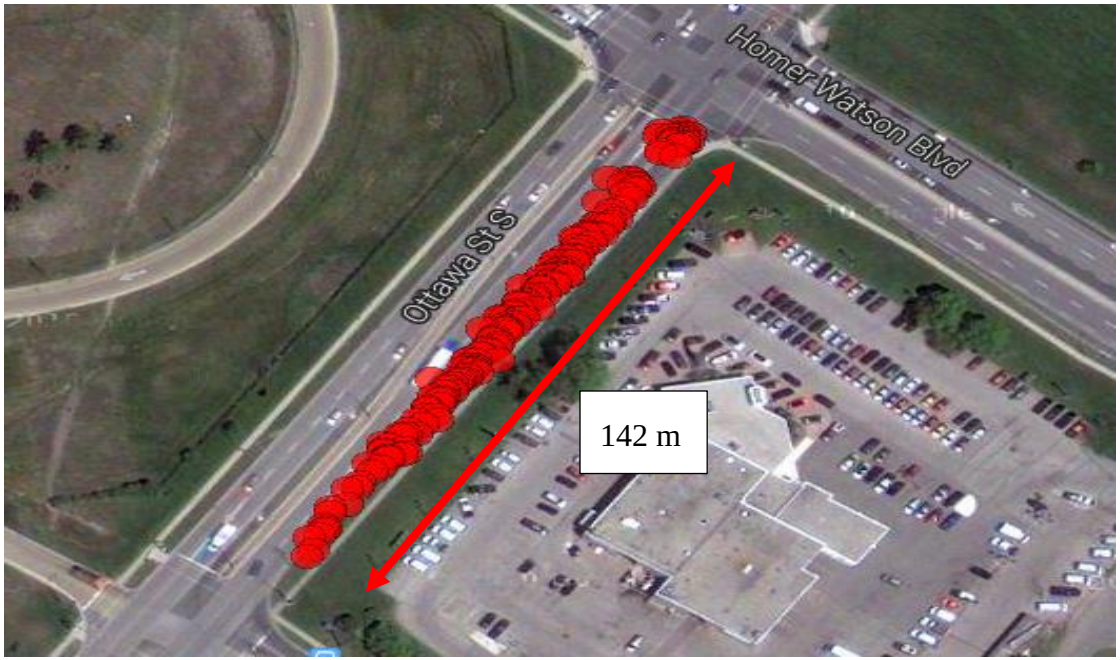

Figure C-12: The unscheduled stop observations superimposed on Google Maps for Homer Watson at Ottawa intersection

In Figure C-11(B) the observations from adjacent segments are excluded from the analysis.

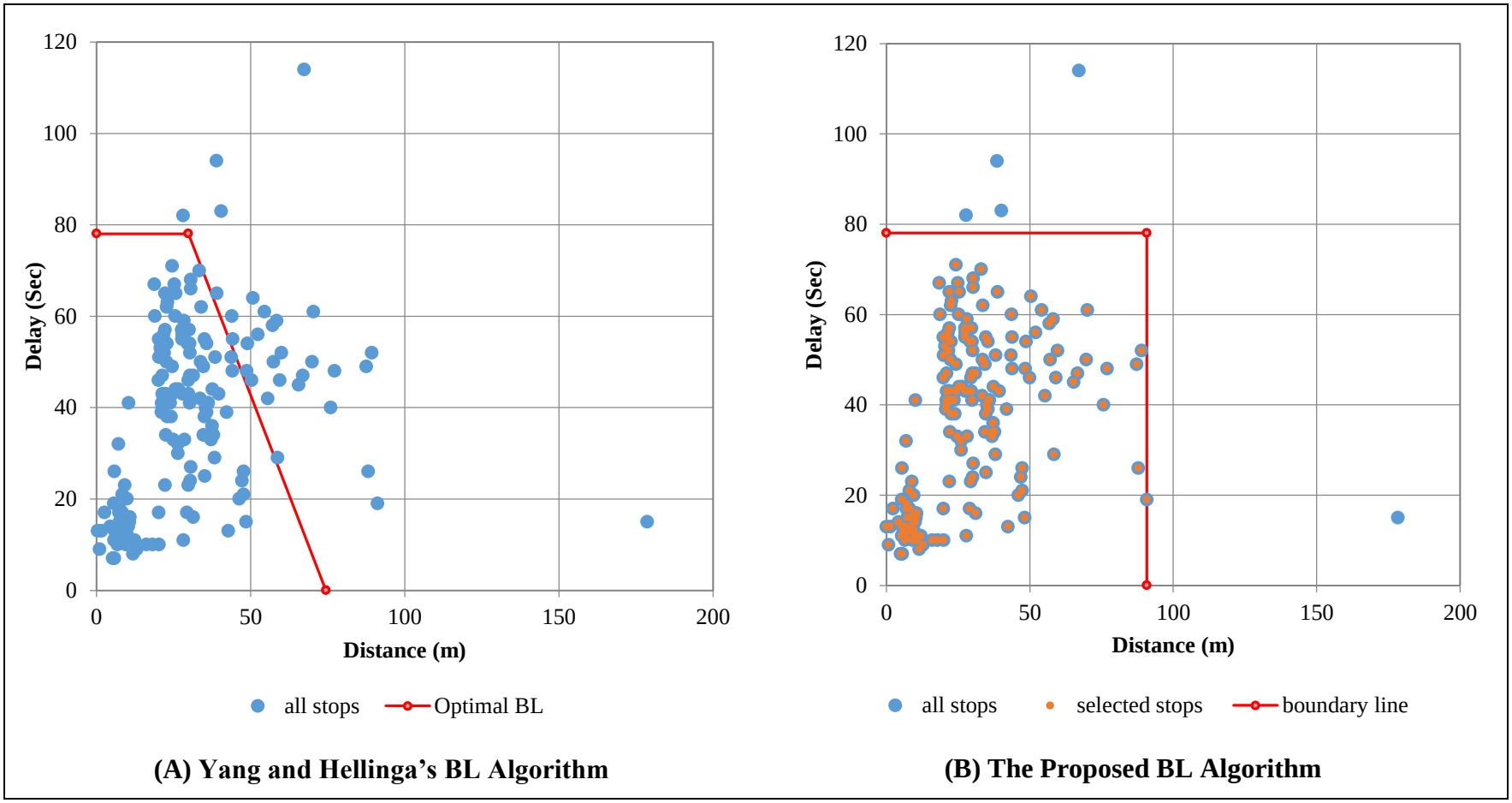

Figure C-13: Comparison of the BL Fitted to Stop Observation of Alpine at Ottawa Intersection

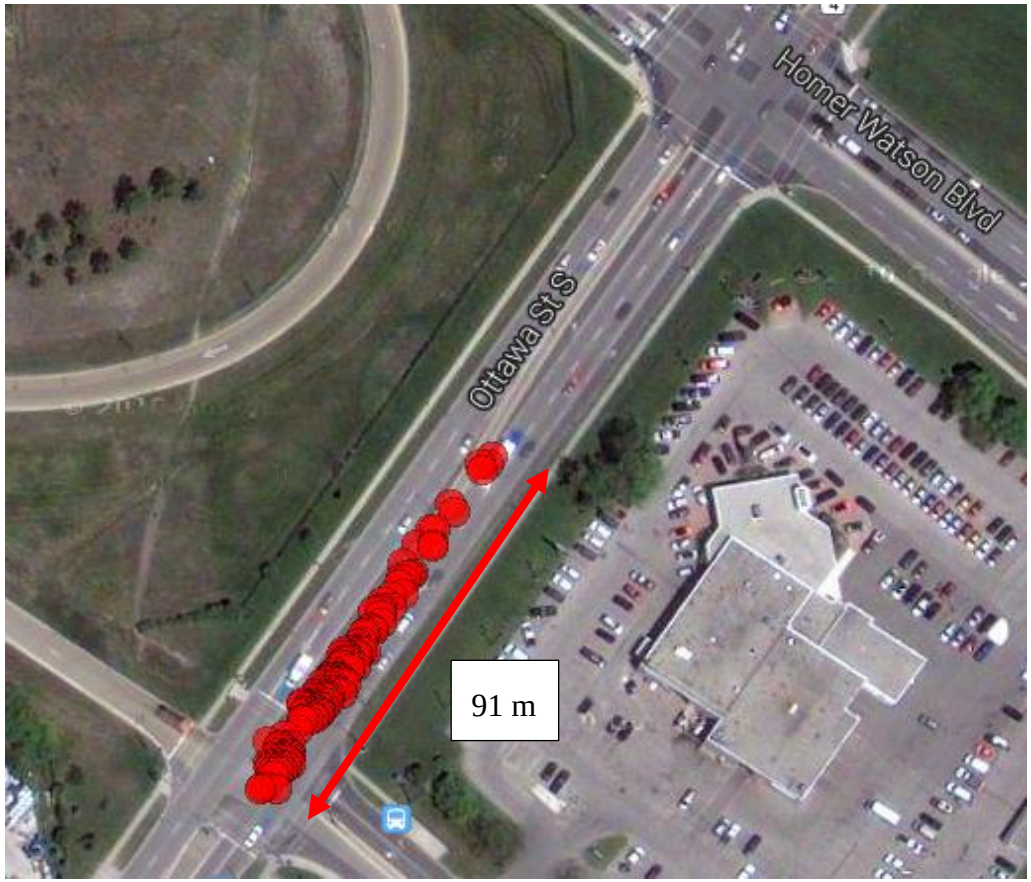

Figure C-14: The unscheduled stop observations superimposed on Google Maps for Alpine at Ottawa Intersection (route 11 OB)

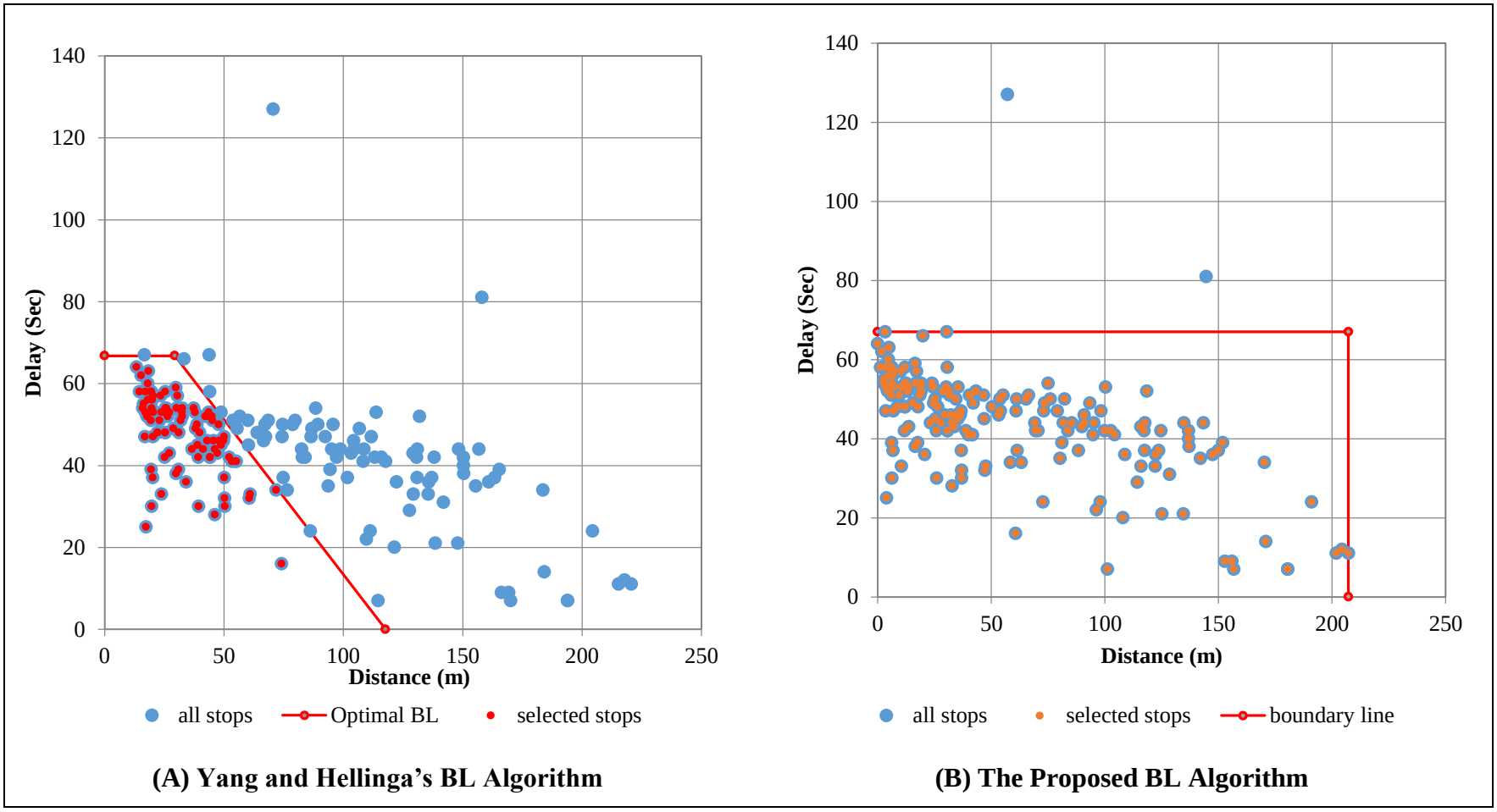

Figure C-15: Comparison of the BL Fitted to Stop Observation of Fountain and Shantz Hill Intersection

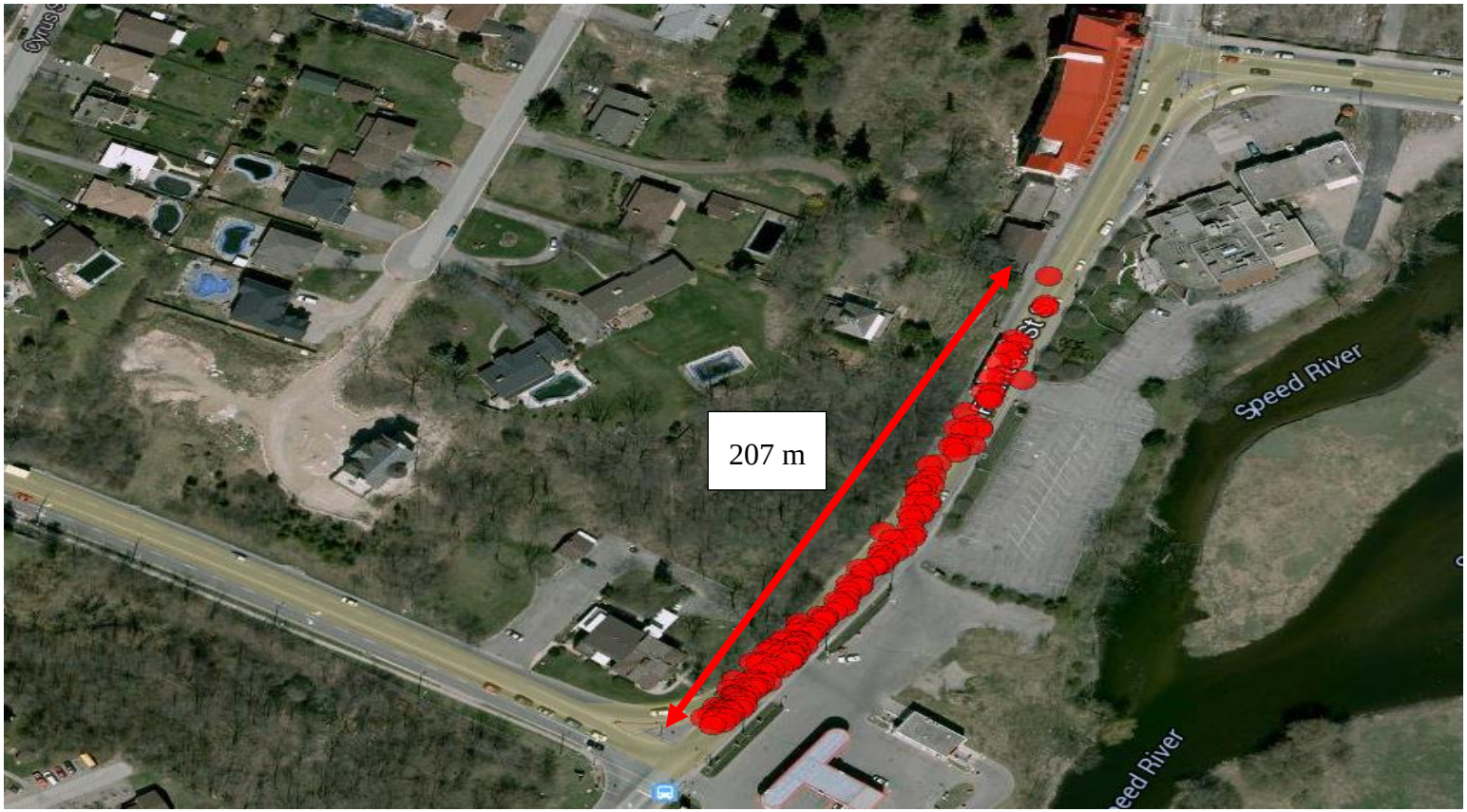

Figure C-16: The unscheduled stop observations superimposed on Google Maps for Fountain and Shantz Hill Intersection

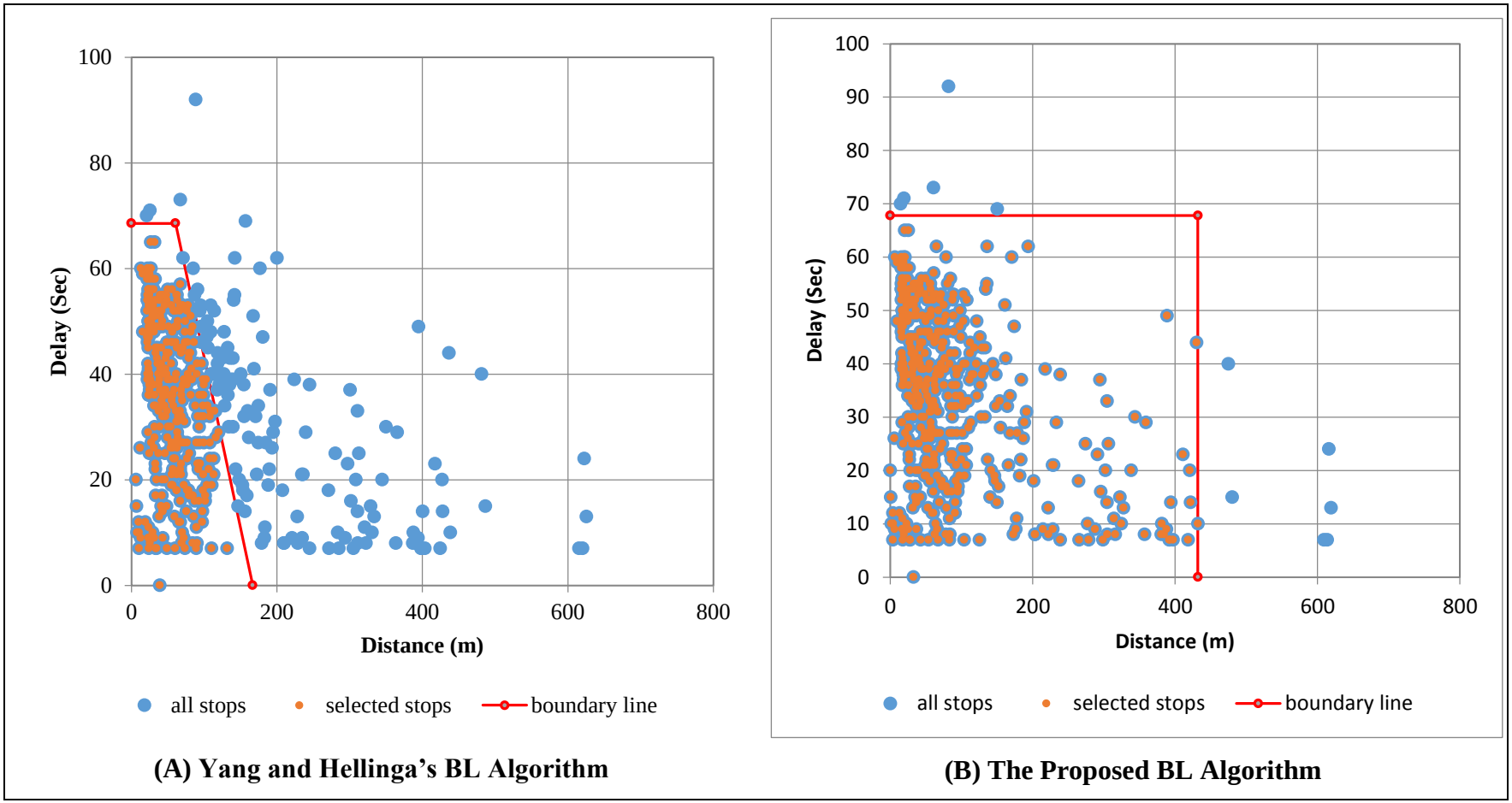

Figure C-17: Comparison of the BL Fitted to Stop Observation of Fischer-Hallman at Columbia Intersection

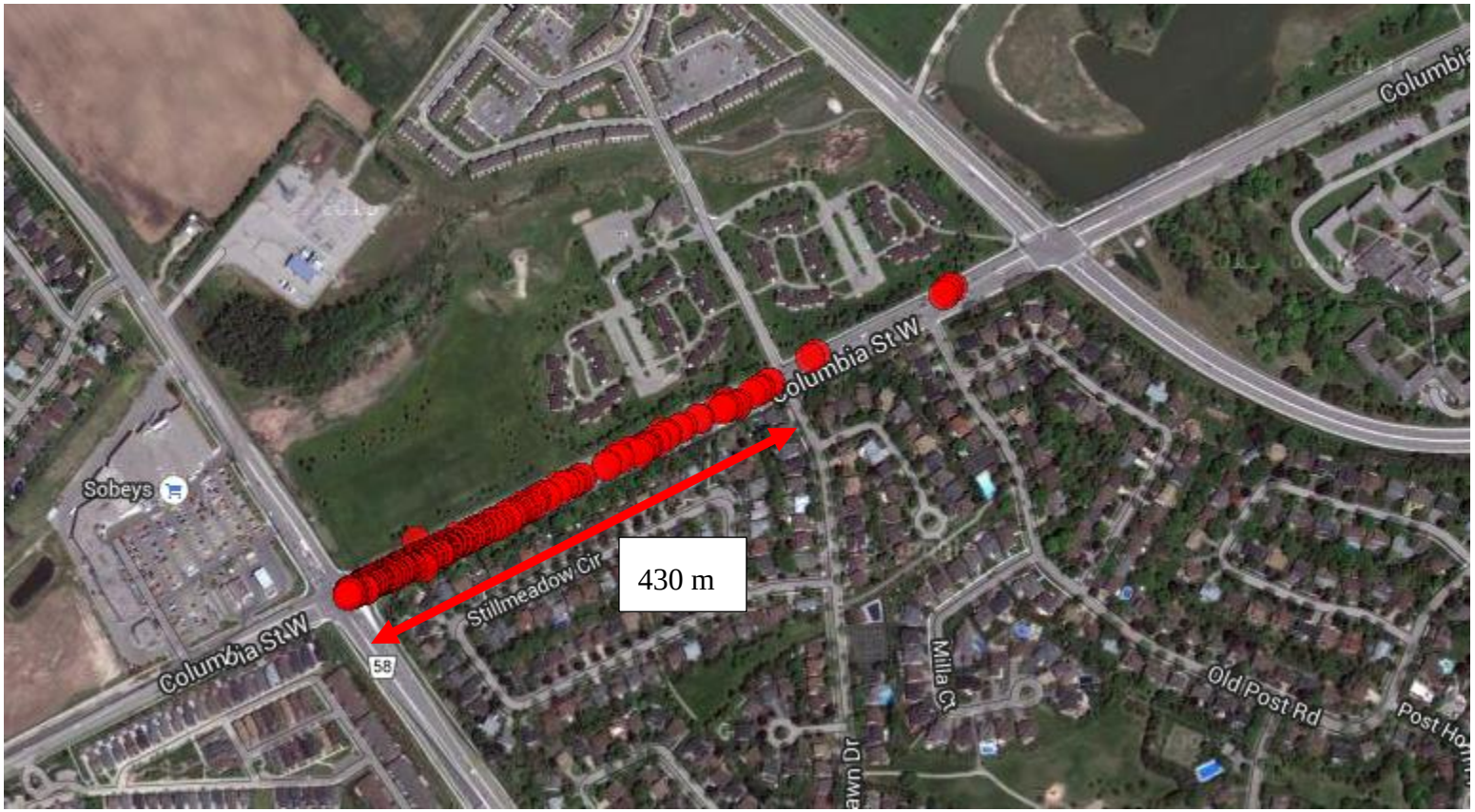

Figure C-18: The unscheduled stop observations superimposed on Google Maps for Fischer-Hallman at Columbia Intersection

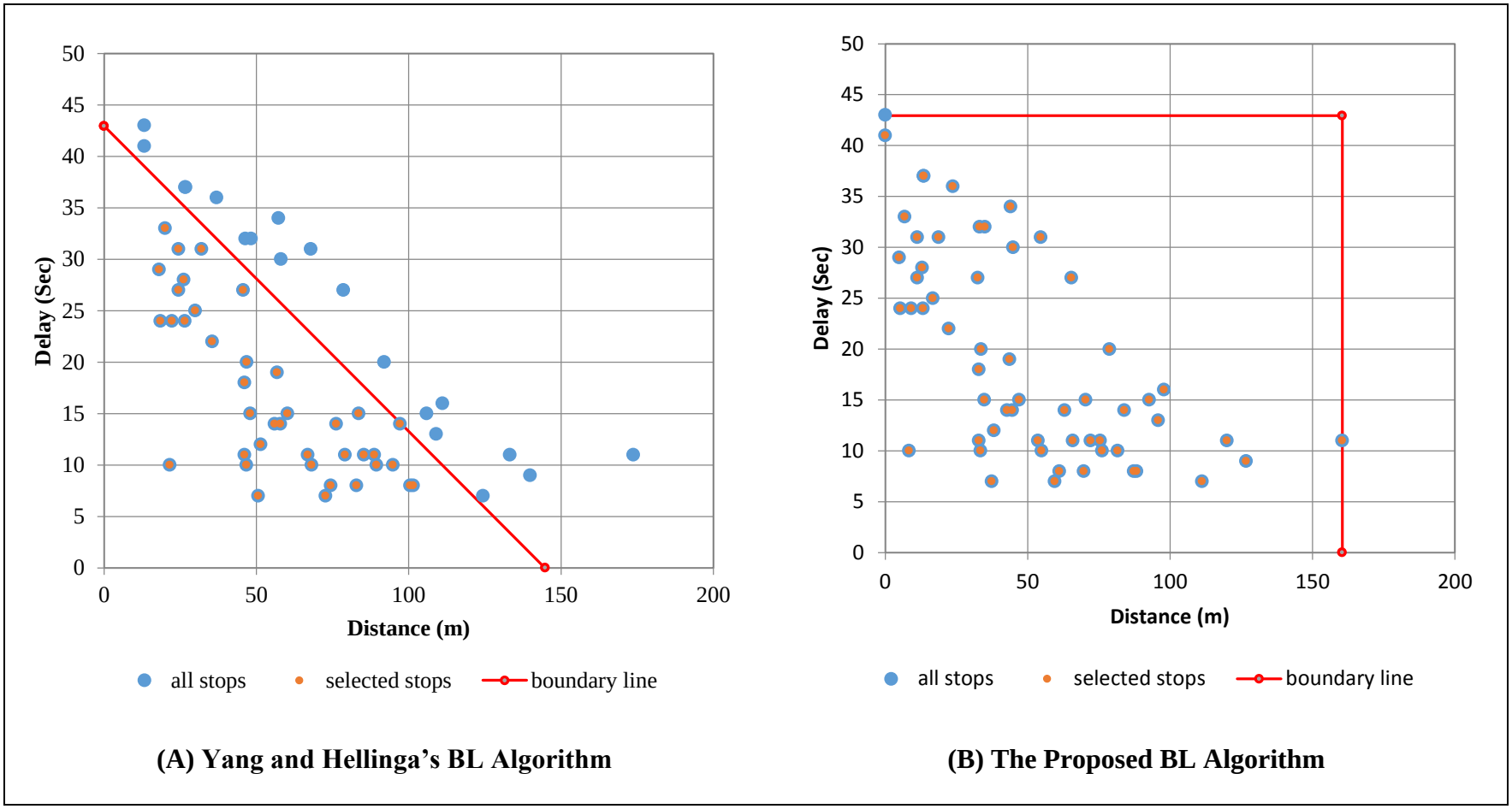

Figure C-19: Comparison of the BL Fitted to Stop Observation of Fischer-Hallman at Glasgow Intersection

Figure C-20: The unscheduled stop observations superimposed on Google Maps for Fischer-Hallman at Glasgow Intersection

Appendix D- List of Ranked Intersections based on the Proposed Ranking Index

Table D-1: Intersection Ranked List based on the Proposed Index

Downstream Intersection	Count of Route	Total trip number	Weighted Average Stopped Delay	weighted 90th percentile delay	Weighted Number of trips with delay	Max of Queue Length	Index	LOS
HESPELER_AT_Eagle_And_Pinebush	3	687	42.94	79.76	0.67	349	0.9	E
HOMER_WATSON_AT_ManitouAndDoon_Village	4	506	31.14	69.04	0.69	224	0.7	D
FOUNTAIN_AT_Shantz_Hill	3	521	27.47	51.95	0.70	266	0.7	D
FAIRWAY_AT_Lackner	1	145	31.99	96.80	0.58	99	0.7	D
VICTORIA_AT_Natchez	1	141	36.61	75.00	0.75	50	0.7	D
FRANKLIN_AT_Pinebush	3	393	17.70	52.51	0.50	370	0.6	C
KING_AT_Fountain	1	142	19.84	43.20	0.76	268	0.6	C
HESPELER_And_WATER_AT_Coronation_And_Dundas	6	1906	27.72	77.00	0.53	170	0.6	D
COURTLANDAndFAIRWAY_AT_Manitou	1	202	24.04	54.00	0.81	157	0.6	C
WESTMOUNT_AT_Glasgow	1	296	14.76	40.00	0.54	365	0.6	B
OTTAWA_AT_Homer_Watson	6	1601	26.47	72.85	0.52	163	0.6	C
FRANKLIN_AT_Savage	1	147	31.54	73.00	0.67	45	0.6	D
WATER_AT_Main	2	282	25.90	48.58	0.73	142	0.6	C
WESTMOUNT_AT_Williamsburg	1	290	27.62	66.00	0.78	35	0.6	D
FISCHER_HALLMAN_AT_Columbia	2	743	23.86	51.96	0.68	155	0.6	C
NORTHFIELD_AT_Kraus	1	297	29.82	72.00	0.67	34	0.6	D
HOMER_WATSON_AT_Conestoga_College	5	664	22.82	65.52	0.52	176	0.6	C
HOMER_WATSON_AT_Bleams	3	557	21.86	62.05	0.57	175	0.6	C
NORTHFIELD_AT_Skylark	1	285	31.02	69.00	0.66	35	0.6	D
FRANKLIN_AT_Elgin_And_Saginaw	2	289	25.44	65.73	0.57	125	0.6	C
UNIVERSITY_AT_Lincoln	1	296	17.78	61.00	0.45	256	0.6	C
FAIRWAY_AT_King	8	1500	20.17	51.77	0.48	256	0.6	C
HOMER_WATSON_AT_Pioneer	2	301	16.12	46.77	0.45	315	0.6	C
FAIRWAY_AT_Wilson	4	842	24.43	62.87	0.58	130	0.6	C

Downstream Intersection	Count of Route	Total trip number	Weighted Average Stopped Delay	weighted 90th percentile delay	Weighted Number of trips with delay	Max of Queue Length	Index	LOS
KING_AT_Farmers_MarketAndHwy_85_SB_Ramp	1	148	28.22	68.30	0.67	39	0.6	D
FRANKLIN_AT_Can_Amera	1	147	23.76	46.00	0.78	93	0.5	C
CHARLES_AT_Ontario	9	2137	21.20	54.76	0.58	168	0.5	C
KING_AT_Tu_Lane	1	245	21.10	83.00	0.35	158	0.5	C
KING_AT_Weber_Wool	1	148	23.39	57.00	0.66	81	0.5	C
VICTORIA_AT_Lackner	1	147	18.31	49.00	0.53	206	0.5	C
HIGHWAY_24_AT_Hwy_401_WB_Ramp	2	588	14.05	35.90	0.40	333	0.5	B
HESPELER_AT_Bishop	4	863	18.98	58.62	0.48	177	0.5	C
DUNDAS_AT_Beverly	1	246	22.85	60.00	0.59	88	0.5	C
ERBSVILLE_AT_Laurelwood	1	286	22.20	42.00	0.80	64	0.5	C
HESPELER_AT_Sheldon_And_Langs	2	588	9.89	40.00	0.31	370	0.5	B
BRIDGE_AT_University	1	202	17.87	55.60	0.49	169	0.5	C
MANITOU_AT_Wabanaki	2	301	17.36	44.03	0.57	178	0.5	C
WESTMOUNT_AT_University	1	296	17.24	45.10	0.57	169	0.5	C
PARKHILL_AT_George	1	97	17.39	38.00	0.67	145	0.5	C
OTTAWA_AT_Alpine	1	290	21.21	55.00	0.58	91	0.5	C
KING_AT_Columbia	1	142	15.47	48.30	0.45	215	0.5	C
FRANKLIN_AT_Main	1	147	19.46	48.20	0.64	97	0.5	C
VICTORIA_AT_Belmont	4	601	13.68	38.50	0.52	228	0.5	B
OTTAWA_AT_Westmount	2	492	21.35	59.06	0.54	84	0.5	C
KING_AT_Eagle	4	766	14.63	33.65	0.54	225	0.5	B
NORTHFIELD_AT_Colby_And_Conestoga	3	867	13.22	35.25	0.41	285	0.5	B
NORTHFIELD_AT_Highpoint	2	582	22.07	58.29	0.61	43	0.5	C
VICTORIA_AT_Lancaster	2	288	15.99	40.34	0.62	139	0.5	C
LANCASTER_AT_Guelph	1	144	22.83	64.20	0.50	44	0.5	C
KING_AT_Northfield	5	1422	18.44	44.42	0.54	123	0.5	C

Downstream Intersection	Count of Route	Total trip number	Weighted Average Stopped Delay	weighted 90th percentile delay	Weighted Number of trips with delay	Max of Queue Length	Index	LOS
UNIVERSITY_AT_Seagram	6	1758	17.55	45.96	0.52	135	0.5	C
COURTLAND_AT_Benton	1	290	18.85	38.00	0.72	63	0.5	C
FRANKLIN_AT_Jamieson_And_Holiday_Inn	4	587	13.92	40.39	0.50	186	0.4	B
NORTHFIELD_AT_Bridge	1	148	18.56	50.60	0.53	96	0.4	C
HOMER_WATSON_AT_Hwy_401_WB_RampAnd_New_Dundee	3	372	16.74	39.58	0.65	81	0.4	C
MANITOU_AT_Bleams	2	498	9.89	34.02	0.43	249	0.4	B
FISCHER_HALLMAN_AT_Highland	5	1344	13.14	40.86	0.43	196	0.4	B
FISCHER_HALLMAN_AT_Victoria	3	756	16.13	52.74	0.43	130	0.4	C
WEBER_AT_CedarAndKrug	2	582	19.21	52.23	0.46	93	0.4	C
FRANKLIN_AT_Avenue	2	294	10.39	34.70	0.39	253	0.4	B
WESTMOUNT_AT_Columbia	4	1492	15.38	48.52	0.44	140	0.4	B
KING_AT_Deer_Ridge	1	245	11.52	37.60	0.43	215	0.4	B
FISCHER_HALLMAN_AT_Queens	8	2364	13.44	44.02	0.41	176	0.4	B
HIGHLAND_AT_Highland_Cres	1	139	20.29	40.00	0.65	30	0.4	C
WESTMOUNT_AT_Highland	3	637	19.26	54.69	0.48	58	0.4	C
WEBER_AT_Victoria	1	146	18.51	50.00	0.48	76	0.4	C
FAIRWAY_AT_Fairview_Park_Mall	5	979	13.23	43.59	0.42	164	0.4	B
MAIN_AT_Wellington	2	391	13.01	37.61	0.46	163	0.4	B
VICTORIA_AT_Edna	1	141	14.45	32.00	0.72	47	0.4	B
DUNDAS_AT_Main	1	147	17.69	48.00	0.52	49	0.4	C
KING_AT_Waterloo	2	388	9.21	34.50	0.32	250	0.4	B
HIGHLAND_AT_Belmont	1	139	14.14	38.00	0.55	99	0.4	B
LANCASTER_AT_Bridgeport	2	284	13.28	38.86	0.52	113	0.4	B
KING_AT_Victoria	2	295	15.87	44.89	0.52	72	0.4	C
OTTAWA_AT_Strasburg	3	777	13.96	43.17	0.35	167	0.4	B
NORTHFIELD_AT_Davenport	3	437	14.18	47.18	0.42	118	0.4	B
CONCESSION_And_MAIN_AT_Chalm	1	147	12.62	34.00	0.48	149	0.4	B

Downstream Intersection	Count of Route	Total trip number	Weighted Average Stopped Delay	weighted 90th percentile delay	Weighted Number of trips with delay	Max of Queue Length	Index	LOS
ers								
WEBER_AT_Frederick	4	731	13.43	41.52	0.45	129	0.4	B
WEBER_AT_Union	2	290	11.75	39.05	0.44	149	0.4	B
FRANKLIN_AT_Bishop	2	294	13.65	50.60	0.33	142	0.4	B
CEDAR_AT_Grand	1	144	13.16	39.60	0.43	132	0.4	B
ERB_AT_Fischer_Hallman	3	1058	12.93	47.99	0.33	148	0.4	B
LANCASTER_AT_Wellington	2	284	13.97	36.15	0.46	125	0.4	B
WEBER_AT_Queen	1	141	15.72	43.00	0.55	37	0.4	C
OTTAWA_AT_River	4	617	14.01	50.16	0.41	86	0.4	B
VICTORIA_AT_Strange_And_West	2	295	10.43	28.00	0.52	145	0.4	B
FAIRWAY_AT_Hwy_8_EB_Ramp	5	1069	13.05	40.43	0.45	110	0.4	B
STRASBURG_AT_Blockline	7	2022	9.73	35.58	0.36	187	0.4	B
UNIVERSITY_AT_King	4	1080	13.12	30.83	0.35	182	0.4	B
UNIVERSITY_AT_Albert	8	2200	10.81	34.65	0.38	172	0.4	B
WEBER_AT_University	2	498	8.23	27.82	0.28	255	0.4	B
KING_AT_Northland_And_Wyman	1	146	14.75	47.50	0.45	53	0.4	B
SPORTSWORLD_AT_Gateway	1	245	15.15	41.50	0.45	60	0.3	B
UNION_AT_Moore	1	147	14.71	42.00	0.51	31	0.3	B
AINSLIE_AT_Main	6	1609	10.47	32.73	0.36	159	0.3	B
WILSON_AT_Kingsway	3	546	12.34	31.28	0.55	66	0.3	B
KING_AT_Conestoga_Mall	5	979	14.56	41.21	0.41	68	0.3	B
QUEEN_AT_Charles	9	2277	10.24	28.93	0.42	141	0.3	B
PARK_AT_Union	2	294	12.43	29.00	0.54	71	0.3	B
ERB_AT_Amos	1	144	11.56	37.70	0.44	89	0.3	B
NORTHFIELD_AT_Parkside	3	1124	8.42	30.85	0.34	180	0.3	B
DOON_VILLAGE_AT_Pioneer	1	155	8.95	22.00	0.53	121	0.3	B
WEBER_AT_Parkside	3	868	11.05	33.81	0.46	93	0.3	B
WEBER_AT_Northfield	2	431	12.34	38.95	0.32	126	0.3	B
WESTMOUNT_AT_Queen	2	588	13.66	48.00	0.38	56	0.3	B

Downstream Intersection	Count of Route	Total trip number	Weighted Average Stopped Delay	weighted 90th percentile delay	Weighted Number of trips with delay	Max of Queue Length	Index	LOS
FISCHER_HALLMAN_AT_University	4	1208	12.38	34.51	0.34	131	0.3	B
FISCHER_HALLMAN_AT_Ottawa	4	1497	10.62	44.19	0.25	149	0.3	B
CHARLES_AT_Benton	11	2961	10.86	32.52	0.38	123	0.3	B
VICTORIA_AT_Frederick	2	288	7.93	26.62	0.36	177	0.3	B
KING_AT_Westminster	4	766	5.67	20.58	0.29	245	0.3	A
FAIRWAY_AT_River	2	230	9.50	29.83	0.40	132	0.3	B
ARTHUR_AT_Listowel	1	150	7.58	32.00	0.30	180	0.3	A
SHANTZ_HILL_AT_Preston_Parkway	1	246	11.75	41.00	0.39	72	0.3	B
MAIN_AT_Elgin	1	147	8.21	24.00	0.43	136	0.3	B
HIGHLAND_AT_Eastforest_Trail	2	287	12.41	35.45	0.49	30	0.3	B
WEBER_AT_Columbia	1	142	13.70	59.90	0.26	33	0.3	B
STRASBURG_AT_Forest_Glen_Plaza	9	2157	7.82	23.68	0.34	169	0.3	B
VICTORIA_AT_Hazelglen	1	148	11.43	40.70	0.38	64	0.3	B
HESPELER_AT_600And611_Hespeler_Road_HomesenseAndTravelodge	2	588	8.46	33.70	0.29	151	0.3	B
WILLIAM_AT_Caroline	2	301	13.37	44.72	0.39	30	0.3	B
HIGHLAND_AT_Queen	4	867	11.23	35.17	0.44	58	0.3	B
BISHOP_AT_Conestoga	3	622	8.25	23.54	0.44	121	0.3	B
PINEBUSH_AT_Conestoga	4	1077	12.26	47.67	0.30	62	0.3	B
QUEEN_AT_Goebel	1	294	9.40	29.00	0.41	102	0.3	B
FISCHER_HALLMAN_AT_Greenbrook_And_Hwy_7And8_WB_Rmp	4	1497	9.16	41.74	0.25	128	0.3	B
CHARLES_AT_Gaukel	13	2859	9.53	31.41	0.33	125	0.3	B
KING_AT_Water	4	585	6.50	28.19	0.29	174	0.3	A
UNIVERSITY_AT_Hazel	4	1069	9.53	29.64	0.41	95	0.3	B
COURTLAND_AT_Stirling	2	489	12.99	38.24	0.30	80	0.3	B
BELMONT_AT_Glasgow	1	147	10.62	31.00	0.45	54	0.3	B
PINEBUSH_AT_WalmartAndHome_Depot	2	588	7.55	30.85	0.28	153	0.3	A

Downstream Intersection	Count of Route	Total trip number	Weighted Average Stopped Delay	weighted 90th percentile delay	Weighted Number of trips with delay	Max of Queue Length	Index	LOS
FREDERICK_AT_Duke	8	1450	7.88	25.38	0.39	119	0.3	B
FRANKLIN_AT_Sheldon	3	393	8.62	31.20	0.23	156	0.3	B
FREDERICK_AT_Edna	2	292	10.06	35.51	0.34	79	0.3	B
FREDERICK_AT_Lancaster	2	290	10.23	32.10	0.40	63	0.3	B
KING_AT_Bridgeport	2	827	10.60	22.24	0.36	110	0.3	B
WESTMOUNT_AT_Gage	2	498	9.71	27.23	0.44	59	0.3	B
FRANKLIN_AT_Clyde	2	294	9.11	32.00	0.38	69	0.3	B
OTTAWA_AT_Lackner	3	324	10.13	29.60	0.43	48	0.3	B
WATER_AT_Dando	2	684	1.99	5.21	0.11	334	0.3	A
HESPELER_AT_Munch	3	873	8.03	30.61	0.30	112	0.3	B
VICTORIA_AT_Charles	1	437	7.46	25.00	0.36	110	0.3	A
ARTHUR_AT_Church	1	148	9.45	29.00	0.46	35	0.3	B
WESTMOUNT_AT_Victoria	5	959	10.61	37.18	0.32	54	0.3	B
OTTAWA_AT_Laurentian_Power_Centre	4	1067	5.66	21.73	0.24	182	0.3	A
SHELDON_AT_Conestoga	1	437	8.90	33.80	0.35	65	0.3	B
FREDERICK_AT_River	2	286	9.01	32.55	0.38	54	0.3	B
KING_AT_Union	1	147	7.85	30.00	0.36	77	0.3	B
OTTAWA_AT_Charles	1	390	10.65	38.00	0.35	30	0.3	B
HESPELER_AT_Dunbar	5	1405	7.85	31.33	0.29	99	0.3	B
STRASBURG_AT_Bleams	3	588	8.70	28.70	0.39	54	0.3	B
BEARINGER_AT_Parkside	1	437	8.59	29.40	0.39	47	0.3	B
OTTAWA_AT_International	1	295	9.77	37.60	0.34	30	0.3	B
FOUNTAIN_AT_Hwy_401_EB_Ramp	1	133	7.72	23.80	0.42	59	0.2	B
PARK_AT_Glasgow	1	147	8.69	27.80	0.40	44	0.2	B
FAIRWAY_AT_Morgan	2	292	8.94	26.58	0.37	61	0.2	B
KING_AT_Deer_Ridge_CentreAndSportsworld_Crossing	1	245	4.70	21.50	0.23	172	0.2	A
KING_AT_Bishop	3	520	7.57	26.55	0.37	65	0.2	A

Downstream Intersection	Count of Route	Total trip number	Weighted Average Stopped Delay	weighted 90th percentile delay	Weighted Number of trips with delay	Max of Queue Length	Index	LOS
KING_AT_Benton_And_Frederick	6	1160	6.61	24.09	0.34	94	0.2	A
FISCHER_HALLMAN_AT_Activa	1	288	8.81	36.00	0.28	59	0.2	B
FISCHER_HALLMAN_AT_WestmountAndMax_Becker	5	1954	8.46	31.11	0.24	91	0.2	B
UNIVERSITY_AT_Trans_Canada_Trail	6	1662	6.40	23.46	0.31	103	0.2	A
COLUMBIA_AT_HageyAndUniversity_Of_Waterloo	5	1640	7.54	26.98	0.27	98	0.2	A
KING_AT_Martin_Grove_And_Hwy_85_NB_Ramp_Wool	2	298	6.66	24.75	0.32	86	0.2	A
FISCHER_HALLMAN_AT_Laurelwood	1	286	7.73	32.40	0.27	72	0.2	B
EDNA_AT_Hwy_7And8_WB_Ramp	2	288	9.43	31.79	0.32	36	0.2	B
CONCESSION_AT_Bishop	2	275	7.09	24.58	0.37	51	0.2	A
ARTHUR_AT_Oriole_Pkwy	2	298	5.79	19.85	0.33	92	0.2	A
LEXINGTON_AT_Davenport	2	444	7.21	31.67	0.28	58	0.2	A
WELLINGTON_AT_Moore	1	147	7.14	25.00	0.39	30	0.2	A
COLUMBIA_AT_Hazel	1	285	9.11	43.20	0.20	30	0.2	B
COLUMBIA_AT_Albert	3	741	5.23	23.90	0.20	124	0.2	A
AINSIE_AT_Parkhill	4	1415	6.52	26.19	0.25	85	0.2	A
OTTAWA_AT_Heritage	3	384	4.58	18.17	0.29	109	0.2	A
ARTHUR_AT_First	2	298	5.49	21.04	0.28	95	0.2	A
HESPELER_AT_Can_AmeraAndYMCA_Driveway	5	1557	6.23	23.62	0.27	84	0.2	A
KING_AT_Lowther	2	491	2.48	11.66	0.16	203	0.2	A
ALBERT_AT_Hazel_And_Bearinger	2	582	6.63	24.29	0.34	47	0.2	A
WESTMOUNT_AT_Blockline	3	955	7.62	27.08	0.30	47	0.2	A
FRANKLIN_AT_Kingsway	2	827	6.58	24.66	0.35	41	0.2	A
HESPELER_AT_Beaverdale_And_Queen	1	294	6.71	28.70	0.26	64	0.2	A
RIVER_AT_Holborn	4	821	6.00	21.14	0.31	72	0.2	A
FREDERICK_AT_Bruce	1	147	6.62	24.00	0.34	46	0.2	A

Downstream Intersection	Count of Route	Total trip number	Weighted Average Stopped Delay	weighted 90th percentile delay	Weighted Number of trips with delay	Max of Queue Length	Index	LOS
HESPELER_AT_Burger_King_580	1	294	6.44	26.50	0.29	60	0.2	A
UNIVERSITY_AT_Phillip	5	1225	4.82	14.20	0.20	156	0.2	A
WEBER_AT_Albert	2	582	5.79	21.11	0.30	77	0.2	A
WESTMOUNT_AT_Chopin_And_Brybeck	3	646	5.44	18.70	0.34	70	0.2	A
HESPELER_AT_Avenue	2	827	3.61	17.87	0.15	170	0.2	A
QUEEN_AT_Courtland	3	728	6.82	24.69	0.29	61	0.2	A
HESPELER_AT_480And499_Hespeler_Road_WinnersAndShoppers	2	588	3.38	13.90	0.19	169	0.2	A
KING_AT_River	1	246	5.70	25.50	0.25	78	0.2	A
FISCHER_HALLMAN_AT_Glasgow	3	1061	3.64	15.72	0.18	160	0.2	A
KING_AT_Francis	3	443	4.41	18.89	0.25	102	0.2	A
ERB_AT_Father_David_Bauer	2	301	6.54	20.62	0.19	105	0.2	A
KING_AT_Dolph	2	378	2.81	12.41	0.20	148	0.2	A
HOMER_WATSON_AT_Doon_South_Rd_And_Monarch_Tr	2	292	5.51	21.00	0.31	47	0.2	A
WELLINGTON_AT_Dickson	1	246	5.50	18.00	0.36	32	0.2	A
KING_AT_Gaukel	3	583	6.67	32.13	0.17	50	0.2	A
KRUG_AT_East	1	289	5.14	21.20	0.30	43	0.2	A
KING_AT_Breithaupt	2	537	6.14	22.03	0.25	52	0.2	A
COLUMBIA_AT_Phillip	2	914	3.24	16.50	0.16	123	0.2	A
OTTAWA_AT_Old_Chicopee	1	85	4.85	18.60	0.29	44	0.2	A
FISCHER_HALLMAN_AT_McGarry	4	1344	3.89	12.54	0.13	139	0.2	A
BRIDGE_AT_Dansbury	1	202	6.42	23.00	0.25	30	0.2	A
MARGARET_AT_Wellington	1	143	4.27	16.80	0.28	55	0.2	A
KING_AT_Erb	2	827	3.98	10.90	0.19	115	0.2	A
FISCHER_HALLMAN_AT_Keatsway	2	914	3.65	17.70	0.18	95	0.2	A
HIGHLANDAT_Highland_Hills_Mall	2	299	5.65	17.08	0.30	30	0.2	A
KING_AT_KCI_AndCentral_Meat	1	437	3.27	14.00	0.24	80	0.2	A

Downstream Intersection	Count of Route	Total trip number	Weighted Average Stopped Delay	weighted 90th percentile delay	Weighted Number of trips with delay	Max of Queue Length	Index	LOS
RIVER_AT_Lorraine	1	145	4.34	16.20	0.26	54	0.2	A
MILL_AT_Stirling	4	1067	4.42	14.95	0.21	72	0.2	A
KING_AT_William	2	547	4.79	8.74	0.19	102	0.2	A
WESTMOUNT_AT_Greenbrook	2	498	3.79	17.58	0.20	73	0.1	A
UNIVERSITY_AT_WLU_Ped	6	1373	2.54	12.77	0.16	110	0.1	A
KING_AT_Green	1	437	3.99	20.00	0.19	56	0.1	A
CHARLES_AT_Cedar	6	1944	2.26	8.39	0.14	132	0.1	A
KING_AT_Willis_Way	2	547	4.52	17.14	0.20	52	0.1	A
HIGHLAND_AT_Westforest_Trail	1	139	3.94	17.00	0.26	30	0.1	A
WESTMOUNT_AT_Westcourt_And_Father_David_Bauer	1	296	3.84	16.00	0.21	56	0.1	A
ERB_AT_Roslin	2	301	5.43	14.40	0.25	30	0.1	A
KING_AT_Marshall	1	437	1.82	9.30	0.14	121	0.1	A
AINSLIE_AT_Dickson	2	684	3.76	20.43	0.19	43	0.1	A
FAIRWAY_AT_655_Fairway	2	498	4.21	20.05	0.19	38	0.1	A
WESTMOUNT_AT_William	1	296	2.35	11.00	0.18	89	0.1	A
CHARLES_AT_Water	2	827	3.23	15.24	0.20	56	0.1	A
CHARLES_AT_Stirling	5	1700	2.41	6.72	0.14	109	0.1	A
WEBER_AT_Randall	1	146	3.30	14.00	0.23	30	0.1	A
KING_And_CORONATION_AT_Concession	2	491	2.51	9.66	0.13	83	0.1	A
KING_AT_WLU_Ped	1	437	1.86	10.30	0.13	85	0.1	A
CONCESSION_AT_Christopher	1	147	2.18	10.40	0.18	56	0.1	A
KING_AT_Agnes	2	827	3.05	10.62	0.17	52	0.1	A
QUEEN_AT_Elm_RidgeAndFire_Station_7	1	294	2.82	16.00	0.16	32	0.1	A
FISCHER_HALLMAN_AT_Highland_Hills_Mall	2	589	3.03	8.06	0.13	69	0.1	A
KING_AT_Ontario	1	293	3.16	7.00	0.10	83	0.1	A
BEVERLY_AT_Kerr	1	245	1.59	9.00	0.14	67	0.1	A

Downstream Intersection	Count of Route	Total trip number	Weighted Average Stopped Delay	weighted 90th percentile delay	Weighted Number of trips with delay	Max of Queue Length	Index	LOS
AINSLIE_AT_SimcoeAndMarket	3	1121	2.38	9.11	0.16	50	0.1	A
KING_AT_Wellington	1	437	2.60	11.40	0.13	38	0.1	A
WESTMOUNT_AT_Erb	3	597	1.83	6.00	0.09	71	0.1	A
HESPELER_AT_Cambridge_Centre	1	294	2.47	11.70	0.13	30	0.1	A
FAIRWAY_AT_500And589_Fairway	1	202	2.19	9.00	0.14	30	0.1	A
CHARLES_AT_Francis	1	437	1.93	9.00	0.11	45	0.1	A
COLUMBIA_AT_Rim_Driveway	3	1056	2.11	6.25	0.12	32	0.1	A
FISCHER_HALLMAN_AT_CraigleithAndRoxton	2	914	1.49	3.55	0.09	40	0.0	A
WATER_AT_Samuelson	1	294	1.06	0.10	0.09	55	0.0	A
DUNDAS_AT_Easton	1	246	1.37	0.10	0.09	46	0.0	A
WEBER_AT_Scott	1	289	1.07	1.40	0.10	30	0.0	A
CHARLES_AT_Borden	2	827	0.76	0.10	0.07	47	0.0	A
KING_AT_Central	1	437	0.73	0.10	0.06	45	0.0	A
ERB_AT_University	2	301	0.67	0.10	0.05	42	0.0	A
ERB_AT_Caroline	1	144	1.06	0.10	0.03	30	0.0	A

Appendix E- Unscheduled Stop Observations of 7 worst Intersection Approaches Superimposed on Google Maps

Figure E-1: Unscheduled Stop Observations for Hespeler at Eagle and Pinebush

The buses traversing this route make a through movement at this intersection.

Figure E-2: Unscheduled Stop Observations for Homer Watson at Manitou and Doon Village

The buses traversing this route make a through movement at this intersection.

Figure E-3: Unscheduled Stop Observations for Franklin at Savage Dr.

The buses traversing this route make a left turn maneuver at this intersection.

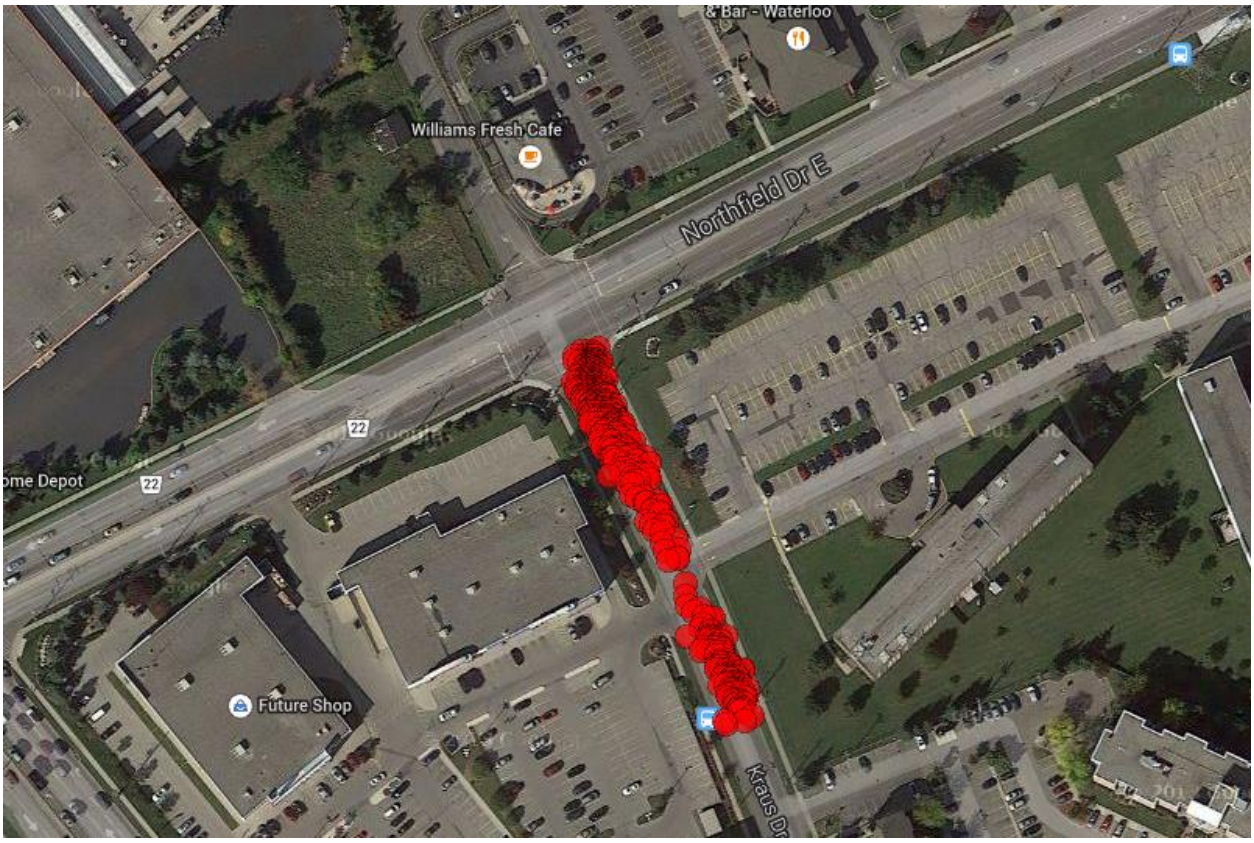

Figure E-4: Unscheduled Stop Observations for Northfield at Kraus

A portion of the buses traversing this route make a right turn maneuver and a portion make left turn maneuver at this intersection.

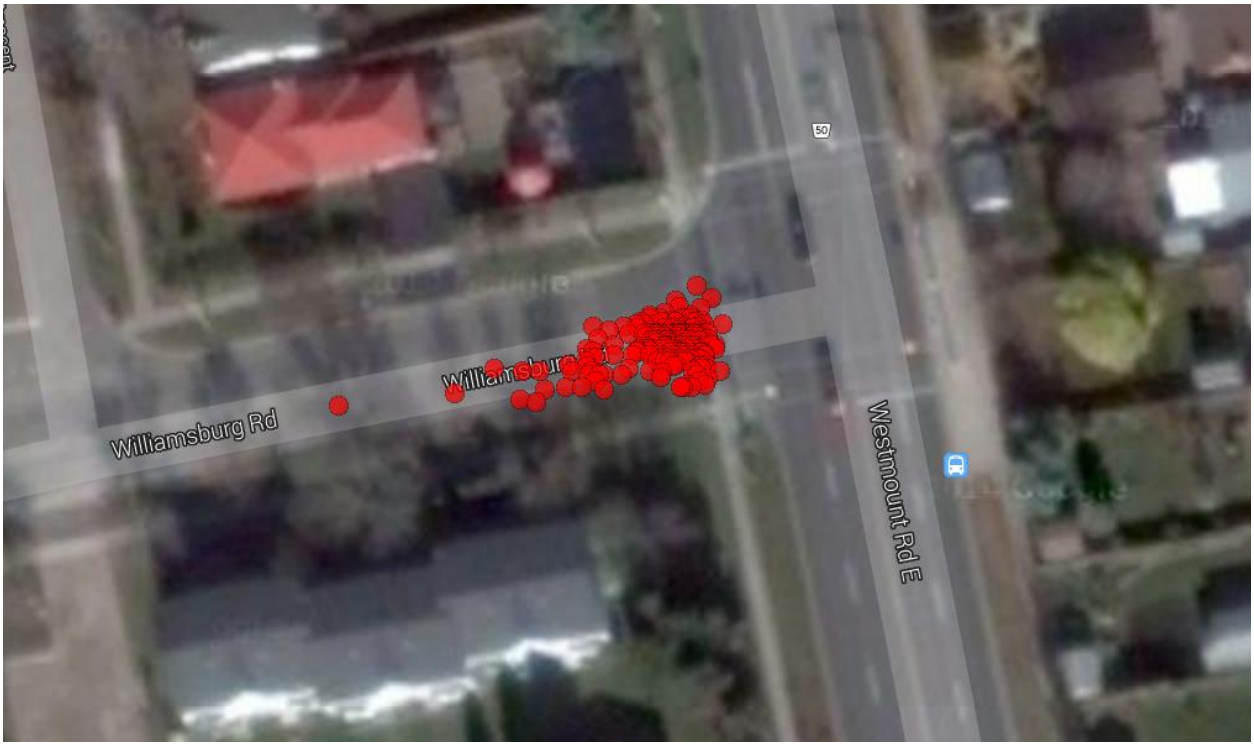

Figure E-5: Unscheduled Stop Observations for Westmount at Williamsburg

Williamsburg is a collector roadway connecting to Westmount arterial. The buses traversing this route make a left turn maneuver at this intersection.

Figure E-6: Unscheduled Stop Observations for Northfield at Skylark

Skylark is a collector roadway connecting to Northfield. The buses traversing this route make a left turn maneuver at this intersection.

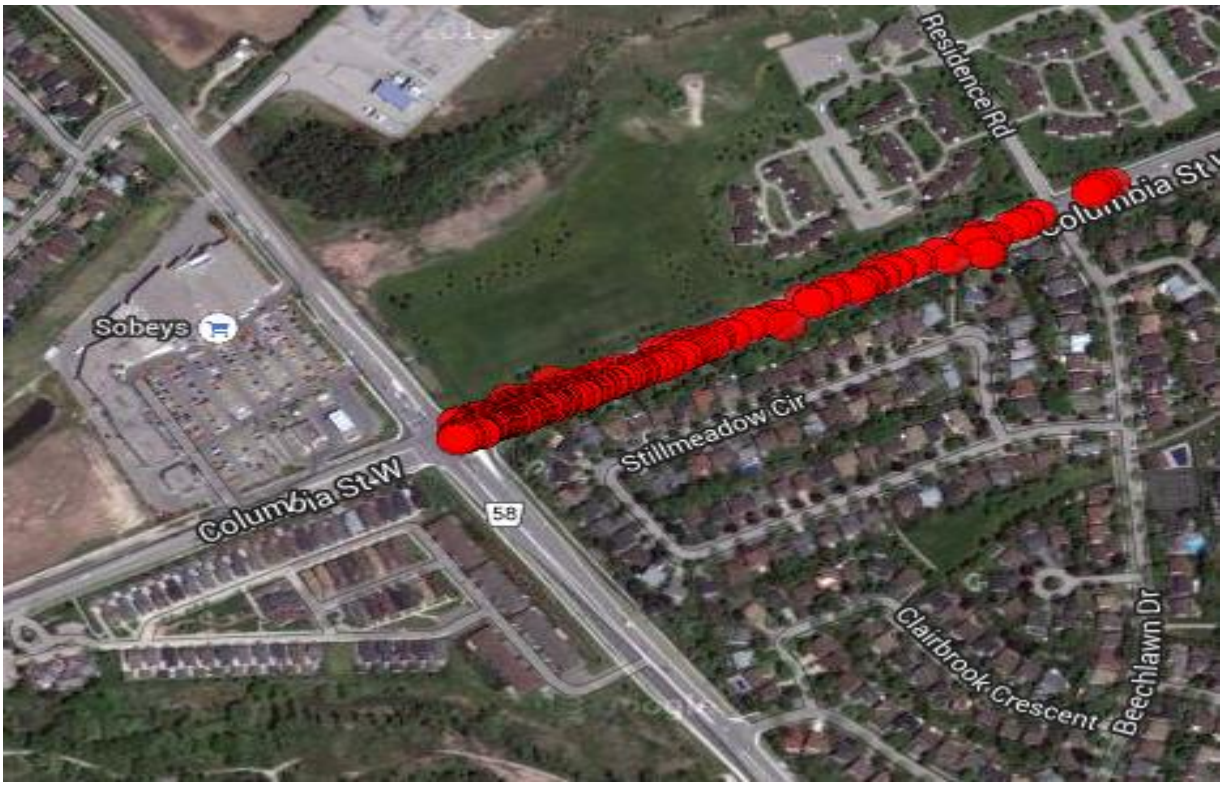

Figure E-7: Unscheduled Stop Observations for Fisher-Hallman at Columbia

The buses traversing this route make a through movement at this intersection.

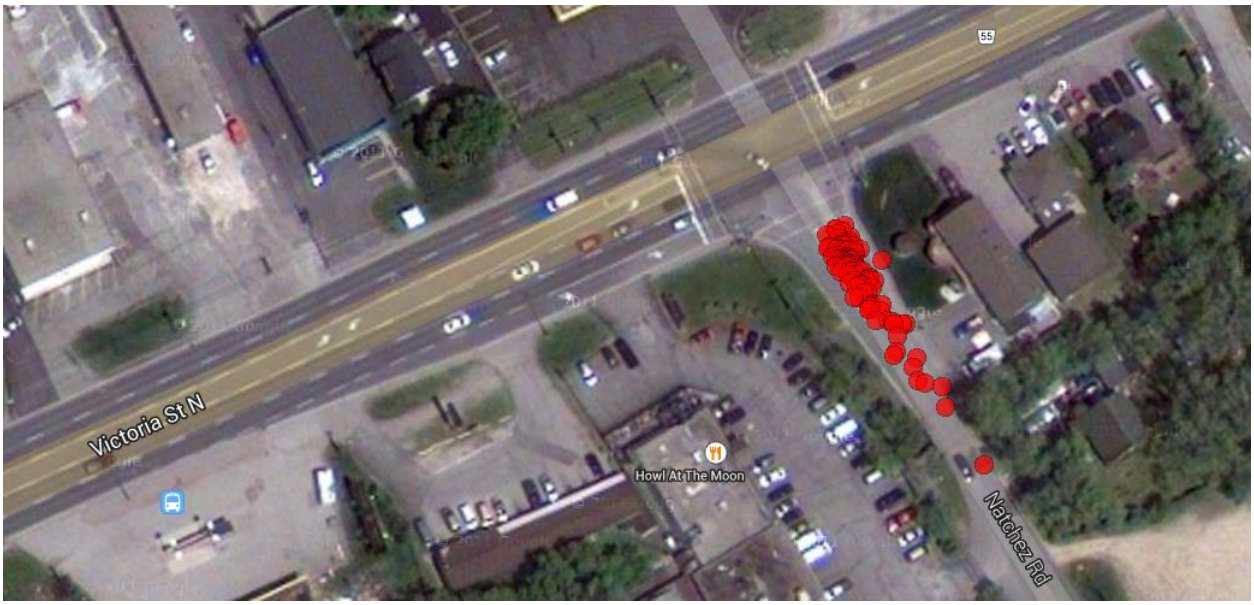

Figure E-8: Unscheduled Stop Observations for Victoria at Natchez Rd

Natchez is a collector roadway connecting to Victoria Street an arterial. The buses traversing this route make a left turn maneuver at this intersection.